Global, Seasonal Cloud Variations from Satellite Radiance Measurements. Part II: Cloud Properties and Radiative Effects

WILLIAM B. ROSSOW AND ANDREW A. LACIS

NASA Goddard Space Flight Center, Institute for Space Studies, New York, New York

(Manuscript received 14 December 1989, in final form 25 April 1990)

ABSTRACT

Global, daily, visible and infrared radiance measurements from the NOAA-5 Scanning Radiometer (SR) are analyzed for the months of January, April, July and October 1977 to infer cloud and surface radiative properties and their effects on the Earth and surface radiation budgets. The analysis makes use of several additional datasets to help isolate the cloud contributions. The cloud properties inferred from satellite data are found to be about as accurate as the validation datasets available from other sources, but significant improvements are needed for better diagnosis of cloud-radiative feedbacks. Consequently, advances in cloud retrievals from satellite data will be like "new measurements" that have no independent validation. Reconstruction of regional, monthly mean Earth radiation budgets (ERB) from cloud, atmosphere and surface data is also nearly as accurate as can be checked with summaries of other, more direct measurements; improvements require detailed intercomparisons at smaller space/time scales. Currently, there is no global dataset with which to validate the reconstructed surface radiation budget (SRB). Comparison of monthly, regional mean quantities with those simulated by the GISS climate GCM shows that the differences are only a little larger than the uncertainties in the results; thus, better data and more detailed comparisons will be needed to improve the GCMs.

Despite important limitations in these results, several fundamental conclusions about the role of clouds in the radiation balance of Earth are apparent. 1) The magnitude of cloud property variations and their effects on radiation increase strongly with decreasing space/time scales, going from global, annual means to regional, monthly means; 2) Cloud properties are systematically different between land and ocean: oceans have larger cloud cover with somewhat larger optical thicknesses and lower cloud top altitudes; 3) Although cloud variations appear to be the primary cause of regional radiation budget variability at 5–30 day time scales, the effects of their seasonal variations at larger spatial scales are less important than the changes associated with changes in solar declination and atmospheric/surface temperatures; 4) The largest seasonal variations in radiation occur in the 30°–60° latitude band in each hemisphere; 5) Cloud variations tend to enhance regional and seasonal radiation variations at lower latitudes and mute them at higher latitudes; however, they also affect the average latitudinal gradients of heating/cooling; 6) Although clouds have a net cooling effect in the global, annual mean radiation balance at both the top of the atmosphere and the surface, their net effect on regional, seasonal balances is much more varied; 7) Conclusions (5) and (6), together, are equivalent to saying that the relation between cloud properties and their effect on ERB and SRB depend crucially on the regional and seasonal circumstances of the clouds; 8) Regional cloud and surface seasonal change amplitudes and phases exhibit a wide variety of values; moreover, the correlations between surface temperature and cloud properties vary greatly; 9) There appears to be no simple relation between global mean surface temperature, global mean cloud properties and their global mean effects on ERB and SRB, implying that cloud radiative effects on the seasonal temperature cycle must be described as multiple feedbacks; and 10) The complexity of the cloud radiative effects and the data accuracy required to diagnose cloud-radiative feedbacks indicate the challenge of this problem.

1. Introduction

Determination of cloud-radiative feedbacks on climate has been a primary focus of climate research (GARP 1975, 1978; Rossow 1981; WCRP 1984). Study of this problem is necessarily indirect because there is no way to measure cloud and consequent radiation changes during *climate* variations except by undertaking a multi-decadal, global observation program. There is no guarantee that such an observation program would work since our near-term climate will be a transient change from a low CO_2 "equilibrium" to some future high CO_2 atmosphere. Progress can, however, come from the improvement of our understanding of the detailed physical processes involved in the treatment of clouds and radiation in climate general circulation models (GCMs) that simulate cloud variations from mesoscales to planetary scales and over diurnal, synoptic, and seasonal time scales. Comparisons of regional differences in the seasonal variations of clouds and their radiative effects in such models and in detailed global observations that resolve these same scales can help to constrain the large number of factors which affect cloud/radiation calculations and to make

Corresponding author address: Dr. William B. Rossow, Goddard Space Flight Center, Goddard Institute for Space Studies, 2880 Broadway, New York, NY 10025.

the *climate* simulations of these models more believable. Moreover, such datasets can also be used for direct diagnosis of cloud-radiative interactions. The International Satellite Cloud Climatology Project (ISCCP) and its associated research programs are designed to provide data and analyses for such studies (Schiffer and Rossow 1983, 1985; Rossow and Schiffer 1990).

Evaluations of cloud effects on the radiative budget have used the variations of clouds and radiative fluxes on a variety of space and time scales (Cess 1976; Hartmann and Short 1980; Ohring and Clapp 1980; Cess et al. 1982), even though the formulation of the effects is usually derived from an assumed radiative balance which does not hold for regional or daily and seasonal variations (see more discussion in Hartmann et al. 1986). The changes in quantities are sometimes estimated by simple flux differences, such as "cloud forcing" (Ramanathan 1987; Hartmann et al. 1986), neglecting all possibility of more complicated relations involving phase and amplitude variations. Such an analysis of cloud effects on radiation may be analogous to estimating changes in power dissipation in a complex AC electronic circuit as if it was composed entirely of ohmic resistors.

The neglect of the dependence of radiative flux variations on changes in other cloud properties is equivalent to the assumption that all clouds have the same cloud top temperature, emissivity, and albedo at all times and locations, yet the "type" of clouds and their properties clearly varies among the climate regimes (e.g., Warren et al. 1985; Sèze and Rossow 1990a). When these other cloud properties are allowed to vary along with cloud cover and account is taken of the distribution of radiative heating/cooling within the atmosphere-surface system, cloud-radiative feedbacks on climate are considerably more complex (cf., Wang et al. 1981; Stephens and Webster 1981; Hansen et al. 1984). For instance, Wang et al. (1981) show that variation of more than one cloud property at a time can make the feedback a function of the space and time **structure** of the climate perturbation, in addition to its amplitude; hence, a more detailed understanding of the distribution and variation of cloud properties is needed.

Most available cloud climatologies (London 1957; Telegadas and London 1954; Van Loon 1972; Schutz and Gates 1971a,b; Berlyand and Strokina 1980; Hahn et al. 1982, 1984; Warren et al. 1985; Warren et al. 1986, 1988; Hughes and Henderson-Sellers 1985; Stowe et al. 1988, 1989; see also Hughes 1984) do not provide complete information on the geographical distribution of clouds, their radiative properties, or their time variations. They do provide key information on "cloud amount" and top and base heights, though with very coarse resolution (in particular, cloud heights are generally reported in three broad categories that are too coarse to determine the quantitative effects of clouds on radiation). However, the physical properties of clouds needed to calculate their effect on radiation are mostly unknown or are known with too little quantitative accuracy.

For the past nine years, we have been investigating one specific approach to the determination of cloud-radiative feedbacks that combines several datasets within a single consistent analysis. The strategy has three steps (Rossow et al. 1989a; cf., Minnis and Harrison 1984a). The first step is to retrieve cloud radiative properties from satellite measured, *spectral radiances* (which are most sensitive to cloud properties) by employing a complete radiative model that is specifically designed to simulate these satellite measurements: to isolate the cloud properties, the model must explicitly account for the separate effects of the Earth's surface, atmosphere, and clouds on the satellite measurements as well as their wavelength and angular dependences. This analysis requires correlative information about atmospheric and surface properties to supplement the information in the satellite data. In the second step, the parameter set describing surface, atmosphere, and clouds is used in a related radiative model to calculate *spectrally integrated fluxes* and to infer the top of the atmosphere (TOA) and surface (SRF) radiation balances (called ERB and SRB) and to diagnose cloud-radiative feedbacks. Some additional datasets are used to specify parameters that are not obtained in the first step of the analysis. The third step is to compare the cloud properties and the associated radiative fluxes, obtained from the combined analysis of the several datasets, to those produced by a climate model over the whole range of accessible time and space scales. This analysis concept involves many steps, some of which are not well understood; hence, results at each step in the analysis must also be verified by additional data comparisons. In particular, before comparing to a climate model, we can compare the deduced radiative fluxes with direct measurements of these fluxes from satellites (ERB) and from the surface (SRB).

This paper and its two companions (Rossow et al. 1989a,b; henceforth, Ro89a,b) report on progress made in understanding and validating some aspects of the analysis scheme discussed above. We have carried the analysis of a limited dataset (section 2a) through all three steps to help identify the key uncertainties and problems that need further study; however, we have not yet completed a validation of all the aspects mentioned above. The focus of Ro89a was to determine the accuracy of the cloud detection step (summarized in section 2b); detailed validation of the measured cloud properties is discussed but not completed. Since the basic cloud detection is done by the identification of changes in the measured radiances away from the values inferred to represent clear conditions, the key to the validation strategy is to verify these clear scene radiance values by comparing them to surface properties deduced from other surface measurements. This avoids problems in the definition of cloud cover frac-

tion (but does not eliminate its importance in modeling cloud effects on radiation, cf. Rossow 1989). Since the accuracy of measuring surface properties also affects the calculation of SRB, a more detailed study of the accuracy of the retrieved surface properties from satellite data is provided in Ro89b. Section 2c summarizes the retrieval of cloud and surface radiative properties from the spectral radiances, and section 2d describes the modeling of total fluxes. The present paper examines the variations of the cloud properties in more detail (section 3) and their consequent effects on the total radiative fluxes (section 4).

One of the key difficulties in modeling the radiative effects of clouds is the treatment of the complex spatial and temporal variability of cloudiness (Stephens 1988; Rossow 1989); hence, one objective of this study is to characterize some of the scales and magnitudes of this variability. In section 3, we examine the results of our analysis to describe the cloud variations on seasonal time scales for length scales from 500 km to planetary scale (section 3). These results complement those of Minnis and Harrison (1984a,b,c), who examined cloud variations on hourly to synoptic time scales over similar spatial scales, and of Sèze and Rossow (1990a) who examined daily to weekly time scales and spatial scales from 5 km to 2000 km. Stowe et al. (1988, 1989) present some results similar to ours. In section 4, we infer the ERB and SRB from these cloud, surface, and atmospheric properties to investigate the magnitude of their variations. These results are compared to ERB measurements from Nimbus-7 (Smith and Smith 1987) to assess in a preliminary way, our ability to diagnose the role of clouds in the seasonal radiation budget. We also compare the variations of clouds, the surface, the atmosphere, ERB and SRB to those in our climate GCM (Hansen et al. 1983, 1984). The summary in section 5 outlines the key issues and objectives for future data analyses.

2. Data and analysis methods

a. Data

The basic satellite radiance data used to determine cloud and surface properties are images from the scanning radiometer (SR) on the NOAA-5 operational, sun-synchronous, polar orbiting weather satellite from January, April, July and October 1977. This instrument measures visible (VIS) and infrared (IR) radiances over the wavelength ranges of 0.52–0.72 μm and 10.5–12.5 μm with a spatial resolution at the subsatellite point of 4 km and 8 km, respectively. Operational data processing provides sampled measurements once per day (morning) at a 15–25 km spacing (NOAA 1977; Fortuna and Hambrick 1974). Visible and infrared radiance calibrations are known to within about 10%; instrument noise levels are estimated to be about 2%–3% (Ro89a).

The atmospheric temperature and relative humidity profiles are taken from the twice daily, gridded analyses produced by the National Meteorological Center (NMC) of NOAA. These data represent an analysis (by assimilation in a forecast model) of conventional weather station reports at 0000 and 1200 UTC every day to produce a uniform 2.5° map grid of profiles on standard pressure levels (1000, 850, 700, 500, 300, 200, 100, 50 and 10 mb) (see McPherson et al. 1979; Rosen and Salstein 1980; and Kistler and Parrish 1982, for more details). Because the satellite data represent observations at approximately constant local time of day, while the NMC data are for two particular UTCs over the globe, we use the daily average of NMC temperature and relative humidity. Uncertainties in these data are estimated to be 3–4 K for temperatures and about 50% for humidities, including both the measurement errors and neglected diurnal variations (Ro89a).

Ozone column abundances used in the satellite radiance analysis are specified by the last year of a seasonal, zonal mean climatology obtained by the SBUV on Nimbus 4, covering the years 1974 through early 1977 (Hilsenrath et al. 1979; Hilsenrath and Schlesinger 1981). Uncertainties are estimated to be about 20%, including both measurement errors and neglected synoptic variations (Ro89a).

Five other datasets are used to describe surface types as a function of location: 1) each point on the globe is specified as land or water using a 0.1° resolution world map (derived from Masaki 1972), 2) topographic heights above mean sea level are derived from the 1° resolution Scripps topography (Gates and Nelson 1975), 3) vegetation type and soil type are specified by data from Matthews (1983, 1985) and from the Oxford World Atlas (1973), respectively and 4) snowline/altitude climatology as a function of latitude and month is taken from Lamb (1972). All of these datasets are used in a statistical analysis of the satellite radiances to obtain maps of the clear sky VIS and IR radiances (Ro89a).

b. Cloud detection method

The NOAA-5 SR visible (VIS) and infrared (IR) radiance data are analyzed to obtain three cloud properties, cloud cover (CC), optical thickness (TAU) and top temperature (TC) – altitude (ZC), and two surface properties, visible reflectance (RS) and temperature (TS) (Ro89a). The primary steps in the analysis involve the determination of which radiance values represent cloudy and clear conditions ("cloud detection") and comparison to radiative model calculations of satellite radiances ("retrieval").

The cloud detection method developed and tested in this study is a bispectral threshold method in which cloudy image pixels are identified by the fact that *both* their VIS and IR radiances differ from clear scene values. The clear scene values are obtained from a statis-

tical analysis of the time/space variations of the radiances at each location, augmented by other surface temperature data. The essential assumptions that underlie this analysis are that clear conditions generally exhibit less variability, especially in time, than cloudy conditions (cf. Sèze and Rossow 1990a) and that similar surface types, defined primarily by land/water/vegetation, have very similar visible reflectances (Matthews and Rossow 1987). Essentially, the satellite radiances are analyzed twice, first to obtain measures of clear conditions and second, to identify cloudy locations (Ro89a). Validation of the surface properties retrieved from clear radiances is discussed in Ro89b and summarized below.

1) OCEAN VISIBLE REFLECTANCES

Ocean visible reflectances are described by a model (Ro89a) in both the retrieval of cloud properties from the satellite radiances and in the calculation of radiative fluxes. Comparison of the model to retrieved visible reflectances as a function of viewing/illumination geometry confirms the model reflectances to within about 2% away from glint conditions and to within about 5% near to glint conditions. When sea ice is determined to be present, the retrieved visible reflectance is used in place of the model. The position of the monthly mean sea ice line is verified to within about 200 km, except for more rapidly varying portions of the line where the errors are as large as 300–500 km. Uncertainties in sea ice visible reflectance values are estimated to be about 10% or more but there is very little data available to validate these results. The VIS threshold is equivalent to a clear radiance uncertainty of 10%. Difficulties with the sea ice edge and the dark bias in high latitude values of RS (see below) may explain a turn-down in our cloud amounts at the highest latitudes in the winter hemisphere.

2) LAND VISIBLE REFLECTANCES

The average visible reflectances obtained for various vegetation types are consistent with available information (Matthews and Rossow 1987). The uncertainty of land reflectances, in the absence of snow, is judged to be about 2%–3% for vegetated surfaces and 3%–5% for the brighter deserts due to the neglect of surface anisotropy. Tropical regions exhibit some cloud contamination. The inferred position of the snow line corresponds to other analyses to within 100 km in most regions, but in more active areas the correspondence is poorer, only to within 200–300 km. The visible reflectances for rapidly varying parts of snow-covered land have a random error of about 10% but only about 5%–10% for persistently snow covered regions. The inadvertent neglect of ozone absorption in the surface reflectance analysis (Ro89a) does not alter low latitude values by more than 1%–2%; however, reflectances of snow-covered land at the highest latitudes are biased low by about 10% (Matthews and Rossow 1987). Since the ozone absorption is included in the retrieval of cloud optical thicknesses, this error is partially compensated by an overestimate of cloud optical thicknesses over snow and ice covered areas. The VIS threshold is equivalent to a clear radiance uncertainty of 10%. The dark bias for snow-covered values of RS may explain the turn-down of our cloud amounts at the highest northern latitudes in January.

3) OCEAN SURFACE TEMPERATURES

Comparison to ship and other satellite analyses of sea surface temperatures shows a random error in our results of about 2 K; however, an underestimate of water vapor absorption effects in the analysis biases our values low by about 1–2 K (Ro89b). We retrieve surface temperatures assuming an emissivity of one, which contributes an additional 1 K low bias. Since the same water vapor absorption and surface emissivity values are used in the cloud retrieval, these biases do not effect the accuracy of the cloud detection. Errors in the sea ice edge location do not cause large errors in surface temperatures. Small scale spatial variations suggest that sea ice surface temperatures may be uncertain by as much as 5 K; however, there is little data available to verify our results. The IR threshold is equivalent to a clear radiance uncertainty of 9 K.

4) LAND SURFACE TEMPERATURES

The random and systematic differences between satellite-based, solid-surface temperatures, and weather station near-surface, air temperature data are both about 5–6 K. There are three effects that contribute to these differences: 1) variations of land surface emissivities with location change the relation of the solid-surface temperatures and the near-surface air temperatures, 2) variations in the temperature contrast between the solid-surface and the near-surface atmosphere with season, and 3) variations in the temperature contrast between the solid surface and the near-surface atmosphere with cloud amount (Ro89b). The first two factors, however, do not affect the clear infrared radiances or the cloud detection. The effects of errors in locating image pixels in mountainous terrain cause larger uncertainties. The IR threshold is equivalent to a clear radiance uncertainty of 9 K.

5) CLOUD DETECTION ACCURACY

If there were no uncertainties in the input data, deduced surface properties, or radiance models, then comparison of measured and modeled radiances would imply values of TAU and ZC that would be either zero (no cloud) or some finite value (cloud). Since the actual values of TAU and ZC can be arbitrarily small, especially since cloud cover of the radiometer field of view can also be small, real values of TAU and ZC may be confused with small values produced by data

noise and analysis errors. The estimated errors in RS and TS are equivalent to errors in TAU and ZC of about 1.0 and 1.0 km, respectively. To prevent spurious cloud detections and to compensate (partially) for incompletely covered fields of view, an image pixel is labeled as cloud covered only if the retrieved values of TAU and ZC are ≥ 1.2 and >1.4 km, respectively (Ro89a).

The global mean sensitivity of the cloud detection, expressed as the change in total cloud cover when the thresholds are doubled, is about 5%. About 10%–15% of the TAU and ZC values that are rejected by the analysis appear to represent actual clouds, generally representing high, optically thin clouds (cirrus) and very low-level, optically thick clouds (primarily marine boundary layer cloudiness). The accuracy of the detection is judged to be about 10%–15%. Comparisons to other cloud climatologies (see section 3) also suggest an uncertainty of about 10%–15%. With the exception of the marine stratus regions in the eastern subtropical ocean basins and the polar regions, the cloud cover errors appear to be nearly uniform over the globe.

c. *Radiance analysis method*

Cloud and surface properties are retrieved from the narrowband visible and infrared radiances measured by NOAA-5 SR using models designed to simulate the angle dependence at these particular wavelengths in clear and cloudy atmospheres. Optical constants have been adjusted to account for the specific spectral response of the SR channels (Ro89a). All quantities are assumed to be constant over an image pixel with an effective size of 8 km; however, the statistical tests used in the analysis, together with the navigation uncertainties and data sampling, effectively smooth all properties over regions of 15–25 km in size. Specific characteristics of the retrieved cloud and surface optical parameters are described below.

Cloud cover (CC) is obtained by counting the number of image pixels found to contain cloud. The finite thresholds on TAU and ZC values imply a threshold in the amount of cloud within the radiometer field of view required for detection that depends on the average optical properties of clouds that vary with location. Using global mean cloud properties implies that cloudiness would be detected with about 20%–30% cover of the pixel. Thus, the monthly mean cloud cover parameter, defined by this analysis, is a frequency of occurrence for a spatial scale of about 15–25 km and time scale of one day.

In the model of the 10–12 μm radiances (Ro89a), a cloud is represented as a single, isothermal, absorbing layer in a layered atmosphere with temperatures and humidities given by the NMC atmospheric data. All cloud and atmospheric scattering effects are neglected and the surface is a blackbody. Surface temperatures are specified by the TS values obtained from analysis of clear IR radiances using the same radiative model and atmospheric conditions with no cloud layer. Day-to-day variations of TS are taken from the NMC data but the monthly mean value is based solely on the satellite analysis. The cloud top temperature (TC) is the temperature of the upper surface of an opaque (black-body) layer, corrected for any water absorption above the cloud; TC < TS, always.[1] If the VIS optical thickness of the cloud is small (< about 4), the cloud temperature is corrected to account for transmission of radiation from below with the cloud emission treated as that from an isothermal layer. The IR absorption optical thickness is taken to be (1/1.24) times the VIS optical thickness (defined below). The altitude of optically thinner clouds is biased low by 1–2 km because the IR absorption optical thickness should be about 1/2.0 or 1/3.0 times the VIS value (e.g., Platt et al. 1987). The cloud top altitude (ZC) is the altitude above mean sea level at which the atmospheric temperature is equal to TC. Precise verification of ZC values is difficult with available information; however, our results are consistent with other climatologies to within about ± 0.5 km (Ro89a, see section 3), except for higher level clouds.

In the model of the 0.5–0.7 μm radiances (Ro89a), a cloud is represented as a single conservatively scattering layer in a layered atmosphere. Ozone absorption occurs in a layer at the top of the atmosphere and Rayleigh scattering occurs in layers above and below the cloud layer. Aerosol scattering is neglected and land and sea ice surface reflection is assumed to be isotropic. Water surface reflectances are represented by anisotropic Fresnel reflection from a rough surface (Ro89a). Surface reflectances, except for water, are specified by monthly average RS values obtained from analysis of clear VIS radiances using the same radiative model and atmospheric conditions with no cloud layer. (Ozone absorption was neglected by mistake.) Cloud scattering effects are modeled by full, multiple, Mie scattering in a plane-parallel layer composed of water spheres with a "gamma" size distribution characterized by a mean effective radius of 10 μm and a size variance of 0.15 (Hansen and Travis 1974). Neglect of variations in cloud particle size is estimated to produce an uncertainty in the value of TAU of about 15%; observations of microphysical variations in marine clouds, for example, suggest that this estimate is conservative (Stephens and Platt 1987). The angular distribution of VIS radiances are modeled explicitly. The optical thickness (TAU) obtained is the value for 0.6 μm wavelength. There are no other climatologies of TAU to verify our results.

d. *Radiation budget analysis method*

Another radiative transfer model is used to calculate upward and downward, solar and thermal fluxes at the

[1] This is not always true in reality; however, if a cloud occurs in a temperature inversion, it is likely to be missed in this analysis.

top-of-the-atmosphere (ERB) and at the surface (SRB); this radiative model is used in our climate GCM (Hansen et al. 1983). The model calculates the spectral variations of solar and thermal IR absorption, using the correlated k-distribution method (Lacis and Oinas 1990; see also Lacis and Hansen 1974) to integrate over overlapping gaseous absorption lines in the presence of scattering and calculates the full anisotropic multiple scattering effects of aerosols and clouds (both solar and thermal IR), using Mie computations (Hansen and Travis 1974). All radiatively significant atmospheric constituents and vertical inhomogeneities are explicitly and separately represented. For our analysis, inputs from other subroutines in the GCM are replaced by the results of the satellite data analyses. Since the cloud and surface properties retrieved from the satellite radiances are defined at the particular wavelengths measured, additional assumptions are required to describe the complete spectral dependence of the cloud and surface properties. There are also some other properties of the clouds, atmosphere, and surface that must be specified to calculate total fluxes even though they do not affect the satellite radiances. Separation of the effects of clouds, atmosphere, and surfaces on the narrowband radiances allows for separate, self-consistent treatments of the other properties of these three components of the climate and their effects on ERB/SRB. In particular, this approach provides a natural way to combine multiple datasets that measure different aspects of the climate system.

1) SPECTRAL DEPENDENCES

The cloud optical thickness and top temperature are defined at 0.6 μm and 11 μm, respectively; together with the atmospheric temperature/humidity profiles, these two parameters also define the cloud top altitude and pressure. Since the retrieval analysis assumes an explicit microphysical model (liquid phase, spherical droplets, and a gamma size distribution with mean radius of 10 μm and variance of 0.15), the complete spectral dependence of the cloud optical parameters can be specified in the flux calculations by using the same microphysical model. Thus, variations of the narrowband radiances caused by clouds are linked to variations of total fluxes in a spectrally self-consistent fashion by just three parameters, cloud cover, optical thickness and top pressure through the explicit cloud model. The accuracy of the reconstruction of ERB/SRB is limited by the assumption that all radiation variations are caused only by changes in cloud cover, optical thickness, and top pressure, but this is a significant improvement over use of a single cloud parameter. The study by Stephens and Platt (1987) suggests that most of the flux changes can be represented by these parameters because the variations of other microphysical parameters are relatively small; however, the role played by variations in cloud macrostructure is not yet understood (Stephens 1988; Rossow 1989). Climatological information about the global variations of cloud microphysical parameters, as well as smaller scale variations of optical thickness and top pressure, are not yet available.

The surface reflectance is defined at 0.6 μm. To obtain the surface albedo, defined in two spectral bands, 0.4–0.7 μm and 0.7–4.0 μm, we must have information about both the angular and spectral variations of surface reflectances. Although much is known about these dependences for specific cases, a global survey and classification of these properties is not yet available (see Matthews 1985; Matthews and Rossow 1987; Ro89b). For these calculations, the retrieved visible reflectances are assumed to represent visible directional albedos since the solar zenith angles do not vary much over one month for sun-synchronous observations and the retrieved values are averaged over several satellite zenith angles. The ratio of near-IR and visible albedos at each location is assumed to be that used in the climate GCM, which depends on the surface type (land/water) and the vegetation/soil type of land (see Hansen et al. 1983; Matthews 1983); the near-IR albedo is given by the retrieved visible reflectance times this ratio. A test of the importance of the latter assumption was made by repeating some calculations with both the visible and near-IR albedos set equal to the visible reflectances, which is equivalent to reducing land albedos from about 20%–30% to 10%–15%. Although this change reduces upward solar fluxes at the surface by 10–30 watts/m^2 in some locations, its effect on zonal or global mean SRB is not as large. The effect of this change on ERB is even smaller.

The surface infrared fluxes depend on both the surface temperature and spectral emissivity. The latter is known for water surfaces but only approximately for land as a function of soil, vegetation and other surface conditions (Ro89b). Since the surface temperatures are retrieved assuming unit emissivity, we use the same assumption for the total flux calculations. Although this assumption neglects effects of changes in soil and vegetation moisture content, it minimizes the error associated with regional variations in emissivity by assuming the integrated emissivity is the same as the 10–11 μm emissivity. A test of the importance of this assumption was made by repeating some calculations using the surface emissivities specified as in the climate GCM, which is equivalent to increasing surface temperatures by about 1 K; the overall effect on upward thermal fluxes is less than 20 W m^{-2} at the surface and less than 10 W m^{-2} at the top of the atmosphere.

The only atmospheric gases that affect the narrowband radiances are water vapor and ozone; but other gases have small effects on total fluxes. The abundances of CO_2, O_2, NO_2, N_2O, CH_4 and two "freons" are specified in these calculations (at 1980 values) as in the GCM (Hansen et al. 1983). Aerosol effects are neglected in the flux calculations as in the radiance analysis.

2) VERTICAL DISTRIBUTIONS

The vertical profiles of atmospheric temperature and humidity are specified for both the satellite radiance analysis and the total flux calculations from the same dataset. Only total ozone abundance is needed for the satellite retrievals but the flux model uses an ozone profile: we adjust the climatological (latitude and month) ozone profiles used for the climate GCM to have the same total ozone as in the radiance analysis.

The radiance analysis assumes only one isothermal cloud layer in an image pixel with a distinct top. We use the same assumption for the flux calculations; however, the location of the cloud base must also be specified, particularly for downward IR flux calculations. Since no global information on cloud base temperatures is available (although conventional climatologies report cloud amounts in three coarse height intervals), we assume that all clouds fill one model layer, equivalent to a physical thickness of about one kilometer. One study of clouds over the North Atlantic (Tian and Curry 1989) suggests that single layer clouds occur more than half the time.

3) AVERAGING

The NOAA-5 data provide observations at only one diurnal phase (local morning) so that we cannot attempt a proper representation of the diurnally averaged fluxes. To calculate total solar fluxes, we hold all parameter values fixed over the diurnal variation of solar irradiance; IR fluxes are assumed to represent the diurnal average. This assumption is not necessary if complete diurnal information is available as with ISCCP results (Schiffer and Rossow 1985).

To complete the calculations of global mean quantities and their seasonal variations, we "fill in" the unobserved winter polar regions by assuming that all cloud, atmosphere, and surface properties are constant with latitude and equal to the zonal mean values of the highest observed latitude. This filling affects the north (south) polar region in January (July), equivalent to about 7% of global surface area; in April and October less than 1% of global surface area is "filled."

To reduce the calculations to a manageable task, we use space and time mean quantities: the cloud and surface properties are separately averaged to 1° by 1° spatial resolution for each day and then averaged over one month. For the flux calculations, these values are further averaged to 7.5° by 10° ($\approx$1000 km) spatial resolution to match the climate GCM resolution. The total fluxes are then calculated for clear and overcast conditions and averaged together using the cloud cover as a fractional weight; the surface and atmospheric properties are the same for both the clear and overcast calculations. In other words, we use the separate monthly averages of the atmosphere/cloud/surface optical properties to estimate monthly mean radiative fluxes. As our results illustrate, this approach neglects significant correlations among the variations of these parameters. This procedure is not a necessary limitation of the accuracy of calculating the ERB/SRB but it is a practical choice made for this preliminary investigation.

The neglected effects of smaller scale optical inhomogeneities enter into the flux calculations in two ways: in the representation of pixel-scale (8 km) narrowband radiances in the retrieval analysis and in the representation of total fluxes at 1000 km scale. The first issue has already been discussed in Ro89a (see also Stephens 1988; Rossow 1989). Although the flux calculations also assume homogeneous optical properties, except for the variation described by cloud cover, the method of averaging cloud and surface properties from pixel to 1000 km scale can affect the resulting fluxes. In this study, the values of TAU, TC, RS and TS were averaged linearly; i.e., the spatial and temporal averages are proportional to the linear sums, which gives equal weight to clouds according to their altitude and mass density. This means that the cloud effects on the fluxes are not equally weighted, but rather, the average fluxes will be dominated by the contributions from larger TAU and somewhat lower TC. Moreover, the independent averaging of the cloud properties may not describe the proper correlation between these two quantities since we have replaced variations of optical thickness and top pressure from pixel-to-pixel with a single layer cloud with average optical thickness and top pressure (see Sèze and Rossow 1990a).

e. Climate GCM radiation calculations

At the end of section 4, we compare monthly mean radiative fluxes inferred from the NOAA-5 SR cloud analysis to those calculated in our climate GCM. Although the basic radiative transfer model is identical in both flux calculations, there are some differences in specifications of some parameter values.

In the flux calculations, the monthly averaged cloud properties are assigned to a single model layer covering a fraction of a GCM grid box specified by the cloud cover. In the GCM, clouds are predicted to occur at many levels (nine in the troposphere); if cloud occurs at more than one level in a single time step, then the vertical extent of a single layer is equivalent to several model layers if they are adjacent and may create multilayer clouds if they are not. The predicted cloud fraction in each layer at each time step is compared to a randomly generated fraction; if the cloud fraction is greater, cloud fraction is set to 100%; otherwise it is set to zero (Hansen et al. 1983). Thus, the GCM monthly mean cloud amount is a frequency of occurrence like the NOAA-5 cloud amount but for a much larger spatial scale. Total cloud amount is always 100% in each layer (when cloud occurs), equivalent to maximum overlap.

TABLE 1. Annual mean cloud properties. Global and hemispheric mean values refer to averages over the lowest 60° of latitude in each hemisphere. (Values in parentheses show the averages over all latitudes but with no winter pole observations included.) The signs on the hemispheric deviations refer to the Northern and Southern Hemispheres, respectively. The estimated random errors apply to daily observation at each location; errors in monthly annual means, as well as in zonal, hemispheric and global means are expected to be much smaller.

Quantity	Global mean	Estimated random error	Deviation of mean hemispheric value	Rms deviation of zonal mean
CC (%)	51.1 (52.8)	5	∓3.6	12.4
TAU	13.1 (16.2)	2	∓2.2	16.0
RS (%)	5 (10)	3	±2	3
ZC (km)	4.6 (4.5)	0.5	±0.2	0.7
TC (K)	265.3 (263.0)	4	∓0.9	13.6
TS (K)	288.3 (284.5)	4	∓0.2	20.7

In the flux calculations, the microphysical properties of the clouds are fixed as in the radiance analysis, whereas in the GCM, clouds colder than 233 K are assumed to be composed of ice spheres with an effective radius of 25 μm and a size variance of 0.2 (Hansen et al. 1983).

In the flux calculations, the surface emissivity is unity, consistent with the radiance analysis; however, in the GCM the emissivity varies with the surface type (and moisture content). The GCM model fluxes include the effects of a specified aerosol climatology but the flux calculations do not. Finally, the monthly mean GCM model fluxes represent the average of a time series with five hour resolution, whereas the flux calculations are performed with monthly mean inputs.

3. Global, seasonal cloud variations

a. Annual mean cloud properties

1) GLOBAL AND HEMISPHERIC MEAN

To indicate the relative magnitude of the cloud variations inferred from this analysis, we will use the annual, global mean of each parameter as a reference value where the average of the analysis results for January, April, July and October 1977 is taken to represent this value. Table 1 shows the global mean cloud and surface properties and summarizes the deviations of the hemispheric and zonal mean values from these. The Earth is about half covered by clouds, to within an uncertainty of about 15% (5%–10% random and up to 10%–15% bias); this compares well with other climatologies (e.g., see Hughes 1984; Hughes and Henderson-Sellers 1985; Stowe et al. 1989, and Table 4). These clouds have an optical thickness of about 13, equivalent to a spherical albedo of 70% over a black surface, and a top temperature of 265 K, about 23 K colder than the mean surface, but warmer than the effective radiating temperature of the Earth. The average cloud top altitude (above mean sea level) is 4.6 km. The values of and contrast between mean cloud top and surface temperatures also agree well with those inferred from Stowe et al. (1989) based on analysis of Nimbus-7 THIR and TOMS data (Table 2).

The two hemispheres (Tables 1 and 2) are not the same: cloud amount is larger in the southern hemisphere (cf. London 1957; Van Loon 1972; Schutz and Gates 1971a,b; Hughes and Henderson-Sellers 1985; Stowe et al. 1989) with a larger optical thickness and warmer cloud top temperature, apparently associated with a small difference in mean cloud top altitude.

2) ZONAL MEAN VARIATIONS

The last column in Table 1 shows that the latitudinal distribution of the cloud properties is not uniform: the rms deviations of zonal mean values from their global mean is much larger than the hemispheric deviations. Figure 1 shows the zonal mean quantities for the annual average. Total cloudiness (Fig. 1a) is concentrated into three zonal bands coinciding with the classical tropical and temperate midlatitude climate zones.

Cloud cover in the tropics is about the same or somewhat lower than in midlatitudes and shows a double peak just north and south of the equator. Both the lower average amount and the double structure are associated with the seasonal variation in the intensity and position of the ITCZ (see next section). The midlatitude cloud band in the Northern Hemisphere has

TABLE 2. Comparison of 1977 global and hemispheric mean cloud top (TC) and surface (TS) temperatures for January and July from NOAA-5 SR to values for 1979/80 from Nimbus-7 (Stowe et al. 1989). Hemisphere means are shown as deviations from the corresponding global mean values. Values for 1977 are retrieved from IR radiances assuming unit emissivity for the surface and variable emissivity for clouds. Averages are over ±60° latitude. TC values for 1979/80 are average IR brightness temperatures whereas TS values are based on conventional ship and land weather station reports. NOAA-5 measurements correspond to early morning local times whereas Nimbus-7 measurements are the average of local noon and midnight conditions.

Date	Global TC	Global TS	Global TS − TC	NH/SH TC	NH/SH TS	NH/SH TS − TC
Jul 1977	266.8	288.9	22.1	±1.3	±3.8	±2.5
Jul 1979	264.5	290	25.5	±2.5	±4.0	±1.5
Jan 1977	264.4	287.7	23.3	∓3.1	∓6.1	∓3.0
Jan 1980	262.5	286	23.5	∓2.5	∓2.0	±0.5

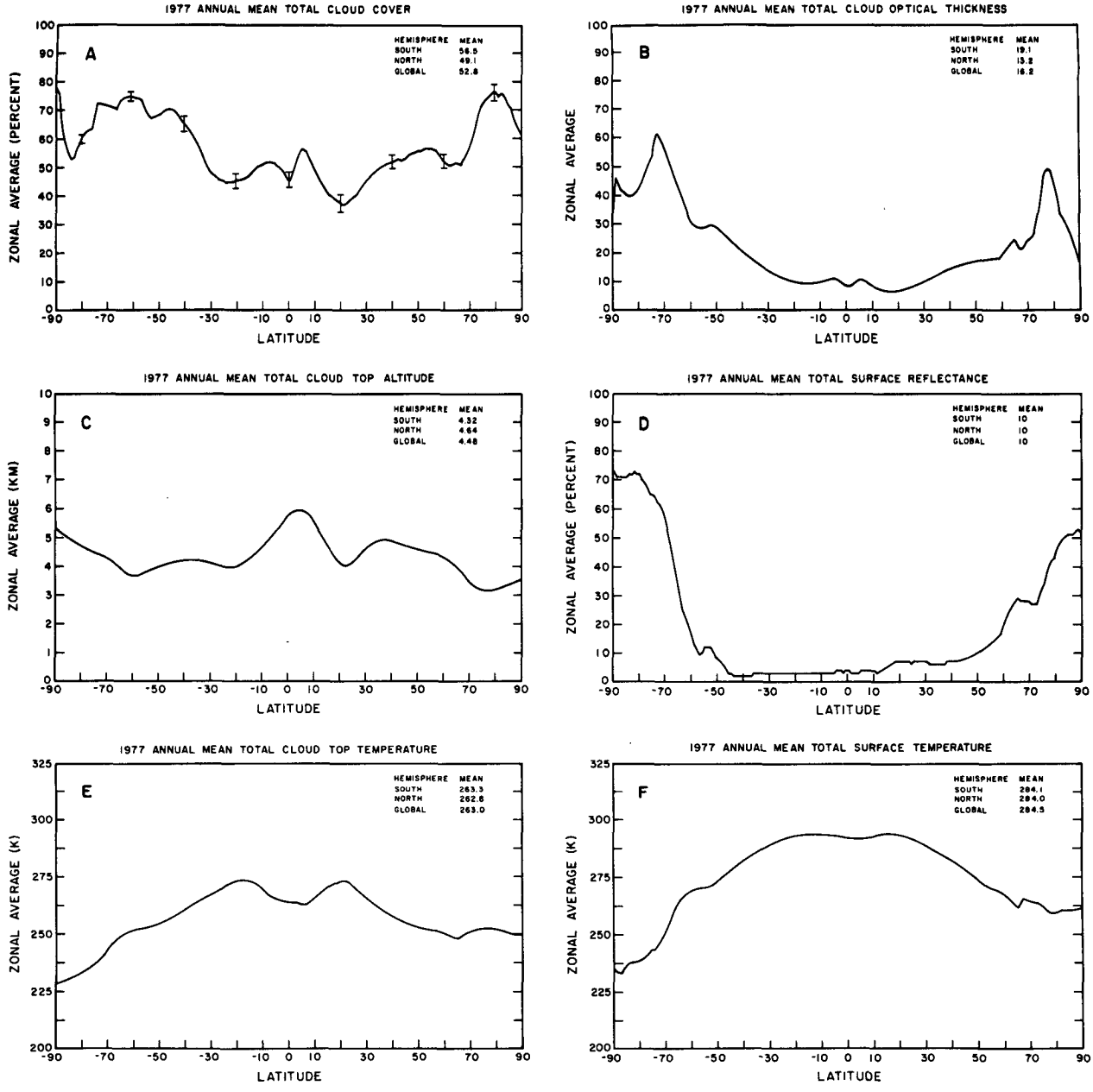

FIG. 1. Annual zonal mean cloud and surface properties: (a) total cloud cover, (b) cloud optical thickness, (c) cloud top altitude, (d) visible surface reflectance, (e) cloud top temperature and (f) surface temperature. Error bars in (a) show the sensitivity of cloud cover to doubling the thresholds.

about 15% less cloudiness than the one in the Southern Hemisphere which is associated both with their differing seasonal behavior and differing land/ocean distributions (see below). The subtropics in both hemispheres are regions of minimum cloudiness; the minimum in the Northern Hemisphere is lower than that in the Southern Hemisphere, which is also related to differences in their land/ocean distributions. The two polar regions exhibit relatively high cloud amounts; however, these results are limited to the sunlit portions of the year and are not as reliable as lower latitude results. All of these qualitative features are exhibited in other climatologies (see Ro89a); but more details can be seen in the results of both Hughes and Henderson-Sellers (1985) and Stowe et al. (1989).

Low latitude clouds have lower values of TAU on average than do middle and higher latitude clouds (Fig. 1b) due to the predominance in areal coverage of the thinner mesoscale anvil and cirrus anvil clouds in the ITCZ. Although the tropical clouds in the ITCZ appear

to be thicker on average than the subtropical clouds, associated with shallow, boundary layer convection, the more highly broken character of the subtropical clouds may be responsible for some of this difference in our analysis. Since only relatively thick (very bright) clouds are detectable over the high albedo surfaces near the poles, the average values of TAU at latitudes > 65°, shown in Fig. 1b, are probably biased high (see discussion in Ro89a). Surface reflectances (Fig. 1d) vary in a similar fashion to cloud optical depths from low values in low to middle latitudes to higher values near the poles; snow-covered land increases the annual mean RS for the Northern Hemisphere.

Cloud top height is relatively uniform when averaged over the globe, hemisphere, or latitude zone. The variations of the zonal mean values, shown in Fig. 1c, exhibit a contrast of only 2 km between the minimum in the subtropics and the maximum in the tropics. Midlatitude and polar cloud heights differ between the two hemispheres, associated with the differences in mean topography.

Cloud top temperatures (Fig. 1e) in the tropics and subtropics, where surface (and atmospheric) temperatures are relatively uniform (Fig. 1f), exhibit variations that are strongly anticorrelated with the variations in cloud top height. In middle latitudes, on the other hand, the latitudinal decrease in cloud top temperature is associated primarily with the decrease of air temperature at constant altitude; however, cloud top temperatures decrease less rapidly with latitude than surface temperatures, indicating an offsetting tendency for higher latitude clouds to occur at somewhat lower altitudes. The qualitative features shown in Figs. 1e and 1f also appear in the results of Stowe et al. (1989) as summarized in Table 2.

3) LONGITUDINAL VARIATIONS

Figure 2 shows the complete geographical distribution of the annual mean cloud and surface properties. The pattern of large longitudinal contrasts apparent in these maps explains the relatively low contrast exhibited in the zonal mean values. For instance, the minimum in zonal mean CC that occurs between 15° and 30° in both hemispheres is actually a combination of very low CC values occurring in the western portions of the ocean basins and over most land areas (deserts) with much higher CC values occurring in the marine stratocumulus regimes in the eastern portions of the ocean basins (Fig. 2a). North Africa and Australia exhibit lower values of CC compared to other subtropical land areas. On the other hand, the maximum in zonal mean CC near the equator is composed of strong maxima over tropical land areas, the tropical Atlantic and Indian oceans, and the "maritime" continent and of a strong minimum over the tropical eastern Pacific ocean. Midlatitude CC values are generally lower over land than over ocean; consequently, the two hemispheres differ in total cloudiness because of their differing land/ocean coverage. If the polar results are to be trusted then this contrast between land and ocean also explains the differences in polar CC values. All of these features of the cloud amount distribution, with the exception of the polar distributions, are also apparent in some of the older climatologies (Hughes 1984) and in the satellite-based results of Hughes and Henderson-Sellers (1985) and Stowe et al. (1989). Detailed regional variations also agree well with the results of Minnis and Harrison (1984b) and Saunders (1986).

Regional variations in TAU and ZC (Figs. 2b and d) are also larger than the variations exhibited by the zonal mean values because of a similar mixing of regions with smaller and larger values. In the tropical convection regions the clouds appear to be thicker over land (particularly Africa) but slightly higher over ocean (however, this relation may depend on the specific diurnal phase of our data). Although the midlatitude clouds exhibit more nearly zonally uniform values of TAU than at low latitudes, some land–ocean contrast is still apparent in ZC. High latitude clouds (poleward of about 45°) appear to be thicker and lower in altitude, in general, compared to lower latitudes (Fig. 1c). The annual mean location of such clouds is at a higher latitude in the Northern Hemisphere than in the Southern Hemisphere.

Regional values of TAU can be compared to the variations of surface reflectance (Fig. 2c); this shows some tendency for the thicker (i.e., more reflective) clouds to occur more over the darker oceans than over the brighter land areas. This tendency reduces the longitudinal contrasts in solar heating associated with surface variations (see section 4); in contrast, the latitudinal variations in cloud reflectances reinforce the latitudinal solar heating contrasts (Fig. 1b).

Regional values of TC in Fig. 2e correspond closely to the variations in ZC combined with the latitudinal decrease in air temperature at constant altitude. Comparison of regional TC values to TS values in Fig. 2f shows that weak zonal asymmetries in sea surface temperatures are partially offset by zonal asymmetries in TC; i.e., warmer water appears to lead to somewhat higher (colder) boundary layer convective clouds. On land the association between TC and TS seems to be related more to the soil moisture: the warmest regions are generally the driest with less cloudiness and higher TC, while moister locales exhibit cooler surface temperatures, larger CC and smaller TC. This correspondence is confused by two considerations, however. The average cloudiness in desert regions may be a combination of cirrus and dust storms detected as clouds, whereas the tropical rain forest surface properties may be distorted by persistent cloud contamination in the surface measurements (see Matthews and Rossow 1987).

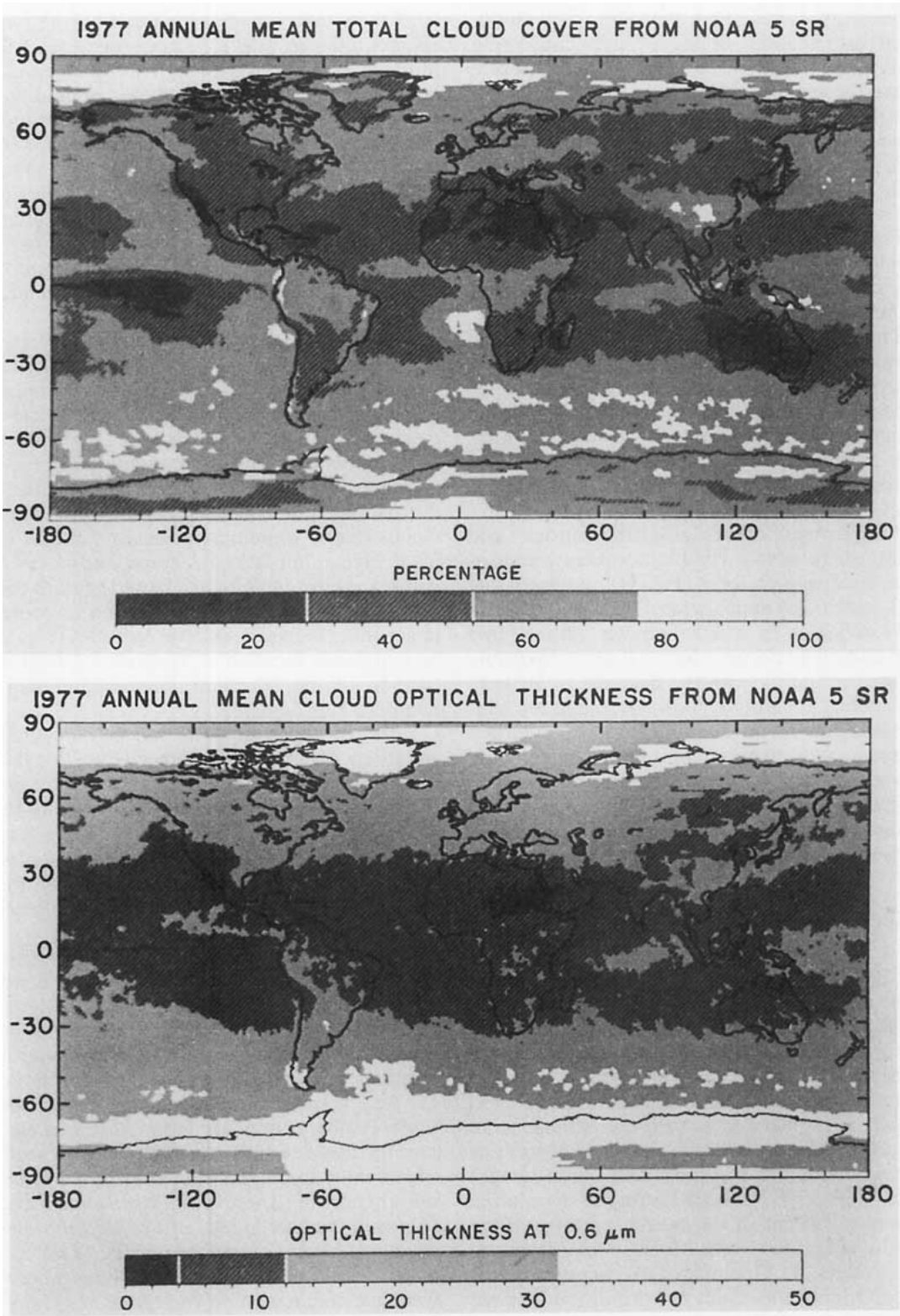

FIG. 2. Geographical distribution of annual mean cloud and surface properties: (a) total cloud cover, (b) cloud optical thickness, (c) surface reflectance, (d) cloud top altitude, (e) cloud top temperature and (f) surface temperature.

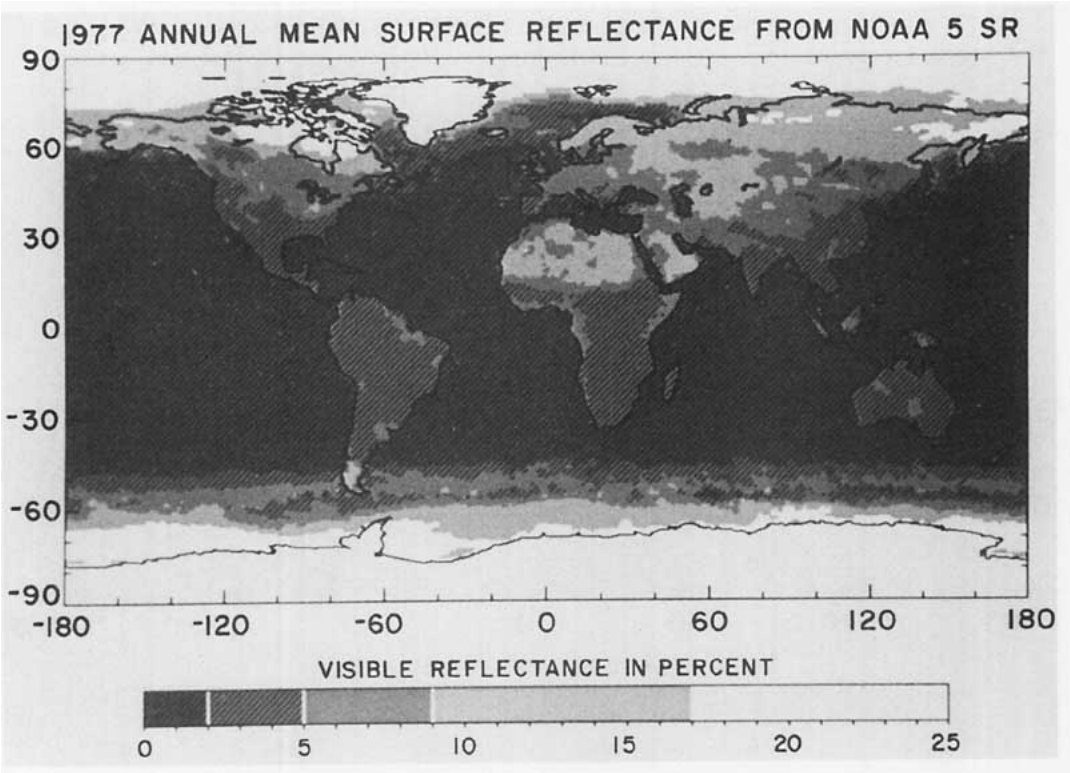

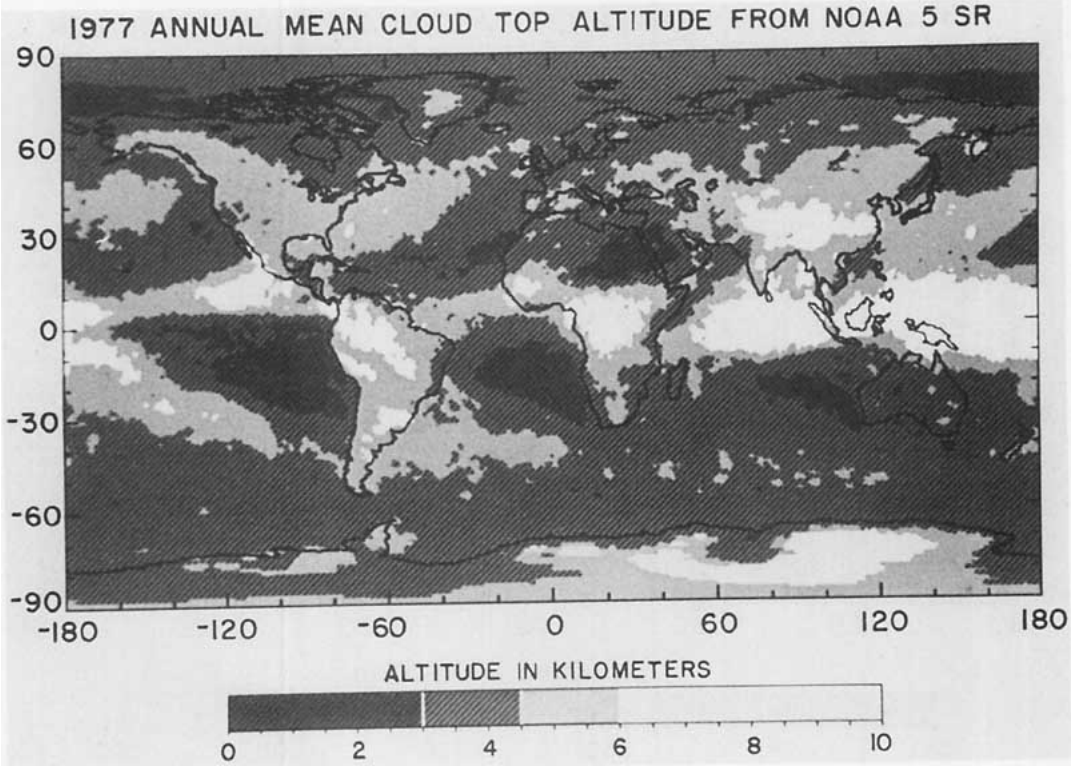

FIG. 2. (*Continued*)

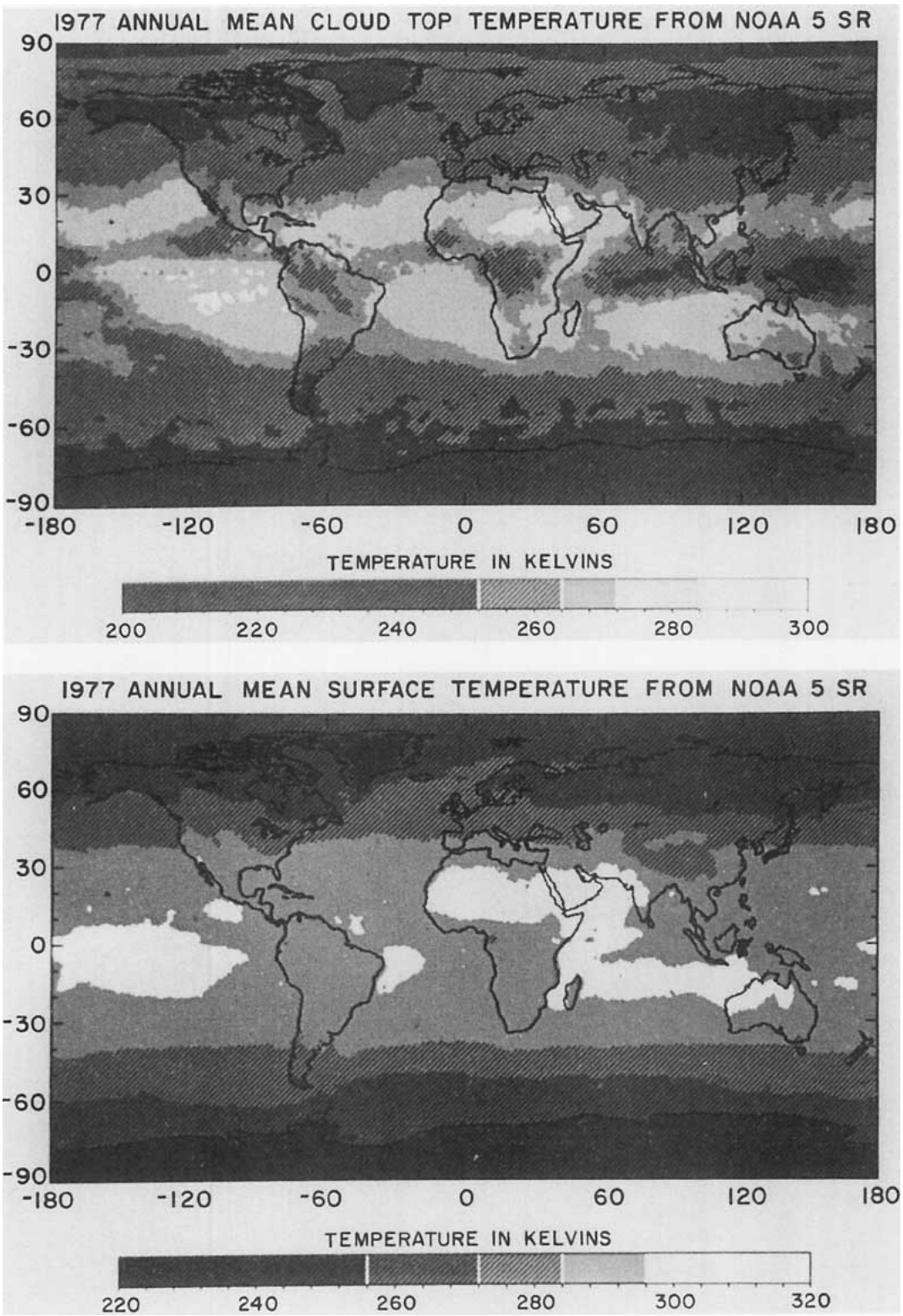

FIG. 2. (*Continued*)

TABLE 3. Seasonal deviations of the global and hemispheric averages of cloud and surface properties from their global annual mean values. The first number in each column is the global mean value (for annual) or deviation from the global annual mean (for each month); the numbers in parentheses are the Northern and Southern Hemispheric deviations from the global annual mean, respectively. Only the lowest 60° of latitude in each hemisphere are included.

Quantity	Annual mean	Jan	Apr	Jul	Oct
CC (%)	51.1 (−3.6/+3.6)	+4.0 (−5.0/+12.9)	−0.5 (−2.5/+1.5)	−2.0 (+0.1/−4.2)	−1.4 (−6.8/+4.0)
TAU	13.1 (−2.2/+2.2)	+0.7 (+2.3/−0.9)	−0.1 (−4.5/+4.2)	+1.4 (−4.1/+7.0)	−1.6 (−2.4/−0.9)
RS (%)	5 (+2/−2)	+1 (+5/−2)	0 (+1/−2)	+2 (0/+3)	0 (0/−1)
ZC (km)	4.6 (+0.2/−0.2)	0.0 (−0.1/0.0)	+0.2 (0.0/+0.4)	−0.1 (+0.4/−0.5)	−0.1 (+0.6/+0.7)
TC (K)	265.3 (−0.9/+0.9)	−0.9 (−4.0/+2.2)	−0.9 (−0.2/−1.7)	+1.5 (+2.8/+0.2)	+0.2 (−2.0/−2.5)
TS (K)	288.3 (−0.2/+0.2)	−0.6 (−6.7/+5.5)	+0.2 (+0.9/−0.5)	+0.6 (+4.4/−3.2)	−0.2 (+0.6/−1.0)

4) SUMMARY

The global annual distribution of cloud properties shows three key attributes. First, the large majority of clouds are distinctly different from the surface in both their visible reflectances and temperatures, except in the polar regions and brightest/hottest deserts: modal values of visible "albedo" are 5%–10% and 50%–70% for surface and clouds, respectively, while modal values of temperature are 270–290 K and 250–270 K, respectively. (This contrast in annual mean quantities is exaggerated by the threshold analysis and by linear averaging of asymmetric distributions but eliminating these effects does not change the qualitative relations.) This large contrast insures that satellite-based analyses will generally agree on most qualitative features of cloud cover distributions and seasonal variations. Specifically, the magnitude of regional variations in cloud and surface properties is much larger than the estimates of our measurement errors (Table 1). However, the large contrast also means that very small *regional* changes of cloud distributions can be significant to the climate (cf. Hansen et al. 1984), therefore, we cannot be reassured by the general resemblance of existing cloud climatologies and climate GCMs.

Second, the magnitude of cloud and surface property variations decreases rapidly as we average over larger spatial scales: variations within latitude zones are similar to variations from zone to zone and much larger than hemispheric differences. However, the hemispheric distributions of cloud and surface properties are not symmetric (see Fig. 12 in Ro89a); i.e., the global averages are sums of larger offsetting hemispheric variations but cannot be assumed to behave like random statistics.

Third, although the cloud variations of "albedo" and temperature generally increase regional contrasts in TOA radiation compared to those associated with the surface (cf. Sèze and Rossow 1990a), the variations of clouds can also serve to decrease some contrasts in radiation, as within latitude zones, or to enhance other contrasts, as with latitude. This already suggests that the precise radiative effect of a specific cloud variation is situation dependent.

b. Seasonal variations of cloud properties

1) GLOBAL AND HEMISPHERIC MEANS

Table 3 summarizes the seasonal variations of the global and hemispheric mean cloud and surface properties by showing their deviations from their global, annual mean values (these values actually represent averages over only the lower 60° of latitude in each hemisphere). The seasonal variations of cloud cover are also compared in Table 4 to those reported by Hughes and Henderson-Sellers (1985), Stowe et al. (1989), and two older climatologies.

The surface visible reflectance is relatively constant except for the effect of seasonal snow and sea ice changes (see Ro89b for more details): the Northern Hemispheric increase in winter is caused primarily by snow cover on land, while the Southern Hemispheric increase in winter is caused primarily by increased ocean reflectance at larger solar zenith angles. Sea ice only influences the global or hemispheric mean surface reflectance in the transition seasons (April and October).[2] The seasonal variation of surface temperature (see Ro89b for more details) also reflects the difference between the mostly-land-covered north and the mostly-ocean-covered south: the seasonal amplitude is about 3 K larger in the north than the south (however, with only 4 months of results, we cannot resolve any effect of a phase lag between the temperature cycles of the oceans in the two hemispheres).[3]

The global mean CC is a maximum in January and a minimum in July because the seasonal variation of CC in the Southern Hemisphere is larger than that in the north (17% versus 7%). Table 4 shows that all the climatologies agree that hemispheric mean CC is maximum in summer and minimum in winter but the dis-

[2] If the whole hemisphere is considered, varying illumination of the Arctic Basin/Greenland and Antarctica amplifies the surface reflectance increase from winter to summer; the latter causes a larger effect on the Southern Hemisphere mean reflectance than the former does for the Northern Hemisphere.

[3] The addition of the polar regions reduces this amplitude difference slightly.

TABLE 4. Annual and seasonal, global and hemispheric cloud amounts from several climatologies. Seasonal variations of global cloud amount are shown as deviations from the global annual mean for each climatology. Hemispheric cloud amounts (Northern/Southern) are given in parenthesis as deviations from the global annual mean values. NOAA-5 results are for ±60° latitude; values in square brackets are USAF results for ±60° latitude.

	Annual	Jan	Apr	Jul	Oct
NOAA-5 SR for 1977[1]	51.1 (−3.6/+3.6)	+4.0 (−5.0/+12.9)	−0.5 (−2.5/+1.5)	−2.0 (+0.1/−4.2)	−1.4 (−6.8/+4.0)
USAF 3-D NEPH for 1979[2]	[56.9 (−2.1/+2.1)]	[+0.9 (−4.0/+5.9)]	[−0.7 (−2.4/+1.1)]	[+0.3 (+2.7/−2.0)]	[−0.7 (−5.0/+3.6)]
	57.5 (−2.5/+2.5)	−0.5 (−4.5/+3.5)	−0.5 (−3.5/+2.5)	+1.0 (+1.5/+0.5)	−1.0 (−4.5/+2.5)
NIMBUS-7 for 1979[3]	53.5 (−1.5/+1.5)	−0.5 (−5.5/+4.5)	+0.5 (−1.5/+2.5)	−0.5 (+0.5/−1.5)	+0.5 (−0.5/+0.5)
London (1957)[4]	51.0 (0/0)	−1.0 (−3.0/+1.0)	+1.0 (0/+2.0)	−1.0 (+1.0/−3.0)	+1.0 (+2.0/0)
B&S (1980)[5]	60.5 (−1.5/+1.5)	+0.5 (−3.5/+4.5)	−0.5 (−2.5/+1.5)	0 (+1.5/−1.5)	+0.5 (−1.5/+2.5)

[1] Satellite-only for early morning conditions (this paper).
[2] Mixture of satellite and conventional observations, covering all diurnal phases (Hughes and Henderson-Sellers 1985).
[3] Satellite-only for noon and midnight conditions (Stowe et al. 1989).
[4] Conventional surface observations covering all diurnal phases in the Northern Hemisphere; results for the Southern Hemisphere are reflections of the northern cloud amounts from the corresponding season (London 1957).
[5] Mixture of satellite and conventional observations with unknown diurnal coverage (Berlyand and Strokina 1980).

agreements in the amplitudes of the opposing hemispheric cycles produce disagreements in the phase of the global variations of CC. Our result is caused, in part, by a large increase of cloud amount near 50°S in January, during the decay phase of an El Niño event, therefore, it may be peculiar to 1977.

TAU is largest in winter in both hemispheres but the combination of the two hemispheric variations produces an apparent semi-annual cycle in the global mean value that has a maximum during the solstices. The seasonal variation in hemispheric mean TAU offsets some of the cloud albedo variation caused by the changes in CC and reinforces the surface albedo seasonal variations.

Seasonal variation of ZC on a global and hemispheric mean basis is essentially negligible (but not regionally, as we shall see); hence, the predominant change in TC is associated with seasonal variations of air temperature at constant altitude and higher latitudes. The amplitude of TC seasonal variations is larger in the north by about 3 K (similar to TS) and acts to offset the radiative effect of CC variations and reinforce the surface temperature variations.

Figure 3 shows the seasonal phase relationships of the hemispheric averages of CC, TAU, ZC and TC with the surface temperature. That the hemispheric seasonal changes exhibit significant differences of both phase and amplitude is readily apparent even though there is a general qualitative resemblance of the seasonal changes. Because of the differences in phase and amplitude between the seasonal cycles of the two hemispheres, the seasonal correlations of globally averaged quantities are completely different. This figure also illustrates two other important conclusions. First, that the simplistic correlations of changes in TS and cloud radiative properties usually sought in such data depend on the space and time scales being considered. These results grow more complicated when examined at regional scales. This scale dependence may also imply that latitudinal and/or seasonal relations cannot be used as proxies for climate relations. Second, the complex differences in the relations of the three cloud properties to surface temperature and to each other (e.g., Fig. 3d) argue strongly against the validity of single parameter representations of cloud radiative feedbacks. For instance, Fig. 3a shows a tendency for mean cloud cover to increase with increasing temperature in both hemispheres; however, the tendency is reversed for globally averaged quantities. This conclusion is reinforced by the flux calculations presented in section 4.

2) ZONAL MEAN SEASONAL CYCLE

In the annual average, the zonal mean CC values are concentrated between 40%–70% and nearly symmetrically distributed about a mode at 50%–60%; however, this distribution is composed of a seasonal oscillation between a broader January distribution, which is skewed towards higher values, and a narrower July distribution that is nearly symmetric at about 50% (see Fig. 12 in Ro89a). The TAU and ZC distributions exhibit seasonal variations in the number of latitudes dominated by larger values. January is characterized by more of the moderate TAU values (20–40) at average ZC (4–5 km), while July shows a bimodal distribution of TAU associated with a small population of larger TAU, high ZC clouds that persists into October (associated with the Indian Monsoon). April and October show the broadest distributions of TAU and ZC with the largest zonal mean values occurring in April. The latitudinal variations of seasonal air temperature changes at constant altitude make the distribution of zonal mean TC values much broader than

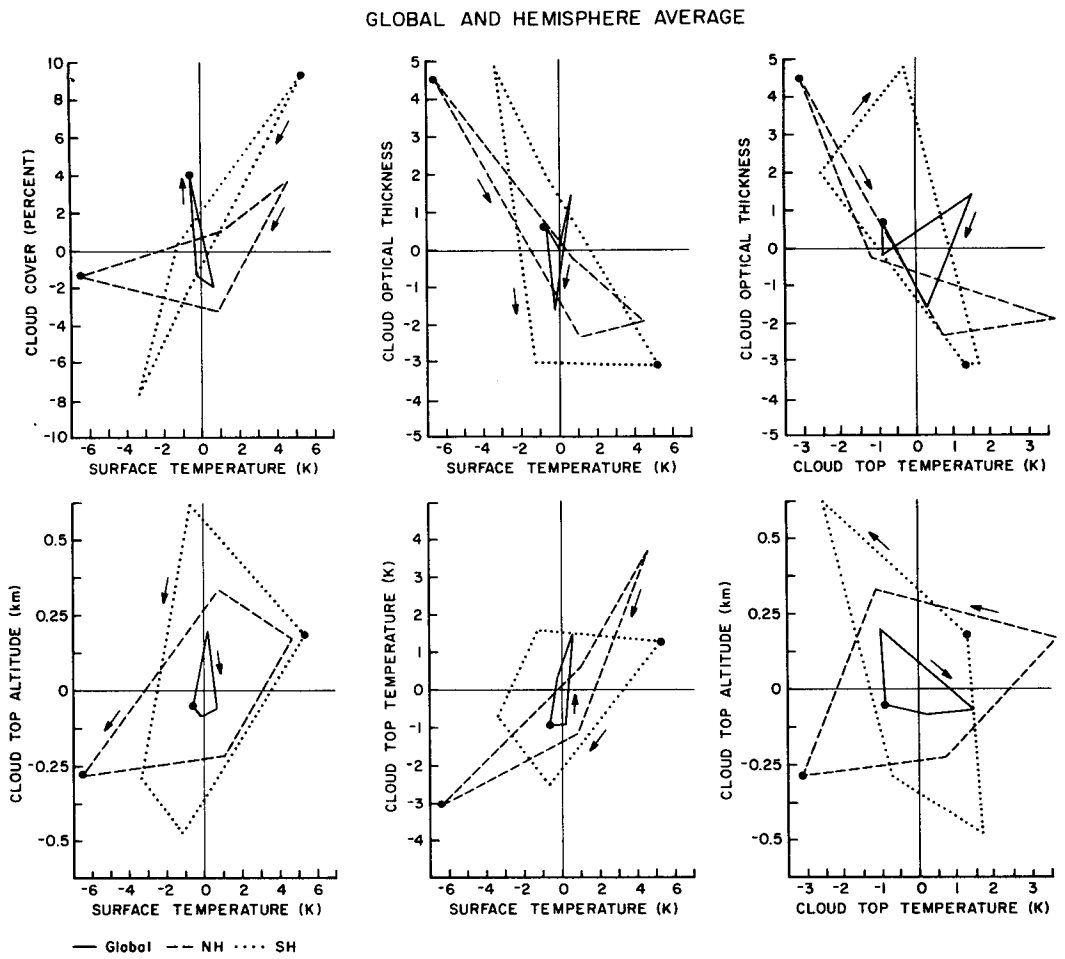

FIG. 3. Phase diagrams showing relations of seasonal variations of global (solid), Northern Hemisphere (dashed) and Southern Hemisphere (dotted) monthly averages: (top row, left to right) CC vs TS, TAU vs TS, and TC vs TS; and (bottom row, left to right) TAU vs TC, ZC vs TC, and ZC vs TS. Seasonal variations are expressed as deviations from the global annual mean values. Averages are for the lowest 60° in each hemisphere. The large dots indicate values for January and the arrows indicate the progression of time, with each month (April, July, and October) lying at a vertex.

that of ZC; however, variations in zonal mean TC are smaller than the corresponding variations in TS.

The simple hemispheric seasonal variations of CC are revealed to be composed of complicated regional variations in Fig. 4. The distinctive patterns of the seasonal changes in different climate zones are apparent in their zonal mean CC variations, which are compared to the range of values from several other climatologies in Fig. 5 (see also Fig. 11 in Ro89a). The Northern Hemisphere displays seasonal CC variations in midlatitudes caused by a latitudinal shift of an otherwise nearly constant CC band; in other words, the mean CC in the storm track zone does not vary by more than about 5%, but the mean latitude of the maximum CC shifts from near 40° in January to near 60° in July. However, the transition back to winter conditions is accompanied by a decrease in CC within the storm track zone during October (Hughes and Henderson-Sellers and Stowe et al. observe an increase in the storm track cloud amount in October 1979). The Southern Hemisphere, on the other hand, exhibits a seasonal oscillation of midlatitude CC with the opposite phase that does not appear to be associated with any shift in latitudinal position. The position of the storm track in the Southern Hemisphere is similar to that in the Northern Hemisphere in Summer. (Stowe et al. show a smaller amplitude variation in 1979.)

The seasonal variations of tropical cloudiness are composed of the oscillation of two maxima of CC with opposite phases although both hemispheric components also show some hint of shifting position in the zonal mean (also in Hughes and Henderson-Sellers 1985; Stowe et al. 1989). The magnitude of the tropical oscillation at a given latitude is about 15%–20% (Stowe et al. show a smaller variation of about 10%), whereas the midlatitude oscillations are only about 10%–15%.

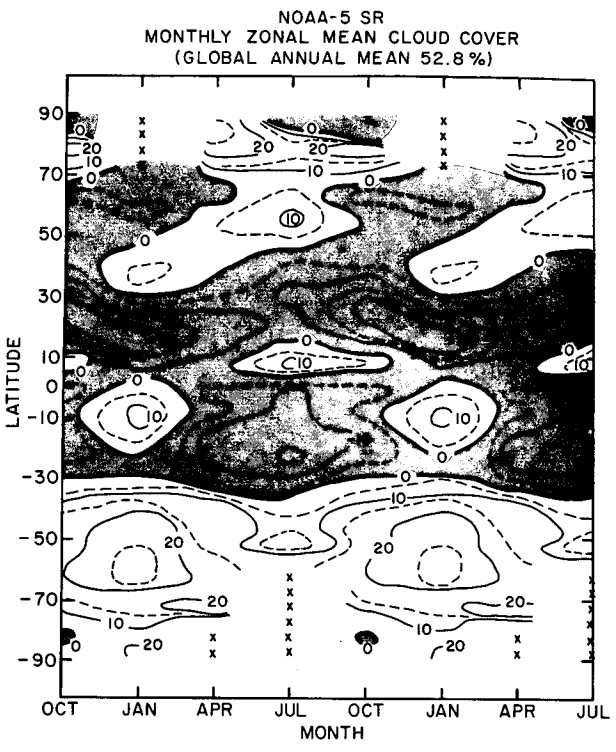

FIG. 4. Seasonal variations in the zonal mean cloud cover, expressed as deviations from the global, annual mean (over all observed latitudes). Note that only four months of data from one year are used to construct this figure, so that the variations can only be taken to be illustrative.

The zonal mean peak cloud cover shifts from about 10°N in July to 10°S in January, producing a double peak in the annual mean (Fig. 1a). Polar region cloudiness variations are incompletely resolved and probably not as reliable but the suggestion of a seasonal variation indicates lower CC in polar summer. Stowe et al. (1989) show lower CC in polar summer, but Hughes and Henderson-Sellers (1985) show the opposite for the same year.

The associated seasonal changes in cloud optical properties (Fig. 6) begin to suggest a dynamical influence on them. TAU at middle and high latitudes shows a general increase in Winter in both hemispheres associated with stronger storms; a similar, though weaker, variation is also apparent at low latitudes, associated with enhanced summer convection. The magnitude of the higher latitude variation is about twice the global, annual mean value of TAU and about 50%–75% of the zonal, annual mean value. The magnitude of the tropical variation is much smaller but still represents a relative variation comparable to the lower, local mean value.

The seasonal oscillation of TC is dominated by the seasonal cycle of air temperature at middle and high latitudes, whereas the tropical variations are caused almost entirely by ZC variations, as can be discerned by comparison of the seasonal variations exhibited in Figs. 6b and 6c. The variation of tropical ZC shows the actual latitudinal shift of the northern component of the ITCZ more clearly in contrast to the southern component which seems to vary in place; but ZC and TC are clearly associated with seasonal changes in the amount of deep convective activity. A weaker seasonal variation of midlatitude ZC values suggests slightly larger values associated with stronger winter storms.

3) LONGITUDINAL DISTRIBUTION OF SEASONAL CYCLES

Another view of these seasonal variations is provided in Fig. 7, which shows the variation of monthly mean CC as a function of longitude for a midlatitude and an equatorial zone. The northern midlatitudes exhibit a longitudinal variation of CC that is associated with the location of the continents. In Fig. 7a, the North Atlantic/Europe and western North Pacific are regions of relatively higher CC, while eastern North Pacific/North America and Asia are regions of lower CC. In the winter, the oceanic cloudy regions generally become more longitudinally extensive; however, this variation also involves an eastward shift in winter and a westward shift in summer. Longitudinal contrast in CC is a maximum in summer with larger CC over the oceans and smaller CC over land; in winter, CC is more nearly zonally uniform. These same features appear in the results of Hughes and Henderson-Sellers (1985) and Stowe et al. (1989).

When CC is averaged over the whole tropical zone, the contribution of the high CC values in the narrow ITCZ is reduced. Also the width of the zone, examined in Fig. 7b, reduces the effect of the seasonal shifts of the ITCZ on land and averages together the seasonal oscillations of the oceanic components. The combination of all these seasonal changes leads to a complicated pattern. The largest variation occurs in the eastern Indian Ocean and western Pacific: the Indian Monsoon peaks in July and October while CC reaches a minimum to the east. The winter Monsoon produces more generally extensive cloudiness over the region starting in October. The eastern Atlantic/Africa complex forms a similar pair of high/low CC regions: the high CC region on the west coast of tropical Africa shows an oscillation of almost 20% from a maximum in January, while the low CC region in the eastern part of Africa shows a smaller and opposite oscillation. The seasonal shifts of the ITCZ in South America produce a double maxima pattern, with the January CC being higher than July. However, over the eastern Pacific CC is larger in July and October, opposite to the variations in the central and western Pacific. Looked at as a whole, the tropical Pacific has four parts: in January and April high CC is found from 100° to 140°E and 160° to 140°W, whereas in July and October high CC is found from 160° to 180°E and 120° to 80°W. Similar features

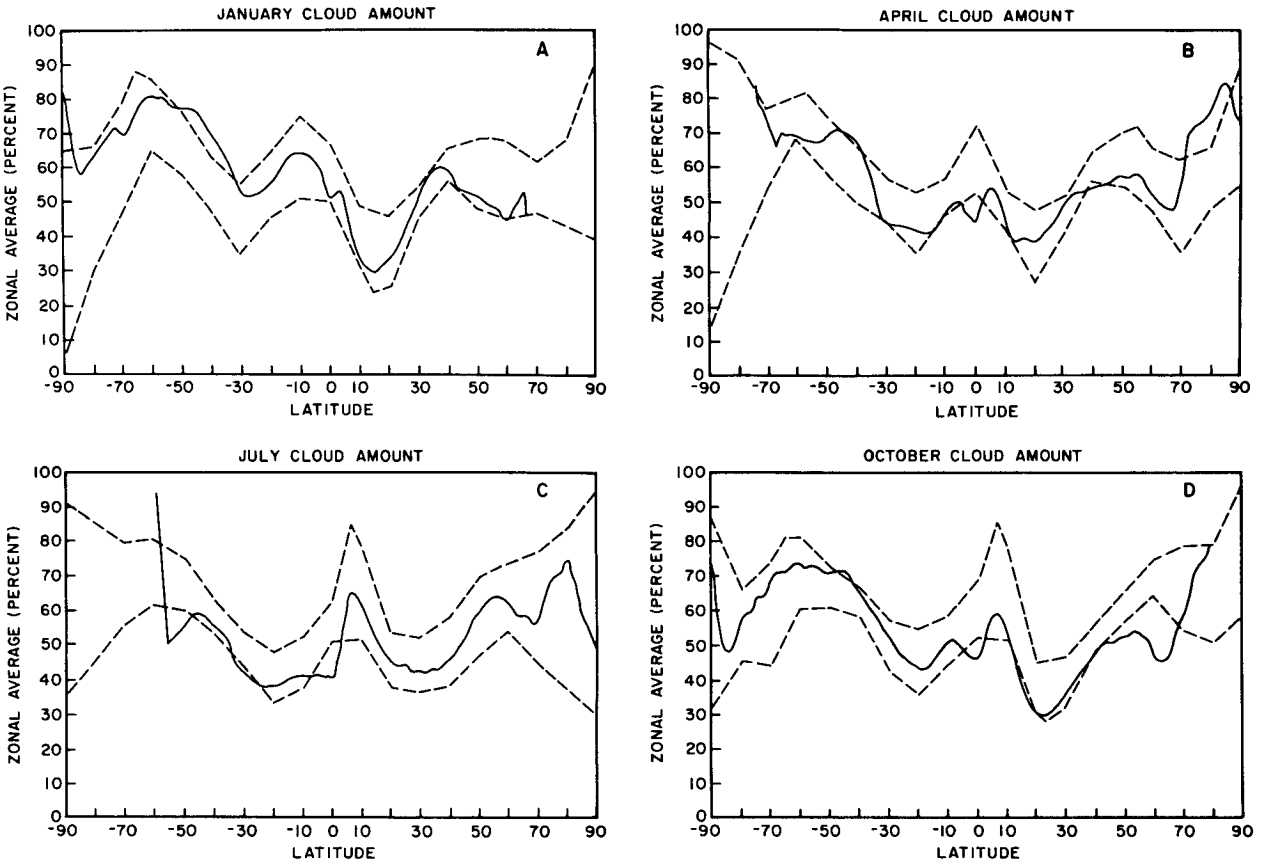

FIG. 5. Zonal mean cloud amounts for January, April, July and October 1977 from NOAA-5 analysis compared to the range of other climatologies: London (1957), Berlyand and Strokina (1980), Hughes and Henderson-Sellers (1985) and Stowe et al. (1989). The dashed lines represent the largest and smallest zonal mean value at each latitude from among these climatologies.

can be seen in the results of Hughes and Henderson-Sellers (1985) and Stowe et al. (1989).

Longitudinal contrasts are as extreme in the tropics as at midlatitudes and also seem to be controlled by the locations of the continents, although in the much larger extent of the Pacific Ocean, almost as much structure is apparent as at land–sea longitudes. Longitudinal contrasts are smaller in southern midlatitudes (not shown). The magnitude of the seasonal variations in the tropics is also comparable to that in midlatitudes. The key conclusion is that the seasonal variations in CC in both latitude and longitude are roughly comparable in magnitude, about 15%–30%.

4) REGIONAL SEASONAL CYCLES

Figure 8 shows the relations of seasonal variations of clouds and surface temperature for several specific climate regimes, namely, 1) the tropics as represented by three segments of the ITCZ over the maritime continent in the western Pacific, Africa and South America, and the Monsoon regions over Southeast Asia and India, 2) the subtropics as represented by the Himalayas, the deserts (North Africa and Australia) and the marine stratus regions off the west coasts of North America and South America, and 3) the midlatitudes as represented by the oceanic storm tracks (off the east coasts of North America and Asia and in the "Roaring 40's" in the Southern Hemisphere) and the associated continental regions in the Northern Hemisphere (North America, Europe, and Central Asia). These results clearly reveal the variability of the seasonal variation patterns among and within the climate regimes.

The ITCZ is characterized by a nearly constant TS over the year (Fig. 8a) but exhibits both shifting positions and variations of cloud properties. CC variations over Africa and South America are very different: CC over Africa is nearly constant at about 60%, whereas CC over South America oscillates between 30% and 75%. The Africa results are averaged over the ±10° at the equator; thus, the CC is constant because this region includes much of the ITCZ as it shifts location. The South America results are averaged only over the land, which is primarily south of the equator (0°–20°S); thus, the larger seasonal shift in location of this part of the ITCZ appears as a large amplitude oscillation

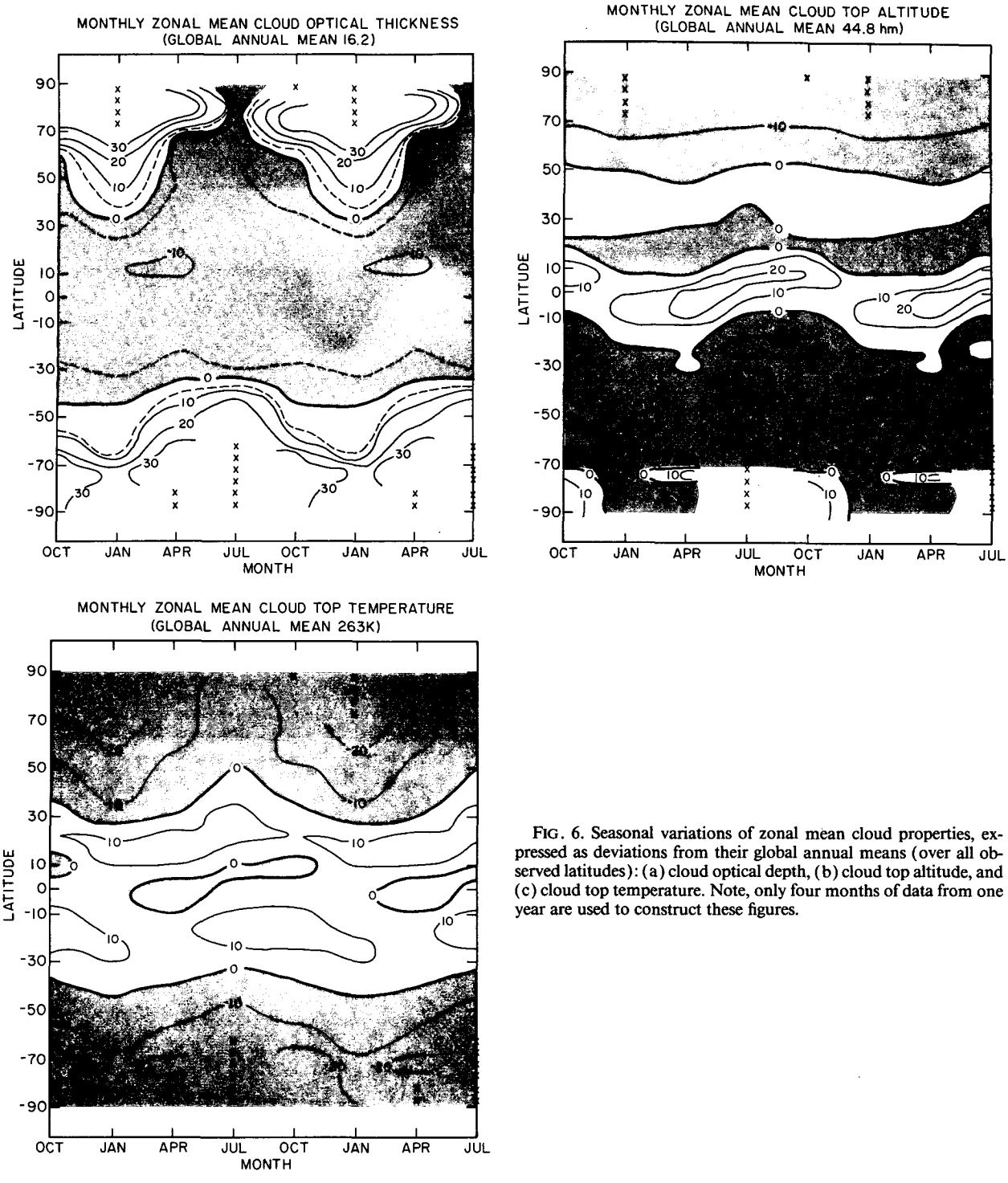

FIG. 6. Seasonal variations of zonal mean cloud properties, expressed as deviations from their global annual means (over all observed latitudes): (a) cloud optical depth, (b) cloud top altitude, and (c) cloud top temperature. Note, only four months of data from one year are used to construct these figures.

in CC. The western Pacific portion of the ITCZ (averaged over ±20° latitude at the equator) exhibits a real oscillation of about 20% in CC but with a different seasonal phase than tropical Africa. The season of decreasing CC coincides with the onset of the stronger Indian monsoon to the west, whereas the season of increasing CC is associated with the winter monsoon in Southeast Asia (Fig. 8b). The values of TAU and TC are nearly constant over the ocean ITCZ represented by the Indonesian sector but both land segments show strong seasonal variations in TC. TC variations are clearly caused by variations in ZC. Although the

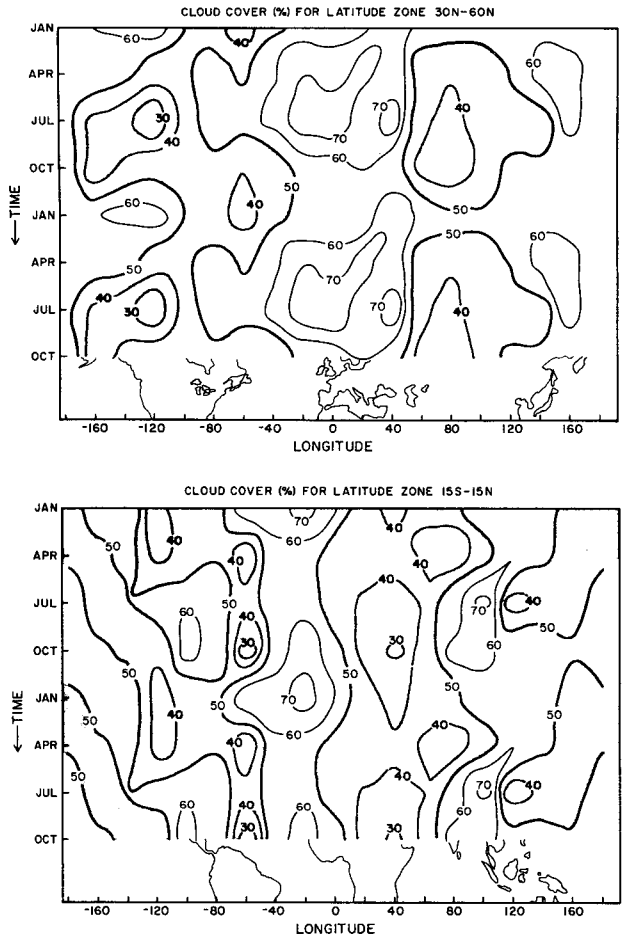

FIG. 7. Variation of monthly mean total cloud cover as a function of longitude for (a) a midlatitude zone and (b) an equatorial zone. The location of land masses is sketched at the bottom. (See note in caption to Fig. 6.)

behavior of ZC over South America may be explained by the shifting of the ITCZ in and out of the region, this explanation does not account for the behavior over Africa. The convection over the drier portions of tropical Africa north of the equator (July) seems to be less intense in 1977 than over the wetter portions south of the equator (January), producing smaller values of ZC and TAU in July than January. Figure 8a also illustrates that the seasonal variations of TAU and TC in the ITCZ are anticorrelated; i.e., albedo changes offset thermal cooling changes.

The monsoon regions (Fig. 8b) are characterized by much larger TS seasonal variations than the ITCZ but a simple seasonal oscillation is not apparent (this may be due, in part, to cloud contamination of TS at the height of the monsoons). The cloud variations associated with the Indian monsoon are very large: CC varies by more than 60%, TAU varies by a factor of two, ZC varies by almost four kilometers, and TC varies by almost 20 K. The TAU and TC variations over India are similar to those in the tropics with offsetting effects on solar and thermal fluxes. The Southeast Asian cloudiness shows a much smaller variation in CC, but exhibits similar variations in TAU, ZC, and TC. In addition, the Southeast Asian region goes through a winter (January) monsoon, semiannual increases in CC and TAU, but with no alteration of ZC and TC at the same time. This produces a more complex radiative feedback in this region that is not simply related to surface temperature. As with the ITCZ, the variations in TC for the monsoon clouds are caused by ZC variations, which contrasts with the Himalayan clouds (Fig. 8c), where TC varies much more than can be explained by ZC variations alone, but less than TS varies. The Himalayan clouds do not exhibit any behavior that appears strongly correlated with the monsoons, except for some increase in ZC that coincides with the intrusion of some of the Indian monsoon into the region. The Himalayan cloudiness also displays CC variations that are almost 90° out of phase with TS variations and TAU-TC changes that have large phase differences.

The deserts undergo a substantial seasonal cycle in TS, as shown in Fig. 8d. CC is generally lower in (local) Summer by 10%–20%. TAU is relatively constant but ZC varies by almost one kilometer. Over the Sahara, both of these parameters are averaged over two distinct cloud types: one with low TAU and high ZC (cirrus) and one with low TAU and low ZC. The latter type often exhibits TC $\geq$ 300 K, suggesting that these clouds are actually dust storms. Over Australia, the cloudiness is composed of cirrus and some midlatitude synoptic cloud types in winter, which may explain the different characteristic seasonal cycles in Australia. TC values vary more strongly than can be explained by ZC variations alone; the roles of ZC and air temperature variations seem comparable in these two regions.

At approximately the same latitude as the land deserts are located the marine stratus cloud regimes off the west coasts of all the continents. These oceanic regions show little TS variation, as expected; however, the recovery from the 1977 El Niño event may have exaggerated the seasonal temperature variations near South America (Fig. 8e). This suggestion is reinforced by examination of the seasonal variation of the marine stratus off the west coast of southern Africa (not shown), which exhibits TS variations that are more similar to the California stratus, but of opposite phase. The normal seasonal variation of these stratus seems to be higher CC in spring and summer but lower TAU and ZC in summer. TC variation is influenced by both ZC and air temperature changes acting together.

The midlatitude oceanic storm track regions exhibit a significant seasonal variation in TS of about 10 K but very different phases of seasonal cloud cover variation (Fig. 8f): the North and South Atlantic seem to vary with the same phase, showing a maximum in northern winter, while the north Pacific varies with the opposite phase. However, this result may be dependent

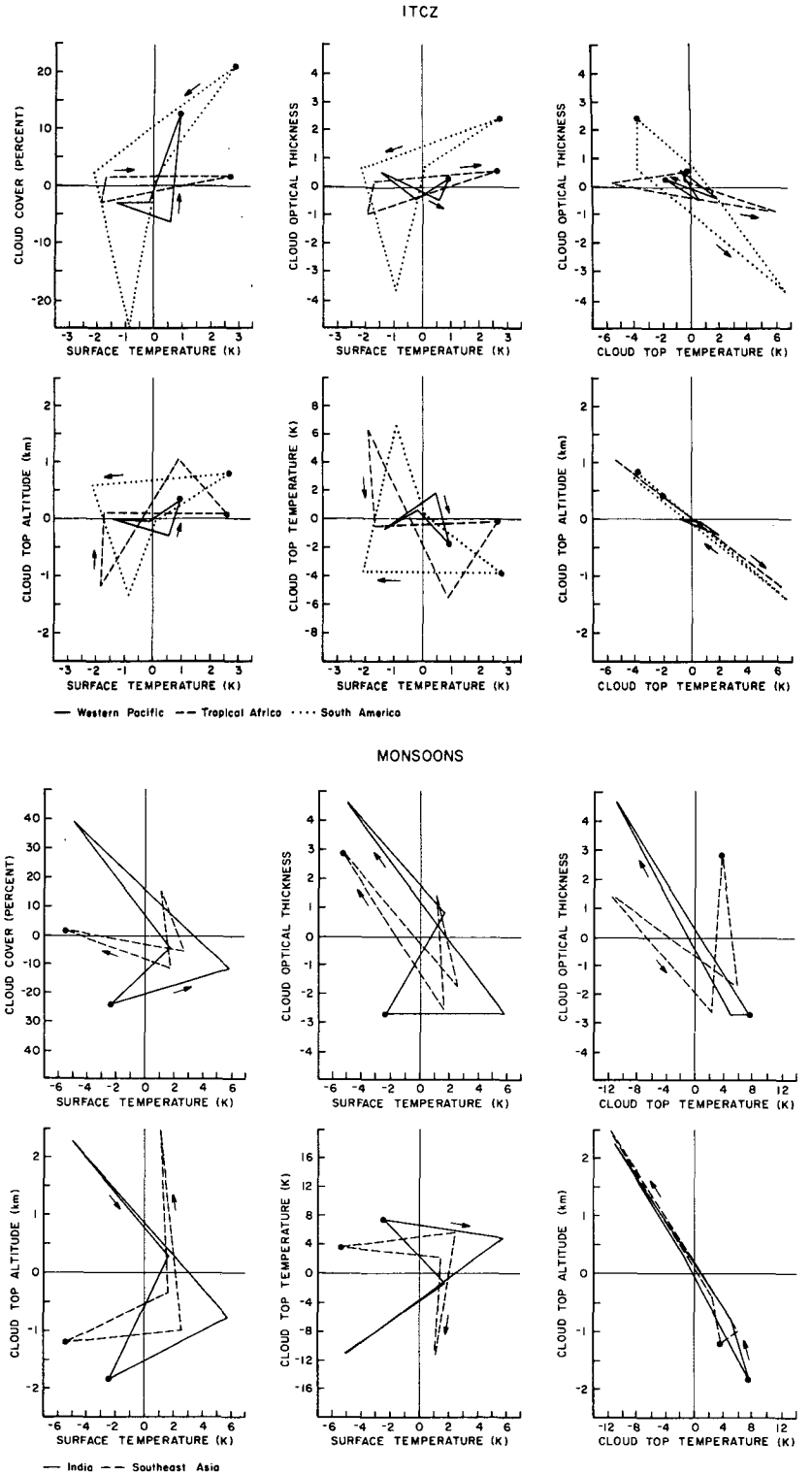

FIG. 8. Seasonal phase diagrams for several specific climate regimes (see caption to Fig. 3): (a) three segments of the ITCZ over the maritime continent in the western Pacific, Africa, and South America, (b) the Monsoon regions over India and Southeast Asia, (c) the Himalayas), (d) subtropical deserts, (e) subtropical oceans in the marine stratus regions off the west coasts of North America and South America, (f) midlatitude oceanic storm tracks off the east coasts of North America and Asia and in the "Roaring 40s" in the Southern Hemisphere and (g) northern midlatitude continental regions in North America, Europe, and central Asia. The large dots indicate values for January and the arrows indicate the progression of time.

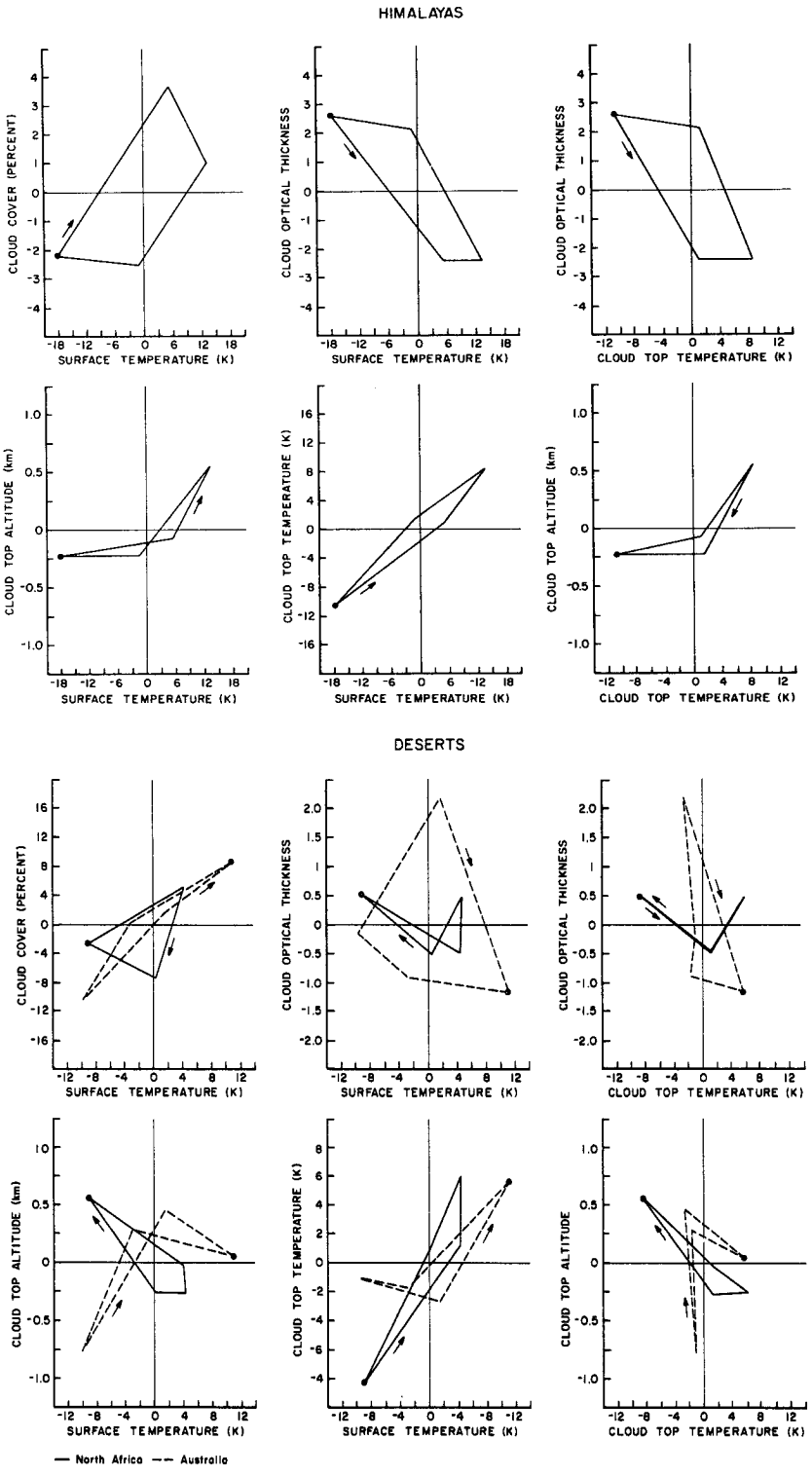

FIG. 8. (*Continued*)

on the precise definition of the regions. The seasonal variation of cloud properties generally shows increasing TAU and ZC with decreasing TS, though the correspondence is not perfect; TC variations correlate more strongly with TS (and air temperature) variations and less with ZC variations than at lower latitudes. The

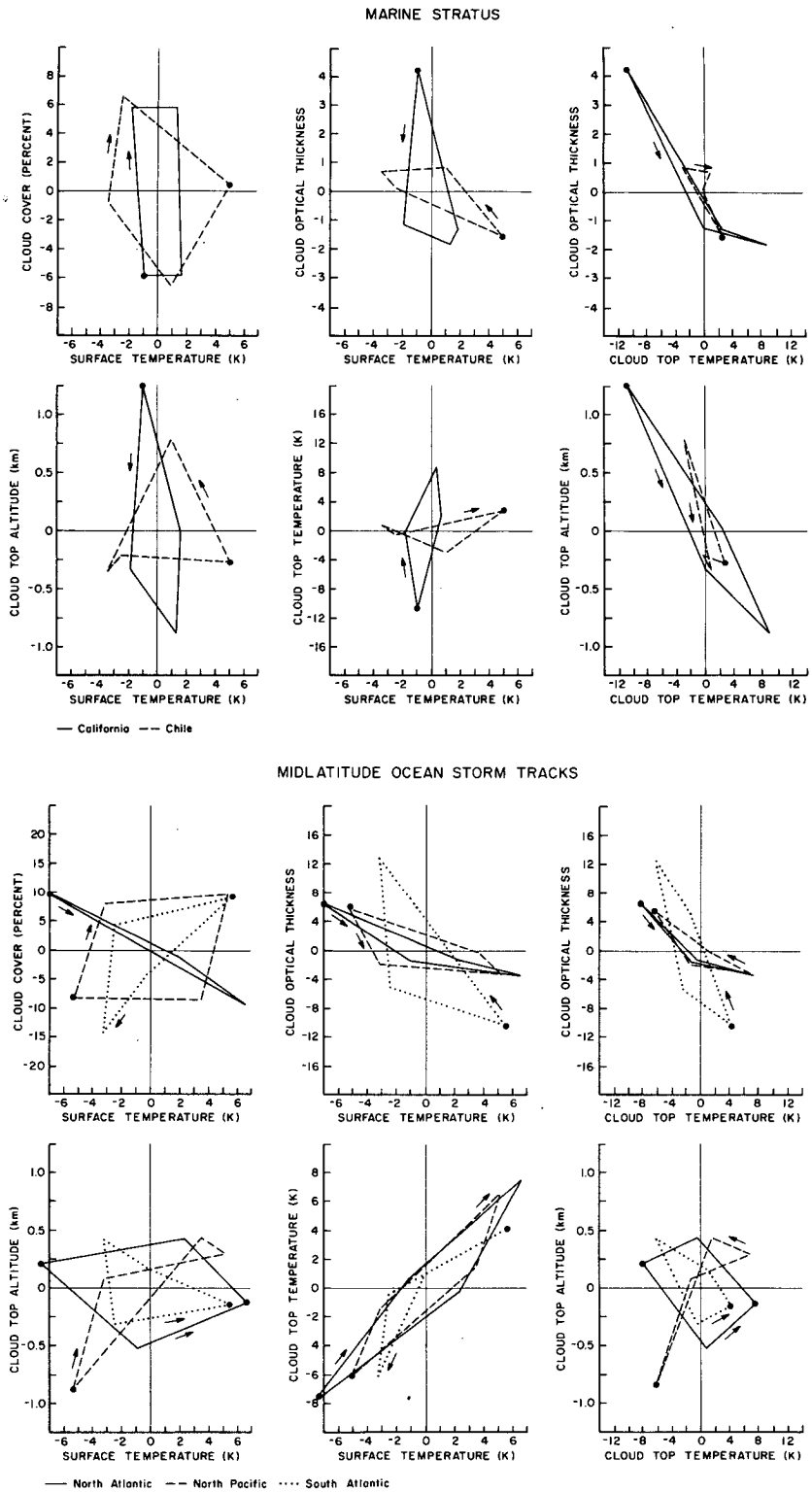

FIG. 8. (*Continued*)

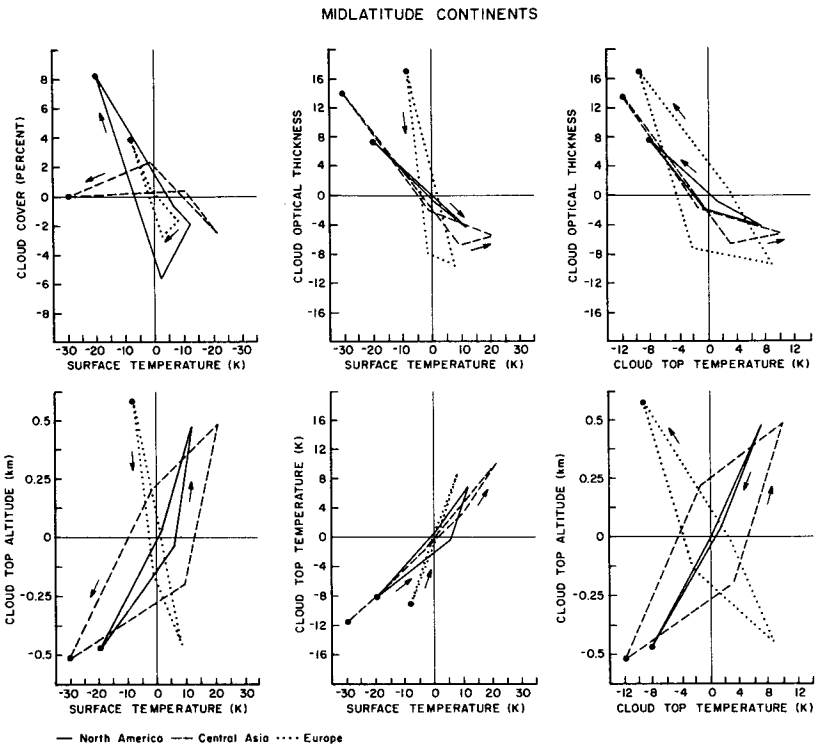

FIG. 8. (*Continued*)

more open shapes of the curves in Fig. 8f may suggest significant phase lags of the seasonal cycle with respect to the sun. Although the TAU-TC variations imply offsetting radiative effects, the amplitudes and phases vary among the ocean basins.

The corresponding midlatitude continental areas in the Northern Hemisphere are characterized by much larger seasonal variations in TS of about 30 K, with central Asia being the most extreme (Fig. 8g). Although CC shows little seasonal variation, both TAU and ZC vary significantly: TAU increases and ZC decreases with decreasing TS. Europe, however, shows the opposite phase in ZC variations that resemble the variations in the North Atlantic closely (Fig. 8f). Unlike the other regions shown in Fig. 8, the ZC and air temperature variations in central Asia and North America oppose each other in determining TC but the air temperature variations completely dominate, making Europe resemble the other two areas in spite of its opposite ZC variations. The amplitude of the seasonal variation in TC is smaller than that of TS, except in Europe.

These general remarks only serve to highlight some of the more noticeable features of the seasonal cloud variations; many of these features are well known, at least qualitatively, from surface meteorological observations. Both Hughes and Henderson-Sellers (1985) and Stowe et al. (1989) highlight some similar features of the geographic complexity of the seasonal variations of cloud cover; Stowe et al. (1989) also discuss seasonal variations of the zonal mean cloud top temperatures. Our results complement and extend their results by including a radiatively complete set of cloud parameters (similar to the study of Minnis and Harrison 1984a,b,c). Comparison of the patterns in Figs. 3 and 8 reinforces the conclusion that the simplicity of seasonal relationships among globally or hemispherically averaged quantities may be highly misleading since they represent the sum of a complex of regional changes with widely varying amplitude-phase relations. If the decaying El Niño "explains" the differences between the marine stratus regions, then this suggests a more subtle way to alter cloud-radiative feedbacks by changing the variation amplitudes and phases in certain regions. Since the global and hemispheric seasonal amplitudes are so much smaller than the regional seasonal amplitudes, indicating a significant cancellation, changes in behavior in a few regions may be sufficient to alter the apparent global mean cloud feedbacks on the seasonal cycle. This situation calls for caution in interpreting limited datasets.

c. *Cloud types*

Conventional ground-based observations of clouds include a classification of clouds by morphology and estimated *base* height above the local terrain (e.g., Warren et al. 1986, 1988). The morphological classes allow for detailed distinctions to be drawn primarily

among convective cloud forms (e.g., Scorer 1972) that are indicative of variations in the dynamic regime in which the cloud is forming. This classification scheme has proved very useful for forecasting of local weather and has been extended, in a qualitative way, to the use of satellite images in weather forecasts on meso- to synoptic scales. Some attempts have been made to identify the classical cloud morphological types in satellite images (Parikh and Ball 1980; Desbois and Sèze 1984; Garand 1988).

Classification of clouds by dynamic regime is valuable but there are other reasons for classification. In particular, classification of clouds according to their effect on the Earth's radiation budget is important to climate studies. This is also the simplest cloud classification scheme for satellite observations since the measured radiances are related to the full radiative fluxes. In this section, we examine a very simple classification scheme: the division of clouds by their top height and/or optical thickness (cf., Minnis and Harrison 1984a; Desbois and Sèze 1984; Stowe et al. 1988).

1) Low, middle, and high clouds

The conventional cloud classification by base height above local terrain has the advantage, when forming averages, of mixing dynamically similar clouds, at least with respect to their location in or out of the boundary layer. The disadvantage is that clouds with very different temperatures may be combined in an average because "low" clouds over high terrain are radiatively equivalent to "middle" clouds over low terrain. Another notable example is the inclusion of cumulo-nimbus clouds (deep convection) with "low" clouds, where from the satellite view they are "high" clouds. If no averaging over latitude or longitude is performed, then the differences in classification by vertical location are not critical. In our case, we lack an accurate specification of surface pressure, but the temperature profiles from the NMC analyses do provide a reasonable estimate of location above mean sea level (as they were intended to do). Therefore, we first classify clouds by their *top* height above mean sea level. To approximate the conventional classification of *base* heights, we add 1 km to the usual definitions: low clouds are those with tops ≤ 3 km, middle clouds have tops $3 < ZC \leq 6$ km, and high clouds have $ZC > 6$ km. Unlike the conventional definitions of low, middle, and high clouds, our definition is the same for all latitudes to preserve uniformity in the statistics. (Note that Stowe et al. (1989) use the conventional definitions that vary with latitude.)

Figure 9 shows the annual, zonal mean CC for total, low, middle, and high clouds. The four major climate zones are characterized by different vertical distributions of total CC. The tropics are covered predominantly by high clouds, the subtropics by low clouds, and midlatitudes are covered by low and middle clouds.

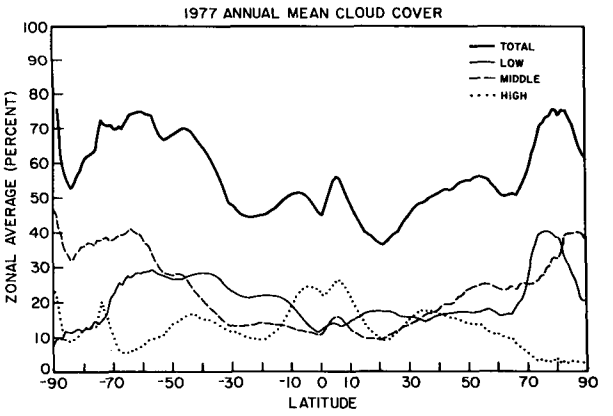

FIG. 9. Annual, zonal mean CC for total, low, middle, and high clouds (see Table 5).

The two polar regions appear to differ: the north polar region is covered by low and middle clouds, while the south polar region is covered predominantly by middle clouds. However, this apparent difference is simply the consequence of the difference in topographic height of the two polar surfaces; i.e., "low" clouds cannot exist over Antarctica. The only large seasonal shifts in the vertical distribution of cloud amount occur in the tropics and in midlatitudes. In the vicinity of the ITCZ, the distribution switches from "tropical" to "subtropical"; i.e., the distribution shifts downward in the "winter" or dry season. This change is associated with the seasonal variation in the location of the ITCZ. In midlatitudes, middle level cloud cover decreases in summer over land, while the oceanic cloud distribution remains essentially unchanged.

This interpretation of the results must be modified by two considerations. First, the satellite viewpoint limits the measurement of middle and low cloud cover to estimates of lower limits. This limitation is most severe where high cloud cover is large; hence, the estimates of low cloud cover are most uncertain in the tropics and most certain in the subtropics. Second, our correction of ZC and TC values for optically thin clouds only works when no other clouds lie below the thin cloud. When other clouds lie below, the thin cloud appears to be optically thicker to the satellite so that the correction is underestimated. This has the effect of underestimating high and overestimating middle or low cloud cover; the effect on middle cloud cover depends on the detailed vertical distribution and optical properties of the clouds that are actually present. Limits on the CC at each level can be estimated from the values of CC in adjacent levels:

$$\text{low CC} \leq \text{"real" low CC} \leq \text{total CC - thin high CC}$$

$$\text{thin mid CC} \leq \text{"real" mid CC}$$

$$\leqslant \text{total CC} - \text{thin high CC}$$

$$\text{high CC} \leqslant \text{"real" high CC} \leqslant \text{high CC} + \text{mid CC}$$

The limits on low CC include the possibility that all upper level clouds, except the thin ones, can be underlain by low clouds (this is the so-called maximum overlap assumption). The limits on high CC include the possibility that all middle clouds are composed of high thin and low clouds. Limits on middle level clouds include both of these possibilities. The analysis of Tian and Curry (1989) reaches two key conclusions for a limited part of the globe: that maximum overlap appears correct for cloudiness in adjacent layers and that less than half of cloud systems are composed of two or more layers. Both of these conclusions, if generally true, would imply a reduction of the estimated ranges of middle and low cloud cover. Based on the actually observed amounts of each cloud type and the Tian and Curry (1989) conclusions, we estimate that global mean cloud cover in each category is 15%–40% (low), 10%–40% (middle), and 15%–35% (high).

Table 5 compares our (1977) zonal mean amounts (as observed) of low, middle and high cloudiness for January and July in the Northern Hemisphere to values reported by Henderson-Sellers (1986) from the USAF 3-D Nephanalysis for 1979, by London (1957) from surface observations climatology (SOBS), by Stowe et al. (1989) from Nimbus-7 for 1979–80, for high clouds in 1972–75 by Barton (1983) from Nimbus-5 and for high clouds in 1979–81 by Woodbury and McCormick (1986) from SAGE. The Nimbus-5 and -7 results are based on downward-looking satellite data and suffer the same interpretive limitations as we do. The USAF results combine surface and aircraft observations with satellite data; the height categories are the same as used for surface observations in the tropics and are constant with latitude. The surface observations suffer a similar limitation as satellites with the role of low and high cloudiness reversed. The results from SAGE use radiometer measurements looking horizontally through the atmosphere and are not subject to the same interpretation limits for high clouds as other satellites. All of these results are obtained with different overlap assumptions, in addition to varying definitions of the height categories. There is some qualitative agreement: 1) a relatively uniform latitudinal distribution of low

TABLE 5. Comparison of zonal mean, low, middle and high cloud amounts for January and July for the Northern Hemisphere from the NOAA-5 results for 1977, from the USAF 3-D Nephanalysis results for 1979 (Henderson-Sellers 1986), from London's surface observation climatology (London 1957), from Nimbus-7 results for 1979/80 (Stowe et al. 1989), from the Nimbus-5 results for high clouds in 1972–75, (Barton 1983) and from SAGE for high clouds in 1979–81 (Woodbury and McCormick 1986). Values in parentheses are replicated values from lower latitudes for the winter pole, that were not observed in the NOAA-5 results.

		Latitude band (deg)									
		0–10	10–20	20–30	30–40	40–50	50–60	60–70	70–80	80–90	NH
Low (Jan)	1977	16	18	17	15	15	12	19	(19)	(19)	16
	1979/80	9	8	9	11	11	9	5	4	1	9
	1979	82	26	30	38	38	33	24	25	20	40
	SOBS	23	18	20	25	30	31	28	22	19	24
Low (Jul)	1977	12	16	19	18	19	20	26	36	28	19
	1979/80	10	10	10	8	9	11	15	20	10	11
	1979	23	52	36	31	32	46	49	34	17	37
	SOBS	27	25	23	22	30	34	34	35	33	27
Mid (Jan)	1977	13	9	15	22	24	25	22	(22)	(22)	18
	1979/80	10	14	21	33	35	31	20	11	4	22
	1979	24	14	19	30	38	39	35	36	65	28
	SOBS	14	9	11	17	24	28	25	19	17	17
Mid (Jul)	1977	15	12	10	11	17	25	24	26	29	16
	1979/80	35	28	22	22	26	32	29	24	26	27
	1979	37	34	24	25	33	42	40	25	21	32
	SOBS	16	13	10	12	18	23	25	26	24	16
High (Jan)	1977	16	8	13	20	14	10	10	(10)	(10)	13
	1979/80	13	3	6	12	11	13	24	41	70	13
	1979	7	5	8	16	16	17	14	5	1	11
	SOBS	19	13	14	17	20	21	18	13	10	17
	1972–75	25	10	12	21	13	10	—	—	—	16
	1979–81	43	25	14	34	41	36	—	—	—	32
High (Jul)	1977	27	23	14	14	15	18	10	5	5	17
	1979/80	21	18	11	11	12	12	14	14	15	15
	1979	16	16	10	11	14	17	4	3	1	12
	SOBS	23	20	16	14	18	22	26	30	25	20
	1972–75	30	27	13	15	19	18	13	6	—	20
	1979–81	57	54	37	39	53	56	56	32	—	49

cloudiness in winter changes to a distribution increasing with latitude in summer, where the cover is less variable with season at low latitudes, 2) an increasing middle cloud cover with latitude with little seasonal variation, and 3) a relative minimum in high cloudiness in the subtropics. Significant disagreements occur in the tropics and polar regions.

As noted, the satellite viewpoint is best for ascertaining high cloud cover (classified by cloud top altitude, whereas surface observations are not only limited by low cloud obscuration but classify clouds by cloud base heights); however, analysis of downward-looking IR radiometer data can mistake optically thin clouds as warmer, lower level clouds. By using the VIS reflectances to measure optical thickness, we have attempted to correct for this effect for *isolated* thin clouds; however, our TAU threshold also causes us to miss some of these thinner clouds, producing similar results to those obtained from Nimbus-5 and -7 (Table 5). Moreover, surface observations suggest that cirrus clouds occur frequently in association with other lower level clouds (Warren et al. 1986, 1988), limiting this type of correction. Multispectral satellite data can be used to detect cloud altitude more directly; one such analysis (Wylie and Menzel 1989) over the continental United States indicates the presence of 10%–15% more high cloudiness than found in our analysis. Scanning the Earth's atmosphere with a horizontal view rather than a vertical view, such as done by SAGE instruments on Nimbus-7, also detects high cloudiness directly (Woodbury and McCormick 1986) and also indicates 10%–15% more high cloud cover than we obtain (although the coarse horizontal resolution of these data may overestimate cloud cover somewhat).

Figure 10 illustrates the distribution of the properties of low, middle, and high clouds by showing histograms of CC and TAU for four climate zones in each hemisphere: tropics (0°–15°), subtropics (15°–30°), midlatitudes (30°–60°) and polar regions (60°–90°). As shown in Fig. 9, the tropics generally have more high clouds whereas the subtropics are dominated by low clouds; however, the Southern Hemisphere tropics and subtropics have more low clouds than the Northern Hemisphere, associated with a larger proportion of ocean. Midlatitudes and the polar regions are dominated by low and middle clouds with southern midlatitudes having relatively more low clouds and southern polar regions relatively less low clouds than the Northern Hemisphere, again associated with the proportion of ocean and high topography in these zones.

All cloud types seem to be optically thicker in the Southern Hemisphere than in the Northern Hemisphere and thicker at higher latitudes than at lower latitudes. (The much higher values of TAU in the polar regions may be incorrect, because of the multivalued solutions encountered when retrieving TAU values over high reflectance surfaces, as discussed in Ro89a. The actual values may be ≤ 10 or a mix of small and large values.) Attempts to correlate TAU with humidity or temperature when climate changes (Wang et al. 1981; Somerville and Remer 1984) are frustrated by these opposing relations: the Southern Hemisphere, being mostly ocean may be more humid, but higher latitudes are colder and less humid than lower latitudes. The seasonal variations, discussed in section 3B, also confound such simple relationships. Moreover, the annual mean TAU distributions in Fig. 10 show a general increase from low to high clouds; however, this result could be interpreted to mean that higher clouds tops are more usually associated with deeper cloud systems.

The TC variations of the low, middle, and high clouds (not shown) simply reflect the latitude and altitude decrease of air temperature, including the effect of generally colder temperatures over the south polar latitudes. Seasonal variations of TC follow those of air temperature, though small shifts of ZC (also indicated by small changes in the amounts of these three categories of clouds) serve to moderate the amplitude of the seasonal variations.

2) BOUNDARY LAYER CLOUDS

A particularly important subclass of clouds are those that are confined to the planetary boundary layer. Not only are they distinguished by the dynamic processes that form them (small scale turbulence as compared with mesoscale complexes and synoptic weather systems), but also this cloud type may play a key role in the modification of the radiation budget (cf., Hartmann et al. 1986). Although the low cloud category defined here may include some clouds that are not dynamically linked to the boundary layer, the distribution determined in these results is probably a qualitative indicator of where this type of cloud is predominant. The importance of these clouds to the planetary and surface radiation balance occurs because these clouds form at such low altitudes that they do not significantly alter the thermal IR component of the planetary radiation balance, but they do alter the planetary albedo and the surface net IR cooling. Although obscuration of low clouds by higher clouds in satellite observations limits measurements of this cloud type, the low clouds that are identified by satellites are the part of the low cloud population that most affects the planetary radiation balance in this way. Figure 11a shows the annual mean geographic distribution of low clouds found for 1977; the key regions, identified by the predominance of low clouds and a larger seasonal variation, are the marine stratus regimes in the eastern parts of the subtropical ocean basins.

3) "STORM" CLOUDS

Figures 11b and 11c show the annual mean distribution of middle and high clouds for 1977. The marine stratus regions are also apparent as local concentrations

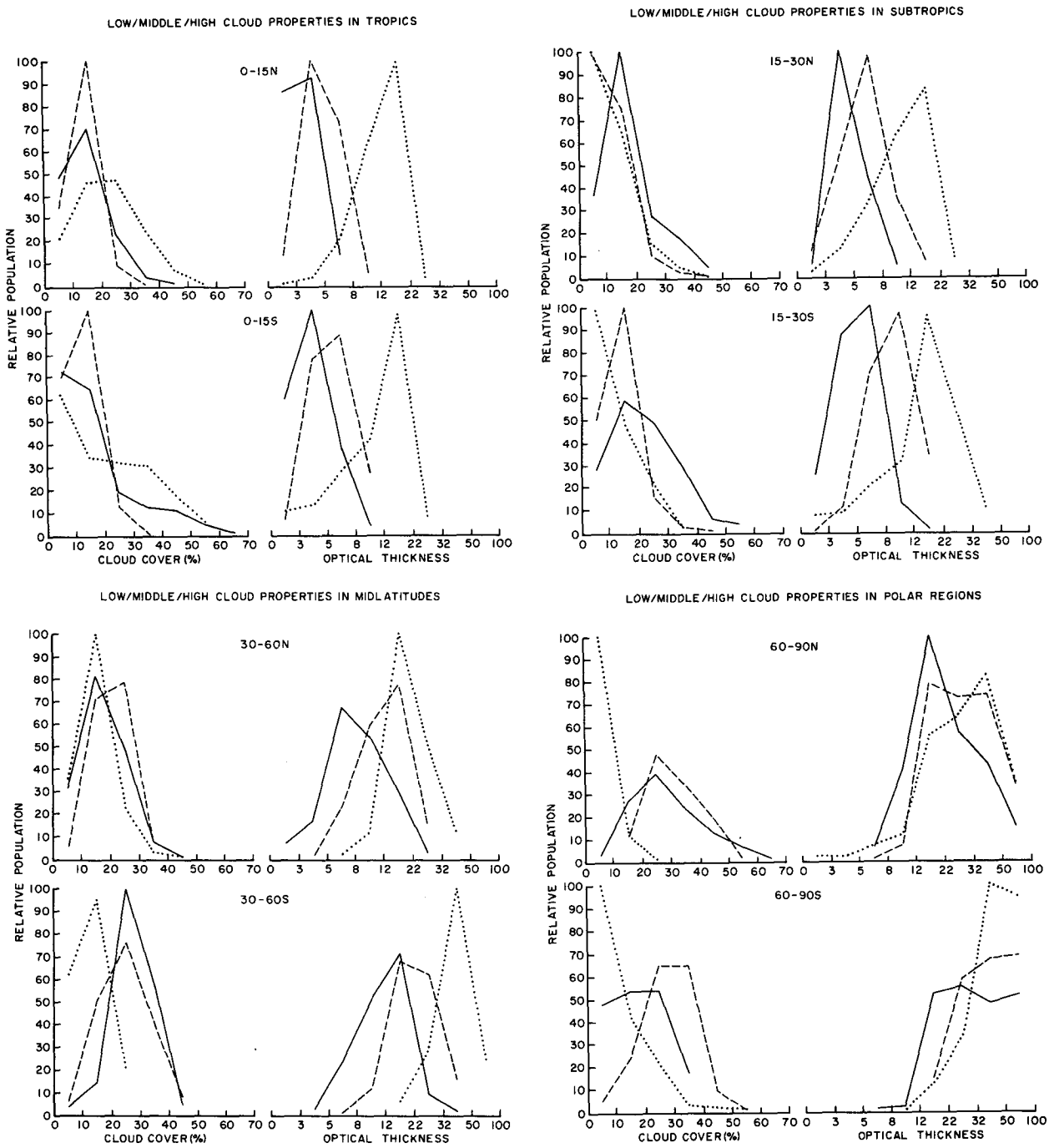

FIG. 10. Distribution of CC and TAU for low (solid), middle (dashed), and high (dotted) clouds in four climate zones in each hemisphere: (a—left) tropics (0°–15°), (a—right) subtropics (15°–30°), (b—left) midlatitudes (30°–60°) and (b—right) polar regions (60°–90°).

of middle cloud but join the clearer ocean regions and deserts as areas of little high cloud amount. Although some low cloud is also present, the midlatitude "storm track" areas are revealed as concentrations of middle and high cloud, with high CC predominant in the cyclogenesis regions off the east coasts of North America, Asia, and South America. The ITCZ and Southern Pacific Convergence Zone (SPCZ) are also regions of large amounts of high cloudiness. These regions of "storminess" are also characterized by optically thicker clouds.

4) DEEP CONVECTIVE CLOUDS

The most violent winds in the atmosphere are associated with strong convection (either isolated or as

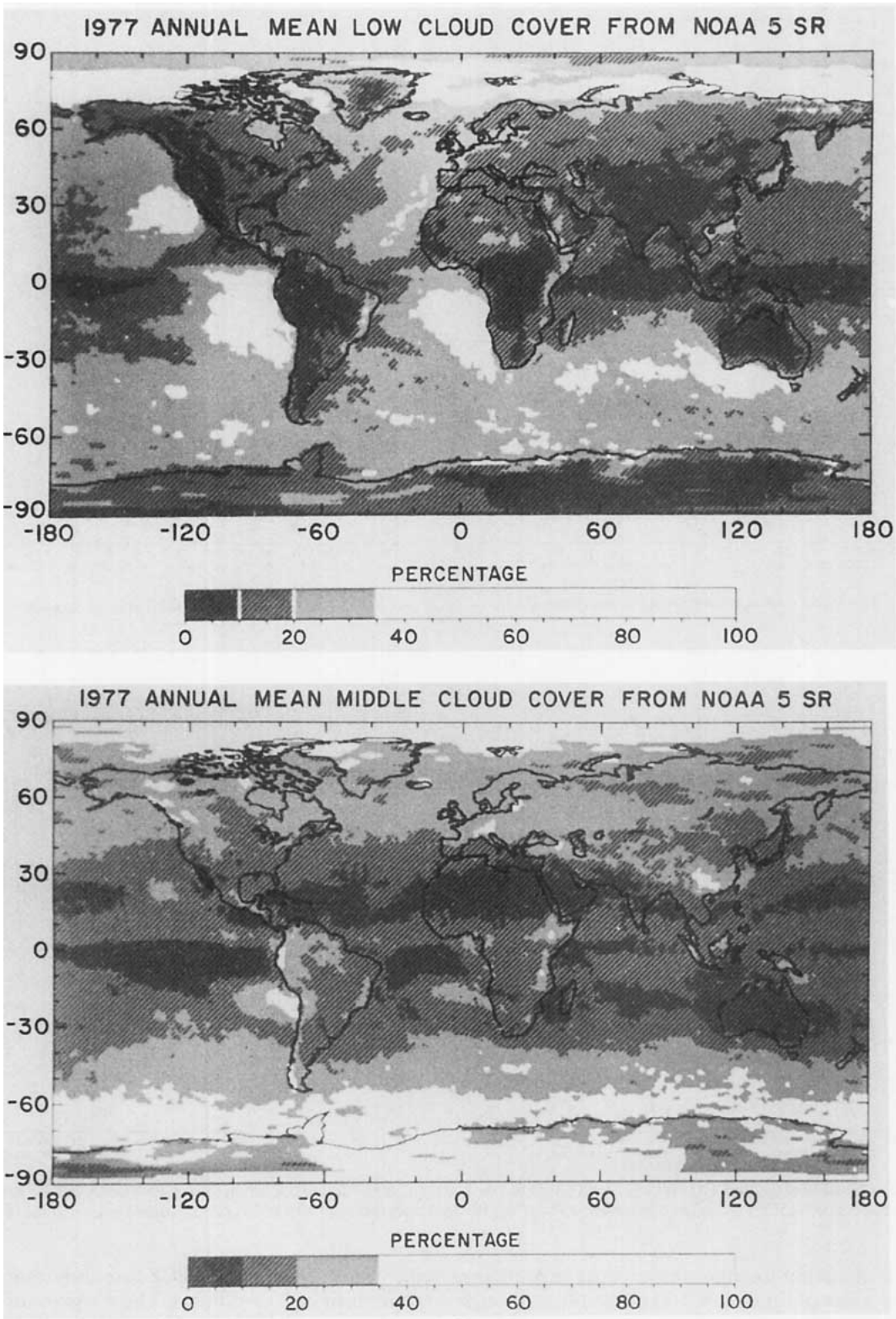

FIG. 11. Geographic distribution of annual mean (a) low, (b) middle, and (c) high cloud cover for 1977.

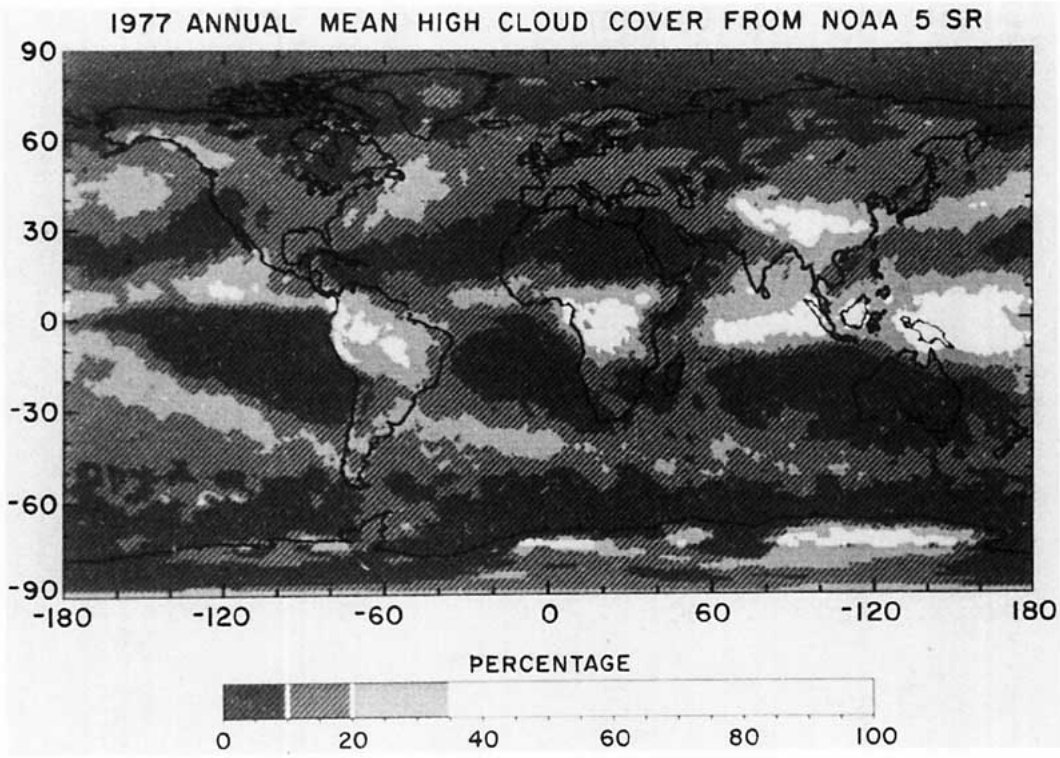

FIG. 11. (*Continued*)

part of strong cyclonic storms), very large cloud liquid water mass densities and precipitation rates, and the most vertically extensive cloud systems. These characteristics also imply very high, cold cloud tops and large optical thicknesses (i.e., large visible brightness). We have attempted to isolate this cloud type by searching for clouds in our analysis with ZC > 6 km and TAU > 32; we refer to them as deep convective clouds.

Figure 12 shows the global distribution of this type of cloud for January and July 1977. The qualitative features of the distributions of deep convection are similar to those shown by Stowe et al. (1989), but we show somewhat more midlatitude deep convection. The ITCZ appears as a much narrower feature in this case than in total high CC (see Fig. 11c), whereas this type of cloud is completely absent from the subtropics. The southward shift of tropical land convection in January and the more northerly extent of the summer monsoon convection combine with a persistent line of oceanic convection north of the equator to produce the double near-equatorial peak in the annual mean cloud optical thickness (Fig. 1b) and its asymmetric seasonal behavior (Figs. 6a and 8a). The seasonal variation of midlatitude distributions, particularly over oceans, is consistent with the presence of stronger winter cyclones compared to summer (Oort 1983). The amplitude of this variation is especially strong in the Southern Hemisphere (Fig. 8f). The contrast between oceans and continents in summer may be exaggerated by the restriction of NOAA-5 observations to early morning. Summer continental deep convection may also produce less extensive cloudiness than over the oceans because of its more isolated occurrences (cf., Klitch et al. 1985). Very little deep convection occurs at high latitudes. Overall, deep convective cloudiness accounts for only about 3% of the total cloudiness in these results, consistent with surface observations (Hahn et al. 1982, 1984).

5) CIRRUS CLOUDS

Cirrus are identified by ZC > 6 km and TAU < 2.5, which isolates only thin, high clouds that do not overlie other clouds. Since the analysis of Warren et al. (1985) suggests that cirrus generally occur in association with other clouds over oceans and about half the time over land, our result is only a lower limit. The comparison of the downward-looking satellite measurements of Barton (1983), which are susceptible to some of the problems discussed above, to those of limb-scanning measurements from SAGE (Woodbury and McCormick 1986), which cannot distinguish between cirrus and the tops of thicker, high layers, shows that the latter give about twice as much "cirrus" cloudiness as the former (Woodbury and McCormick 1986). In addition, our requirement for detection in both spectral channels eliminates some thinner cloudiness in our results (Ro89a). Nevertheless, the part of the cirrus pop-

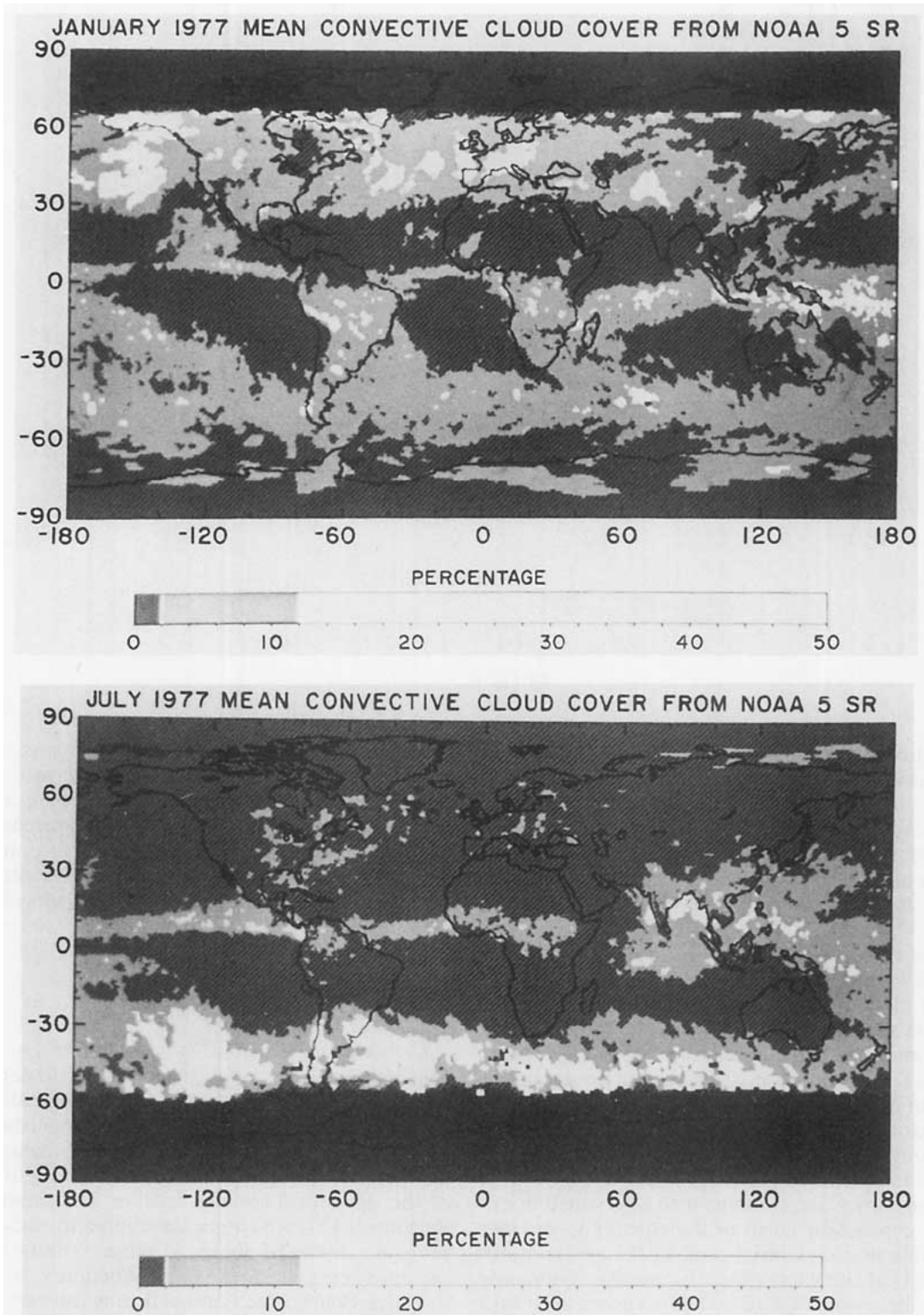

FIG. 12. Global distribution of deep convective clouds for (a) January and (b) July 1977.

ulation identified by this type of data has the strongest "cirrus effect" on the radiation budget. Figure 13 shows that the amount of cirrus identified also depends on the thickness of high clouds included in the category, since most high cloudiness is neither as thin nor as thick as our cirrus and convective categories. The cri-

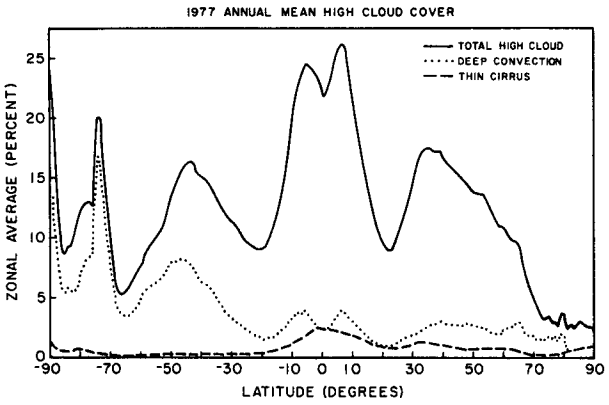

FIG. 13. Partitioning of total high cloud cover into cirrus, deep convective and other cloud cover.

terion we used represents the value of TAU thought to be "typical" of cirrus (Stephens and Webster 1981); if cirrus are identified by the optical properties required to give a positive radiative feedback on surface temperature, then ZC > 6 km and TAU < 6 would be better criteria and would raise our estimate of the global, annual mean amount from about 2% to about 10%.

Comparison of our results to others is difficult, given the range of sensitivities and definitions used; nevertheless, the geographic distribution and seasonal variations of peak concentrations of cirrus in our results (Fig. 14) and those of Woodbury and McCormick (1986), Barton (1983), and Stowe et al. (1989) are similar. Notable features are the much broader ITCZ and SPCZ features, the intrusion of cirrus cloudiness over North Africa in January, and the strong seasonal variation of cirrus amount in the midlatitude storm track zones. Land/water contrasts and their seasonal changes in these results are opposite to the cirrus occurrence frequencies reported by Warren et al. (1985); but at least one factor that affects this comparison is our "morning" observation time, when amounts of land cirrus associated with convection in summer are a minimum (Wylie and Menzel 1989). Estimates of total cirrus cover (thinner high clouds) range from 10% to 30% (Hahn et al. 1982, 1984; Woodbury and McCormick 1986; Stowe et al. 1989; Wylie and Menzel 1989).

4. Assessment of radiative implications

As an additional check on the accuracy of the cloud and surface properties obtained in this analysis, we use these values to infer the total solar and thermal infrared fluxes that constitute the ERB and SRB. The primary motivation for this calculation is to check the cloud TAU values, since this is the first systematic attempt to measure this quantity. This comparison also checks the validity of the radiance calibrations used, though indirectly. A second motivation is to begin the investigation of the accuracy of calculating ERB, SRB, and the seasonal cloud-radiative feedbacks using such cloud data by determining how well we can validate the results with available information. We also compare ERB and SRB values with those simulated by our climate GCM.

a. Global ERB

1) ANNUAL MEAN

The global, annual mean planetary albedo and effective temperature, inferred from these results, are 31% and 251 K, which agree fairly well with the values obtained from Nimbus-3 (Raschke et al. 1973), Nimbus-7 (Smith and Smith 1987), and ERBE (Ramanathan et al. 1989) shown in Table 6. The inferred annual mean, global flux imbalance is <20 watts/m^2, which provides one estimate of the accuracy of this reconstruction of the ERB from the cloud measurements. The good agreement of these values confirms the general validity of the retrieved cloud TAU and TC values as well as providing confirmation of the radiance calibrations employed.

Hemispheric deviations from the global, annual mean values are also shown in Table 6 for our results and those from Nimbus-3, Nimbus-7, and ERBE. Our results imply that the Northern Hemisphere is darker and warmer than the Southern Hemisphere while all the other results show a brighter Northern Hemisphere, though with a smaller difference. The hemispheric difference in our results is due to a larger average CC and TAU in the Southern Hemisphere. The Nimbus-7 measurements at visible wavelengths, however, show no hemispheric difference, suggesting that some of the error in our results may be associated with our prescription of the near-IR component of the surface albedo, combined with the lower than average cloud cover over land in early morning at the time of the NOAA-5 observations. All the other results confirm our sign of the hemispheric temperature difference but indicate that the difference is smaller. However, the daytime Nimbus-7 measurements show a larger difference between the hemispheric temperatures than the diurnal average so that this result may also be dependent on the particular diurnal phase of our sample. Despite these problems our global and hemispheric annual mean TOA fluxes appear correct to within about 5%.

2) SEASONAL VARIATIONS

Table 7 compares the seasonal variations of the global and hemispheric mean radiation obtained from NOAA-5 and Nimbus-7. The seasonal variations of the mean Northern Hemispheric temperature are very similar in both results. The variations in the Southern Hemisphere are also very similar, except for January,

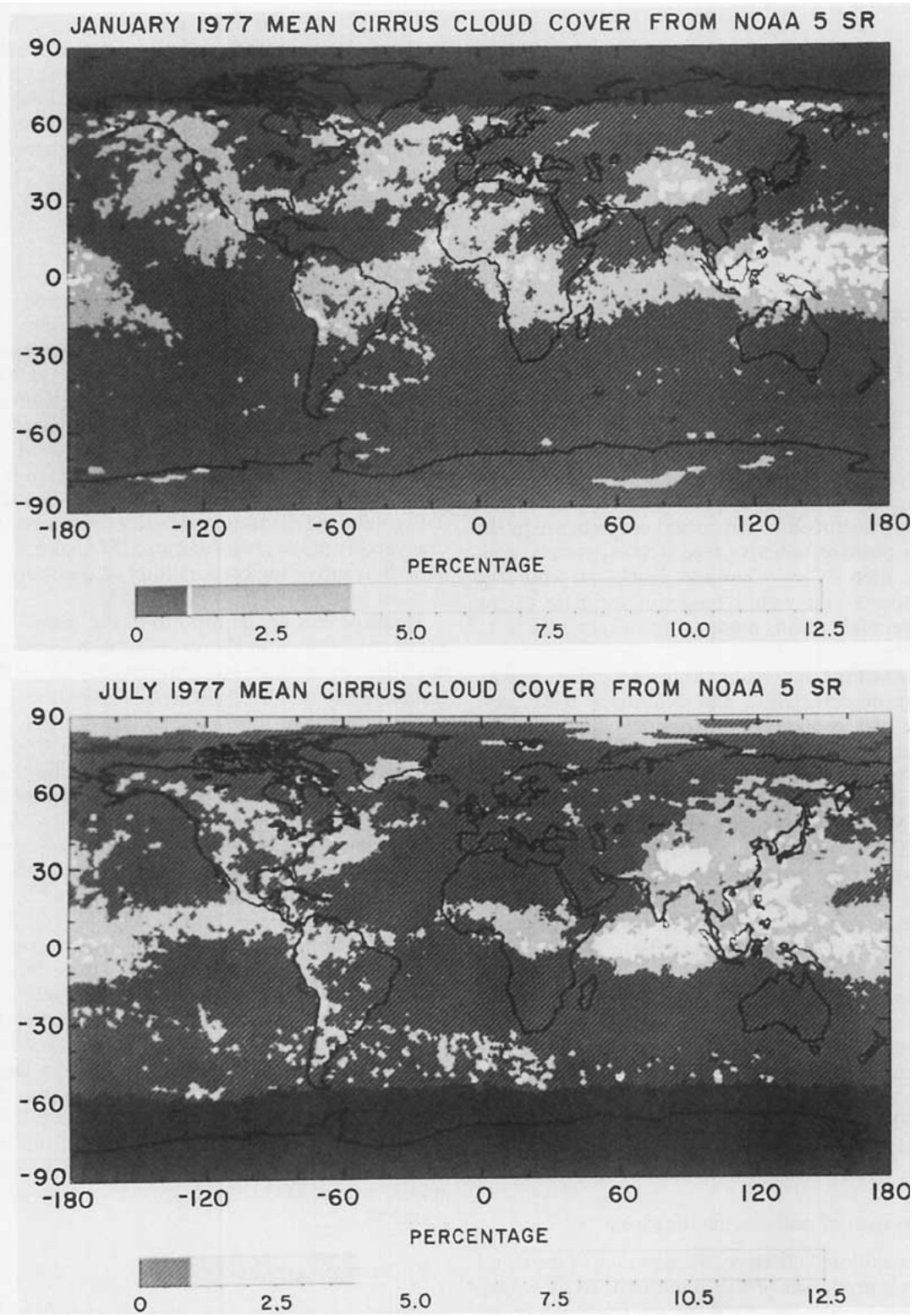

FIG. 14. Global distribution of thin cirrus clouds for (a) January and (b) July 1977.

TABLE 6. Global and hemispheric, annual mean planetary albedos, and effective temperatures calculated from NOAA-5 cloud properties compared to those inferred more directly from multiwavelength narrowband measurements by Nimbus-3 (Rashke et al. 1973) and from broadband measurements by Nimbus-7[1] (Smith and Smith 1987) and ERBE (Ramanathan et al. 1989).

	Albedo (%)	Temperature (K)
NOAA-5 (1977)	30.7 (∓2.3)	251.0 (±1.3)
Nimbus-3	28.4 (±0.7)	255.3 (±0.4)
Nimbus-7 (1979)	29.5 (±0.5)	254.0 (±0.3)
	VIS [33.5 (±0.0)]	DAY [254.8 (±0.5)]
Nimbus-7 (1983)	29.6 (±0.6)	253.9 (±0.2)
	VIS [34.2 (±0.2)]	[254.7 (±0.2)]
ERBE (1985)	29.5	253.6

[1] Several other values for planetary albedo and effective temperature from Nimbus-7 have been quoted in the literature: nonscanner—30.67% albedo, 252.1 K temperature; and scanner—33.1% albedo, 253.1 K temperature (Jacobowitz et al. 1984); nonscanner—31% albedo, 25.21 K temperature; scanner—33.1% albedo, 253.2 K temperature (Hartmann et al. 1986); and Slingo et al. (1989)—30.2% albedo and 254.0 K temperature.

which is much colder than the global, annual mean value in our results but are slightly warmer in the Nimbus-7 results. The seasonal changes in Northern Hemisphere albedo exhibit the same pattern but are generally darker than the global, annual mean in January in our results and brighter in the Nimbus-7 results. The variations of the Southern Hemisphere albedo are more similar in magnitude and pattern (with our results being brighter than the global, annual mean rather than darker), except for January. In fact, it is the large planetary albedo of the Southern Hemisphere in our January results that explains much of the bias between the NOAA-5 and Nimbus-7 albedos. Hence, these differences may be caused by the El Niño in 1977, which is also suggested by their resemblance to the changes associated with the 1982/83 El Niño in the Nimbus-7 observations (Smith and Smith 1987).

3) CLOUD EFFECTS

The global mean albedo and temperature are produced by the combination of mean "cloudy" and "clear" albedos of 45% and 15%, respectively, and mean "cloudy" and "clear" temperatures of 247 K and 255 K, respectively.[4] The difference between the average net solar and "clear" net solar fluxes is -55 W m^{-2}, as compared with a value of about -46 W m^{-2} inferred from ERBE (Ramanathan et al. 1989). The difference between the average net thermal and "clear" net thermal fluxes is $+16$ W m^{-2}, as compared with values of $+24$ and $+31$ W m^{-2} inferred from Nimbus-7 (Ardanuy et al. 1989) and ERBE (Ramanathan et al. 1989), respectively. Another way to represent the cloud effects is by the differences between completely cloudy and clear net fluxes. For the NOAA-5 results these values are -105 W m^{-2} and $+31$ W m^{-2} for net solar and thermal fluxes, respectively; in their review of previous estimates, Hartmann and Short (1980) give a range of values of -68 to -154 W m^{-2} for the difference between the cloudy and clear net solar fluxes and a range of $+40$ to $+80$ W m^{-2} for net thermal fluxes. These comparisons suggest that the errors in reconstructing ERB from the cloud data are not too large; however, the significance of these simple global quantities (and good agreement of their values) is not an obvious cause for complacency when the complexity of seasonal variations at regional scale are considered.

b. Global SRB

We report four flux components of the surface radiation budget: 1) downward solar flux is given as the atmospheric transmissivity of solar radiation (the ratio of solar flux incident at the surface to that incident at the top of the atmosphere), 2) upward solar flux is given as the surface albedo, 3) downward thermal flux is given as the effective temperature of the atmospheric thermal radiation and 4) upward thermal radiation is given as the effective surface temperature.

1) ANNUAL MEAN

The global, annual mean atmospheric transmissivity is 0.54, composed of "cloudy" and "clear" transmissivities of 0.36 and 0.74, respectively (Table 8). The surface albedo is 8.6%; the average albedo of cloudy regions is slightly lower than for clear regions because of the higher cloud amounts over ocean than land and because bright deserts are usually cloud free. The atmospheric temperature is 280.6 K and the surface temperature is 288.5 K (calculated from the mean fluxes that give a slightly different value than the average temperature itself). The atmospheric temperature is composed of "cloudy" and "clear" temperatures of 285.2 K and 275.2 K, respectively, equivalent to an average cloud base altitude of about 1.5 km. As with ERB, the effect of clouds on the solar radiation is stronger than on the thermal radiation.

Hemispheric deviations from the global mean values show that the Northern Hemisphere transmits more solar radiation than the Southern, both because it is less cloudy and because the clouds are optically thinner. However, the mean surface albedo in the Northern Hemisphere is also larger because of a larger proportion

[4] Since the total fluxes are calculated by the weighted average of the fluxes calculated with 0% and 100% cloudiness, all other quantities being the same, we can also obtain the average fluxes for completely clear and completely cloudy conditions. This is not necessarily the same result that would be obtained by averaging over the fluxes separated by actual cloud amount (e.g., Ramanathan et al. 1989), since persistently cloudy or clear regions may well differ in other respects from variably cloudy locations. These differences may bias the averages and could explain, in part, why the clear values inferred by Ramanathan et al. differ from ours.

TABLE 7. Seasonal deviations of global and hemispheric values of the planetary albedo and effective temperature from their global annual mean values, obtained from NOAA-5 SR results (first number in each column) and from Nimbus-7 (second number) (Smith and Smith 1987). The numbers in parentheses in each column are the Nimbus-7 values for visible albedo and daytime temperature, respectively.

	Jan			Apr			Jul			Oct		
Albedo	Global annual mean = 30.3 29.3 (33.4)											
G	+3.4	+0.7	(+0.6)	−1.1	+0.2	(+0.4)	−2.3	−0.8	−0.4)	+0.1	−0.1	(−0.4)
NH	−1.3	+1.5	(0.0)	−2.5	+1.7	(+1.2)	−2.8	+0.5	(+0.4)	−3.7	−0.5	(−1.4)
SH	+5.6	−0.1	(+1.0)	+0.8	−1.3	(−0.4)	−1.3	−2.1	(−1.2)	+2.8	+0.3	(+0.6)
Temperature	Global annual mean = 250.3 253.8 (254.8)											
G	−2.0	−0.8	(−0.8)	+0.4	−0.2	(−0.0)	+1.4	+1.0	(−0.8)	+0.3	−0.0	(0.0)
NH	−1.3	−2.2	(−2.2)	+1.4	−0.2	(0.0)	+3.8	+3.4	(+3.4)	+1.3	−0.0	(+0.4)
SH	−2.8	+0.6	(+0.4)	−0.7	−0.2	(−0.4)	−1.1	−1.0	(−1.2)	−0.7	−0.0	(−0.4)

of land. The larger mean surface temperature in the Northern Hemisphere is also offset by the larger mean atmospheric temperature; the latter seems to be caused primarily by a difference in average air temperature rather than a difference in mean cloud elevation.

2) SEASONAL VARIATIONS

Seasonal variations of the two hemispheres show a more complex interplay among the surface and cloud properties controlling the SRB (Table 8). The Northern Hemisphere peak surface albedo occurs in April, when more snow and sea ice are illuminated than in January; the Southern Hemisphere surface albedo peaks in January when all of Antarctica is illuminated. The Northern Hemisphere solar transmissivity is roughly constant throughout the year, associated with a decrease from winter to summer of the clear transmissivity due to increasing water vapor abundance and an increase from winter to summer of the cloudy transmissivity due to reduced optical thicknesses. The winter cloud optical thickness is so large, however, that the total solar transmissivity is lower in January than for any other month. Seasonal changes in the Southern Hemisphere show the same cycle; however, the stronger corresponding changes in total cloud cover in the Southern Hemisphere reverse the sense of the weak seasonal variation in total solar transmissivity.

The seasonal variations of the atmospheric temperatures are essentially coupled to the surface temperature changes; the differences between these two temperatures are nearly constant over the year with clear temperature variations associated primarily with changes in water vapor abundance and cloudy temperature variations associated with changing cloud optical thickness.

TABLE 8. Annual and monthly mean components of SRB averaged over the globe and each hemisphere. The temperature difference between the effective surface temperature (TS) and effective atmospheric temperature (TA) is shown in the last three lines.

		Annual G/NH/SH	Jan G/NH/SH	Apr G/NH/SH	Jul G/NH/SH	Oct G/NH/SH
Transmissivity	total	0.54/0.57/0.51	0.51/0.54/0.50	0.55/0.58/0.51	0.56/0.57/0.53	0.53/0.57/0.51
	cloudy	0.36/0.40/0.33	0.33/0.26/0.37	0.33/0.41/0.26	0.33/0.42/0.21	0.33/0.33/0.33
	clear	0.74/0.73/0.74	0.74/0.78/0.74	0.79/0.75/0.82	0.79/0.73/0.80	0.74/0.77/0.75
Surface albedo	total	8.6/9.2/7.9	8.0/6.2/8.9	6.7/8.7/3.6	5.9/6.7/4.1	6.5/5.6/7.2
	cloudy	8.6/9.0/8.2	7.8/5.1/8.6	6.6/8.5/3.2	5.6/6.2/3.1	5.5/4.5/6.1
	clear	8.6/9.4/7.8	8.1/6.6/9.2	6.8/8.8/3.8	6.1/7.0/4.4	7.0/6.0/7.8
Atmospheric temperature	total	280.6/281.8/279.4	276.6/275.1/278.2	281.6/280.7/282.5	282.7/288.3/276.8	281.0/282.2/279.8
	cloudy	285.2/286.6/283.9	281.1/286.0/281.6	285.8/285.7/285.9	287.3/291.7/282.8	285.6/287.0/284.2
	clear	275.2/277.0/273.3	270.6/269.6/271.3	276.7/275.5/277.9	278.0/284.5/271.2	275.9/278.0/273.6
Surface temperature	total	288.5/289.9/287.1	284.4/283.7/285.1	289.0/288.7/289.2	290.3/294.9/285.5	288.5/290.2/286.8
	cloudy	—	—	—	—	—
	clear	—	—	—	—	—
Δ temperature (TS − TA)	total	7.9/8.1/7.7	7.8/8.6/6.9	7.4/8.0/6.7	7.6/6.6/8.7	7.5/8.0/7.0
	cloudy	3.3/3.3/3.2	3.3/2.7/3.5	3.2/3.0/3.3	3.0/3.2/2.7	2.9/3.2/2.6
	clear	13.3/12.9/13.8	13.8/14.1/13.8	12.3/13.2/11.3	12.3/10.4/14.3	12.6/12.2/13.2

c. *Regional variations of ERB/SRB*

1) SEASONAL, ZONAL MEANS

Figure 15 shows the zonal mean components of ERB for all four months compared to the Nimbus-7 climatological values. The rms differences range from about 4% in July to 2% in January and October; differences at particular latitudes are as large as about 10%. The pattern of albedo differences can be plausibly explained by two effects: averaging of cloud optical thickness values and diurnal variations in total cloudiness. The former can explain our overestimate of the planetary albedo in the ITCZ that exhibits the largest range of TAU values (Fig. 10a; cf., Sèze and Rossow 1990a). By averaging TAU linearly, we give more weight to the very large TAU values associated with the convective towers and the mesoscale anvils, which do not cover as much area as the thinner cirrus and low level convection (see Figs. 12 and 14). The differences in phase of the diurnal variations of cloud cover over ocean and land (cf., Minnis and Harrison 1984b) can cause a morning satellite, like NOAA-5, to measure a larger planetary albedo over ocean (Southern Hemisphere) than that measured by a noontime satellite, like Nimbus-7. Likewise, the morning satellite would obtain a lower albedo than the noontime satellite for land (Northern Hemisphere). The effect of linear TAU-averaging on the thicker winter clouds may explain the change in the diurnal bias in January for the Northern Hemisphere.

The rms differences in zonal mean planetary temperatures range from 1.5 K in April to 3.0 K in July; a few individual differences are as large as 10 K. Our generally lower planetary temperatures, especially in the subtropics, are probably accounted for by the cold bias in retrieved surface temperatures caused by an underestimate of water vapor absorption in the radiative retrieval model (Ro89a). The differences in the ITCZ location may be associated with interannual variations.

Some of the difference between these two sets of data is expected, since our results are for 1977 (an El Niño year) and the Nimbus-7 results are a composite of measurements covering 1979–1983. Nevertheless, our monthly zonal mean planetary albedo values are within 10% of the Nimbus-7 values and our monthly zonal mean planetary temperatures are within 10 K at all latitudes and seasons. Although the magnitudes of the seasonal changes at particular latitudes are similar to

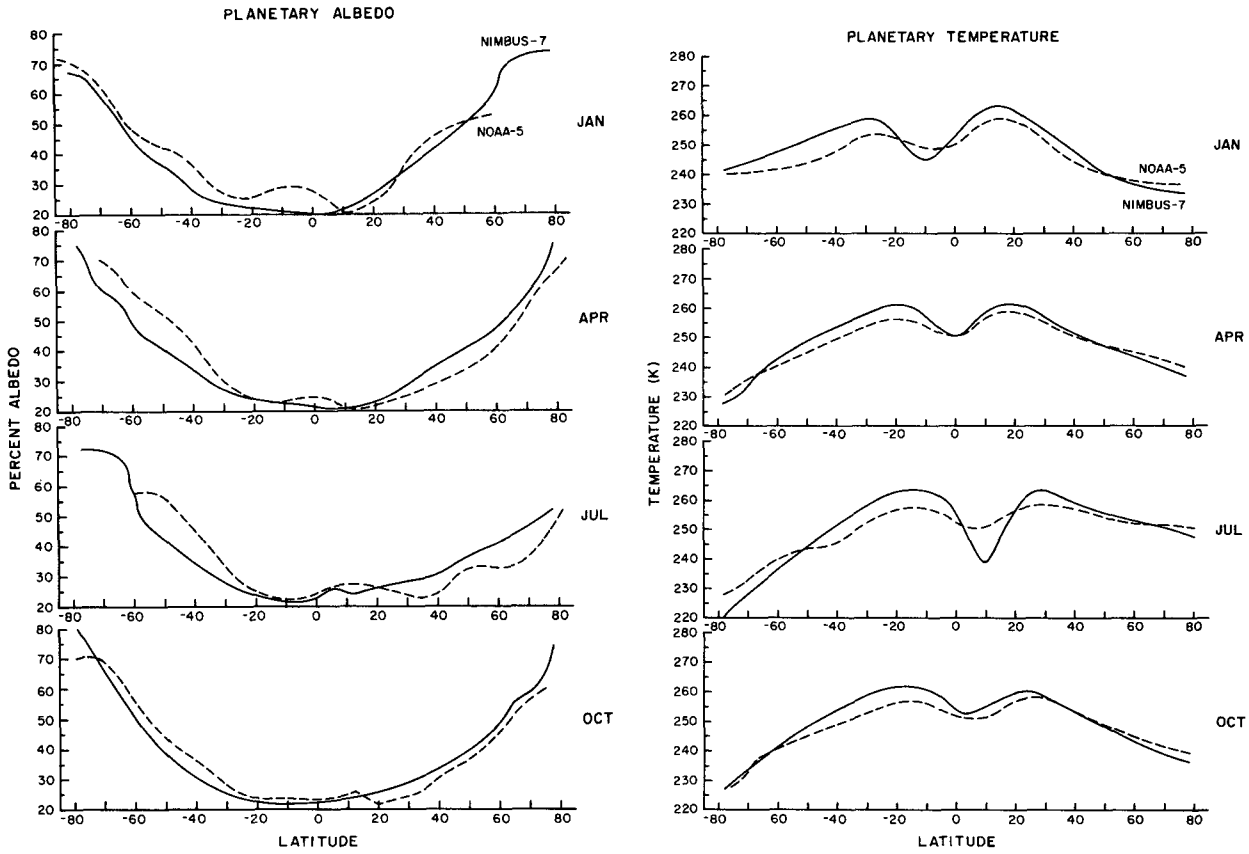

FIG. 15. Zonal mean ERB components (left—planetary albedo and right—temperature) from NOAA-5 (for 1977—dashed) Nimbus-7 (composite over 1979–83—solid) for January, April, July and October.

these differences, the comparison in Fig. 15 suggests that we have enough accuracy in these results to get the sense of the seasonal variations. However, our measurements of seasonal amplitude cannot be confirmed to better than a factor of about two; e.g., our single-year results imply a larger seasonal amplitude than the composite Nimbus-7 results.

2) SEASONAL, REGIONAL VARIATIONS

Deviations of individual components of ERB/SRB from their monthly zonal means are associated with variations both of the surface properties (primarily the contrast between land and ocean) and of the clouds. The largest deviations (>25%) in planetary albedo occur at low latitudes; northern midlatitudes show deviations of 15%–20%, caused by cloud cover variations associated with land–water contrasts while the Southern Hemisphere is more nearly zonally uniform with deviations $\leq$ 10%. With the exception of North Africa and land areas in winter, the regional deviations of the surface albedo are generally smaller than that of the planetary albedo; i.e., cloud variations control and increase the regional albedo contrasts at low latitudes and in the Southern Hemisphere. In the Northern Hemisphere, there is less cloudiness over the brighter land than darker ocean, which serves to reduce the longitudinal variations of planetary albedo, more so in winter than in summer.

The most prominent low latitude albedo features are, in January: 1) minima in the nearly cloud-free areas in the western-central, sub-tropical oceans in both hemispheres, 2) minima over northern subtropical land areas (central America, Sahel, and India), and 3) maxima over three southern subtropical land areas (Amazon Basin, Congo Basin, and Indonesia) associated with strong convection. The eastern portions of the subtropical oceans are mostly cloud covered and have larger planetary albedos, particularly off the coasts of North America and southern Africa, while Australia is relatively clear with a low planetary albedo. In July, the subtropical ocean minima change shape and extent but they persist. The minima over Central America and Australia expand poleward and shift eastward while a new minimum appears over the eastern Mediterranean and Middle East. The other prominent January minima over northern subtropical land areas become maxima in July, particularly India during its summer monsoon. All of the prominent January albedo maxima undergo large transformations in July: 1) the one over the Amazon Basin is replaced by a large minimum, with a small maximum remaining over the headwaters of the Amazon, 2) the one over the Congo Basin is replaced by a large minimum, and 3) the Indonesian feature is much less prominent but still a local maximum. All of these features agree in both position and magnitude with those shown by Hartmann and Short (1980) and those in the Nimbus-7 results (Smith and Smith 1987), except the small scale winter minima over the Sahel and Australia and the summer minimum over the Mediterranean, which Hartmann and Short (1980) do show but may be missed in the Nimbus-7 analysis because of its lower spatial resolution.

The largest planetary and surface albedos are produced by the Greenland and Antarctic ice sheets (60% and 75%, respectively); only the southern tip of Greenland is illuminated in January while Antarctica is not illuminated at all in July. In April and October, when both are illuminated, Antarctica has an albedo about 10%–15% higher than Greenland (Hartmann and Short 1980 show a similar difference but with a magnitude of only 5%–10%). Some snow-covered land areas (particularly the plains to the east of the Canadian Rockies and northeast of the Caspian Sea, cf., Hartmann and Short 1980; Smith and Smith 1987) have surface albedos as high as 50%; their planetary albedos are increased by about 10% by cloudiness. Surface and planetary albedos of Arctic sea ice are about 50% and 55%, respectively, in July. The lowest planetary and surface albedos are associated with low latitude ocean areas. (See Ro89b for more discussion of surface albedos.)

The largest regional deviations of planetary temperature also occur at lower latitudes (tropics and subtropics); the surface temperatures are nearly zonally uniform—again clouds are the primary producers of regional variability. At northern midlatitudes, large deviations of surface temperatures from the zonal mean in January and July are associated with the land–ocean contrasts; however, the clouds reduce the longitudinal variations of planetary temperatures at higher latitudes, particularly in winter. The seasonal shift of the storm tracks causes an increase in the latitudinal extent of the northern subtropical, highly variable zone in the summer hemisphere; the Southern Hemisphere storm track does not shift as much seasonally.

Prominent longitudinal features in planetary temperature all occur at low latitudes: 1) maxima associated with the subtropical oceans, with the drier winter hemisphere maxima being stronger, 2) maxima associated with the Northern Hemisphere land areas (Central America, northern Africa and India) and Australia in January and with Southern Hemisphere land areas (Brazil, southern Africa and northern Australia) in July, 3) additional maxima in July over southwestern North America and extending from northern Africa through the Middle East to the east of the Caspian Sea and 4) minima over Brazil, central Africa and Indonesia in January and over Columbia/Central America, north-tropical Africa and India-Indonesia in July. The planetary temperatures generally decrease from equator to pole, but Siberia, Greenland, and the high plateau of Antarctica exhibit the lowest values in both January and July. The planetary temperature over the highest part of Antarctica in July falls below 220 K (Hartmann and Short 1980). Middle and high latitudes are gen-

erally more zonally uniform than lower latitudes, although there is more longitudinal variation in the Northern Hemisphere (especially in January) than the Southern Hemisphere, associated with land/ocean contrasts. All of these features agree in both position and magnitude with those shown by Hartmann and Short (1980) and Smith and Smith (1987), except for a relative maximum off the coast of South America in January associated with El Niño (this feature resembles the El Niño anomalies in planetary temperature illustrated by Bess et al. 1989).

The surface temperatures show behavior opposite that of planetary temperatures, exhibiting much more seasonal and longitudinal variability at higher latitudes, particularly in the land-dominated Northern Hemisphere, than at lower latitudes. Peak values occur in narrow zones over the Northern Hemisphere subtropical oceans in January; these regions expand northward and into the Southern Hemisphere in July. In addition, northern Africa, the Middle East and India become large maxima in July. Relative minima occur at low latitudes in the highlands of southern Africa and South America in January and in the Himalayas in July. (See Ro89b for more discussion of surface temperatures).

The highest planetary temperatures (over 270 K) occur over the Middle East in July (Hartmann and Short 1980), associated with some of the highest surface temperatures and minima of cloud cover and water vapor abundance. Although other arid subtropical land areas exhibit similar surface temperatures, higher humidities and more cloud cover reduce their planetary temperatures to about 265 K and below. The lowest planetary temperatures occur over Antarctica throughout the year, although northernmost Siberia and central Greenland are as cold as Antarctica in January. In July, the planetary temperature over Antarctica falls below 220 K, significantly less than the surface temperature of about 255 K. (Since we did not directly observe Antarctica in July from NOAA-5 data, these values are estimates produced from conditions near 60°S; therefore, the actual surface and planetary temperatures in July may be colder still. Climatological surface temperatures are about 220–230 K, e.g., but Hartmann and Short (1980) show similar planetary temperatures to those reported here.)

Downward solar and thermal fluxes at the surface are controlled primarily by the variation with latitude and season of solar zenith angle and atmospheric temperature. The major longitudinal modulations are produced by clouds: maxima of downward solar fluxes occurring in the relatively clear subtropical ocean areas and minima in the areas of ITCZ cloudiness and the midlatitude storm tracks. Cloud effects on the downward thermal fluxes are weaker than on the solar fluxes at lower latitudes, where water vapor influences the thermal fluxes the most and are more apparent at higher latitudes where the effects of water vapor are weaker. Downward thermal fluxes are reduced over major topographic highs that shift cloud base altitudes upward. Slightly larger downward thermal fluxes are exhibited in the regions of predominantly low level cloudiness over subtropical oceans.

The combination of all these effects results in a distribution of net radiation at TOA and at SRF that differs considerably in detail from the patterns of the individual components (Figs. 16 and 17).

Spatial variability of the net fluxes is largest (about 15%–25% relative) at low latitudes and somewhat larger in relative magnitude at SRF than TOA; seasonal variability is larger at higher latitudes and at SRF. The peak solar absorption (heating) at TOA (Figs. 16a and 16b) occurs in a band near 30° latitude, south in January and north in July. Major longitudinal modulations are associated with cloud variations: 1) in January, low values in the South Pacific convergence zone (SPCZ), in the marine stratus regions off the west coasts of South America and southern Africa, and the ITCZ components over South America and Africa, 2) in January, high values in the Indian Ocean, south Atlantic Ocean and Australia, 3) in July, low values in the marine stratus regions off the west coasts of North America and northern Africa and 4) in July, a high value over the North Atlantic Ocean due to the shift of the storm track latitude. The solar heating decreases with latitude, falling to less than half of its peak value polewards of 30°N and 70°S in January and 80°N and 30°S in July. Middle and higher latitude net solar heating distributions are nearly zonal.

The pattern of solar heating at SRF (Figs. 16c and 16d) follows that at the top of the atmosphere fairly closely, though it exhibits reduced magnitudes and more variability.

The peak thermal emission (cooling) at TOA (Figs. 17a and 17b) has already been discussed above as the planetary temperature. At SRF (Figs. 17c and 17d), the thermal cooling is strongly enhanced over land, even in the winter hemisphere: 1) in January, Australia, northwestern Africa, and India are strong maxima while Argentina, southwestern North America, and northeastern Asia are weaker maxima and 2) in July, northern Africa through the Middle East and southern Africa are strong maxima while southwestern North America, Australia, and Greenland are somewhat weaker maxima. In January, the thermal cooling in the North Atlantic (Greenland Sea) and the north Pacific are as strong as that over many land areas, though not as strong as over North Africa and India. In July, the strongest thermal cooling over the oceans occurs in the south Atlantic, although there is a secondary maximum in the southeastern Pacific. These patterns are associated with the formation regions for ocean bottom waters (Gordon 1986; Broecker 1987). The weakest thermal cooling is associated with major dense cloud formations: 1) in January, these are the winter monsoon over southeast Asia, the ITCZ and marine stratus off the coast of South America and southern

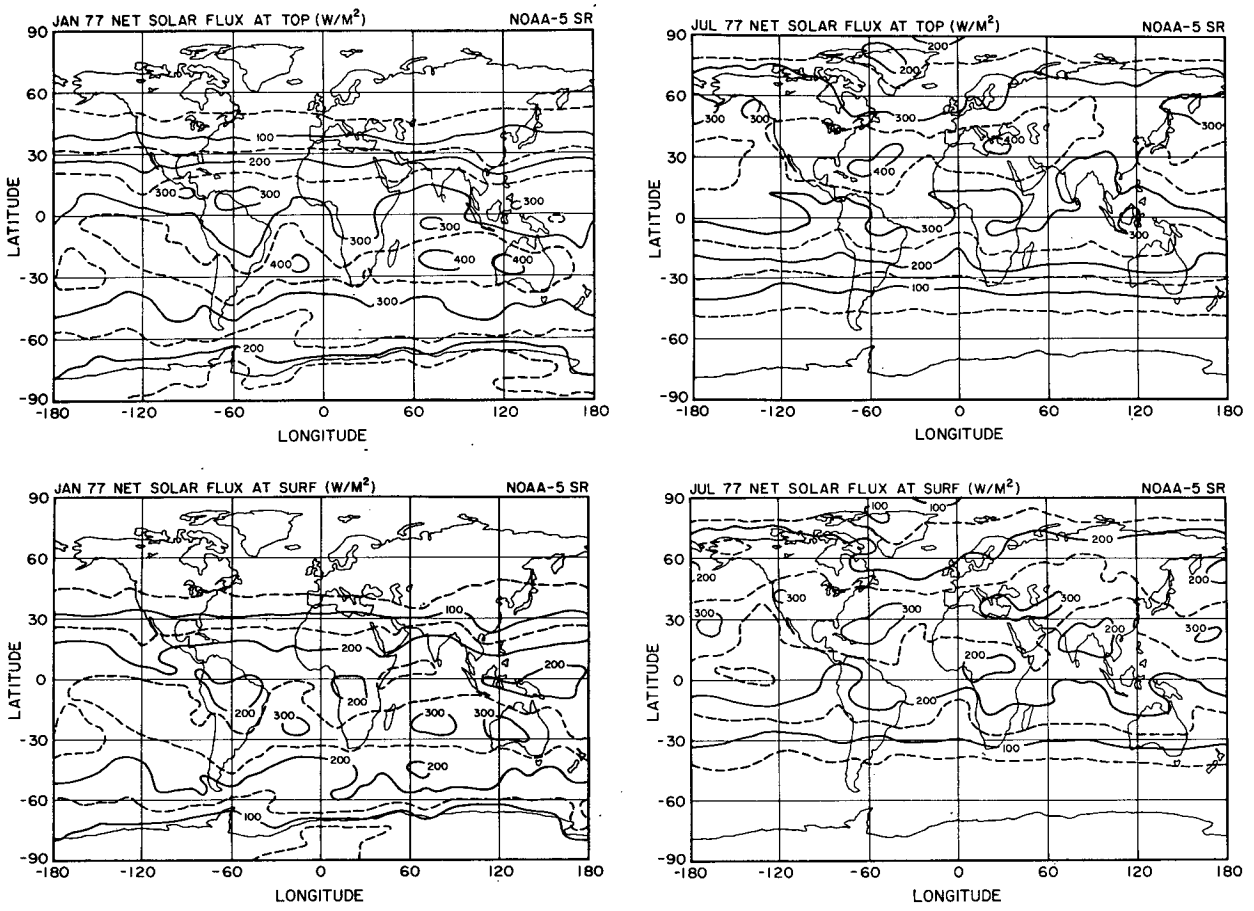

FIG. 16. Geographic distribution of net solar heating at TOA and SRF for January and July 1977.

Africa, and the oceanic storm track zone in the southern midlatitudes and 2) in July, these are the summer monsoon over India and the Himalayas, the ITCZ and marine stratus regions in both hemispheres, and the oceanic storm track regions in the northern midlatitudes. The Atlantic region of suppressed thermal cooling extends into the Arctic Basin between Greenland and Scandinavia and parallels the Arctic coastline of Asia and North America. Comparing the patterns of net thermal fluxes at TOA with those at SRF shows much less resemblance between these two than evident for the net solar fluxes.

The net radiation (solar minus thermal fluxes) at TOA and SRF shows even less regional variation than the net fluxes (Fig. 18); variations are $\leqslant 20\%$. In other words, as we add up the contributions from individual flux components to the net solar and thermal fluxes and then these net flux contributions to the net radiation, the complex regional patterns are almost completely cancelled out, leaving an essentially zonal pattern of the net radiation balance. The largest remaining regional variations, both at TOA and SRF, occur in the zone of peak net energy input that follows the seasonal variation of the subsolar latitude. These local maxima and minima are directly associated with the variations of total cloudiness in this zone; however, the July northern midlatitude pattern is a little less zonal in association with the major continents. Overall, more area at the SRF experiences net heating than at TOA.

Figure 19 shows the differences between the January and July net radiation at TOA and SRF. The pattern of the seasonal variations is strongly zonal, with the largest deviations from the zonal mean of <80 W m^{-2}; almost all of the longitudinal features apparent in Figs. 16, 17, and 18 have been reduced in relative magnitude. Net heating occurs in the summer hemisphere at both TOA and SRF. The maximum difference between summer and winter heating occurs in a zone extending from 30° to 60° in each hemisphere although the zone is shifted slightly more poleward in the Northern Hemisphere. This latitudinal pattern of seasonal variation is controlled predominantly by solar declination variations (changing the solar heating) and associated air and surface temperature variations (changing the thermal cooling). Although clouds alter the total solar heating and thermal cooling rates significantly (the dif-

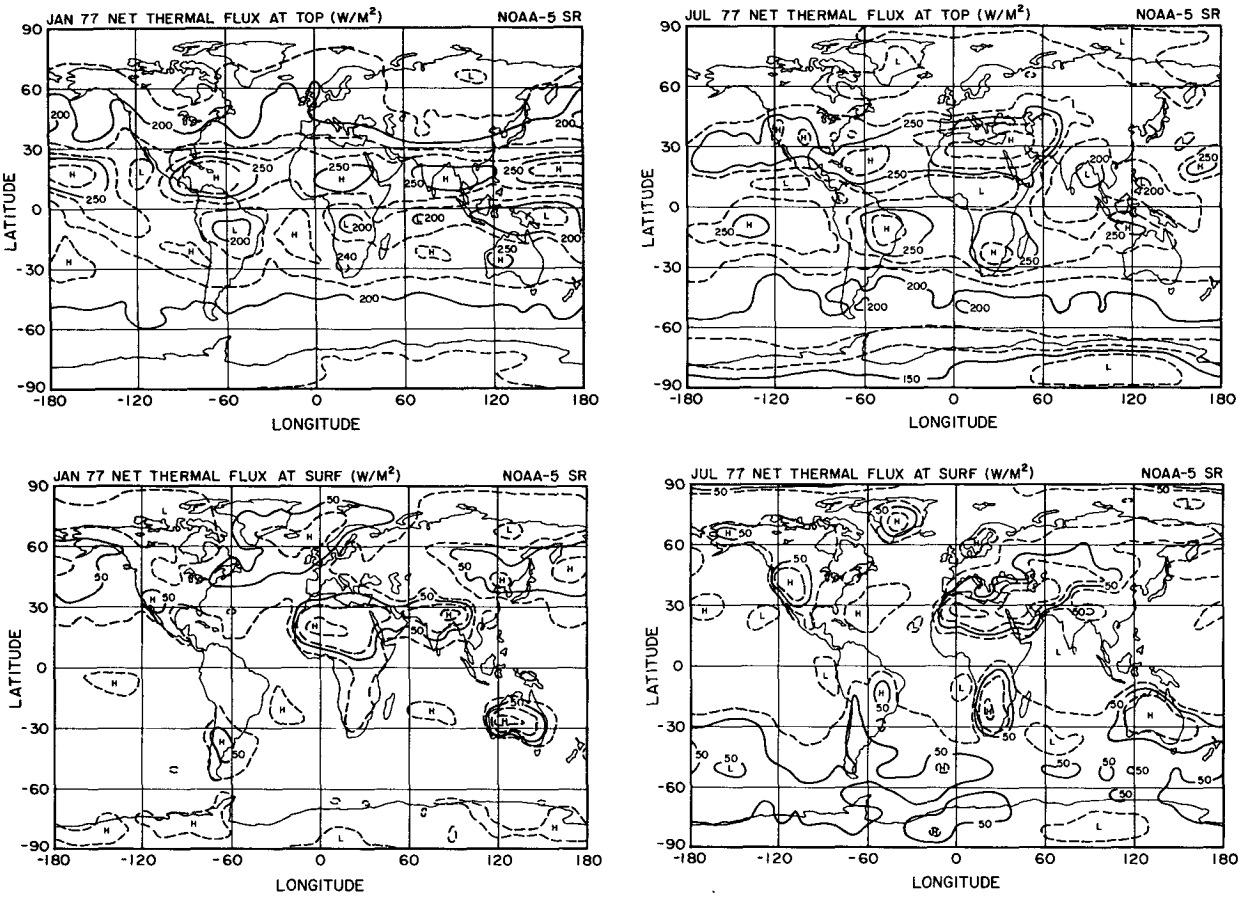

FIG. 17. Geographic distribution of net thermal cooling at TOA and SRF for January and July 1977. Local maxima and minima are indicated by H and L, respectively.

ference between cloudy and clear net solar heating is about 100 W m^{-2} at TOA and SRF while the difference in cloudy and clear net thermal cooling is about 30 W m^{-2} at TOA and 50 W m^{-2} at SRF), their total effect on this primary seasonal cycle is much more subtle. The predominantly zonal character of the seasonal change pattern in Fig. 19 indicates that the main cloud effect is to alter the equator-to-pole gradient and the magnitude of its seasonal variation of the net solar and thermal fluxes. (We do not have sufficient time resolution to determine the seasonal phases of the net fluxes.) The global radiation budget is summarized in Table 9.

Peak heating differences within the maximum change zone are seen at TOA and SRF in central-western Asia, over Alaska, and over Baffin Bay in the Northern Hemisphere, and over Argentina and the southern Atlantic–Indian Ocean storm tracks in the Southern Hemisphere. The line of zero seasonal change in net radiation runs nearly along the equator but is distorted by three significant features, especially at SRF: dipole patterns in the South American, African, and southeast Asian portions of the ITCZ. Northern-central Europe is unusual in being a local minimum of seasonal change at SRF but a local maximum at TOA. All of these features are caused by cloud variations.

The average magnitude of the net fluxes, shown in Fig. 18, is roughly 100 W m^{-2} at TOA and 150 watts/m^2 at SRF. The magnitude of the seasonal changes are somewhat larger at higher latitudes, about 150 W m^{-2}, and somewhat smaller at low latitudes, less than about 75 W m^{-2}. The comparison of ERB components to those inferred from Nimbus-7, together with comparisons of other estimates of global average flux balances and cloud effects, suggest an error in the reconstruction of the individual flux components that is at least 20 W m^{-2}. The error may be larger for some specific components, especially at SRF, since we do not have adequate validation data for the SRB. The geographic and seasonal patterns of the net radiation do correspond with our qualitative knowledge (e.g., Budyko 1974), implying that the errors do not eliminate information about cloud effects on the net radiation. In particular, small changes in net radiation are apparent at low latitudes, associated with well-known seasonal variations in the ITCZ.

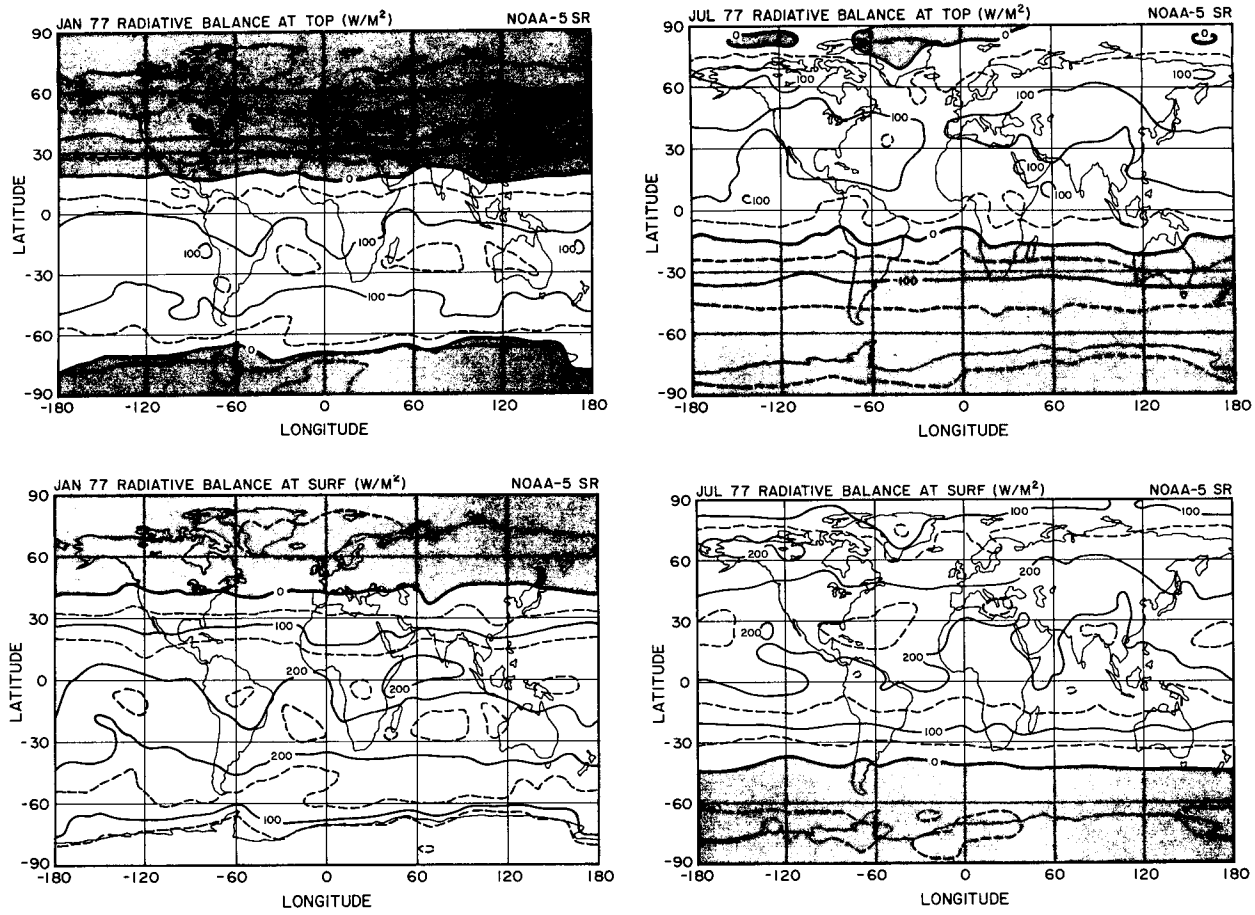

FIG. 18. Geographic distribution of net radiation at TOA and SRF for January and July 1977. Shading indicates regions of net cooling.

d. Comparison with a climate GCM

We compare our results, both the cloud and surface properties and the inferred ERB and SRB, with our climate GCM to illustrate some of the problems that are encountered in attempting the validation of such a model. Figure 20 shows the zonal, annual mean ERB and SRB as well as the net solar heating and net thermal cooling at TOA and SRF from the NOAA-5 results and from the GCM climatology. Table 9 summarizes this comparison for the global annual averages. The "greenhouse effect" of the atmosphere is revealed in the differences between the ERB and SRB: whereas the whole planet is in radiative equilibrium (ERB is zero to within our errors), with an equator/pole, heating/cooling contrast, the surface experiences net heating (nearly) everywhere (Fig. 20a); the global mean surface heating is 128 W m^{-2} (Table 9). This surface heating occurs despite the fact that the solar heating of the surface is somewhat less than the solar heating of the surface and atmosphere together, (Fig. 20b) because the net thermal cooling at SRF is so weak (Fig. 20c). The difference between the net solar heating at SRF and at TOA is larger in the tropics where there is more water vapor (Fig. 20b). The global net solar heating at TOA is decreased by more than 100 W m^{-2} by clouds that appears mostly as a change in the net solar heating at SRF (Table 9). The net thermal cooling of the surface also differs more from that at TOA in the tropics because of larger humidity (Fig. 20c). The global net thermal cooling at TOA is reduced by about 30 W m^{-2} by clouds; however, the reduction of global net thermal cooling at SRF is about 50 W m^{-2} (Table 9).

The rms differences between the NOAA-5 and GCM values of ERB are about 15 W m^{-2} with a bias of about 5 W m^{-2} in the global total; for SRB these differences are both about 25 W m^{-2}. The climate GCM exhibits smaller surface heating than in the NOAA-5 results by almost 25 W m^{-2}, caused about equally by weaker solar heating, especially in the Northern Hemisphere, and stronger thermal cooling, primarily at low latitudes. Both the GCM and the NOAA-5 results show a small residual flux imbalance at TOA (Table 9). (The particular control run used in this comparison is that for the century-long transient experiments, reported in Hansen et al. (1988) that calculates ocean surface tem-

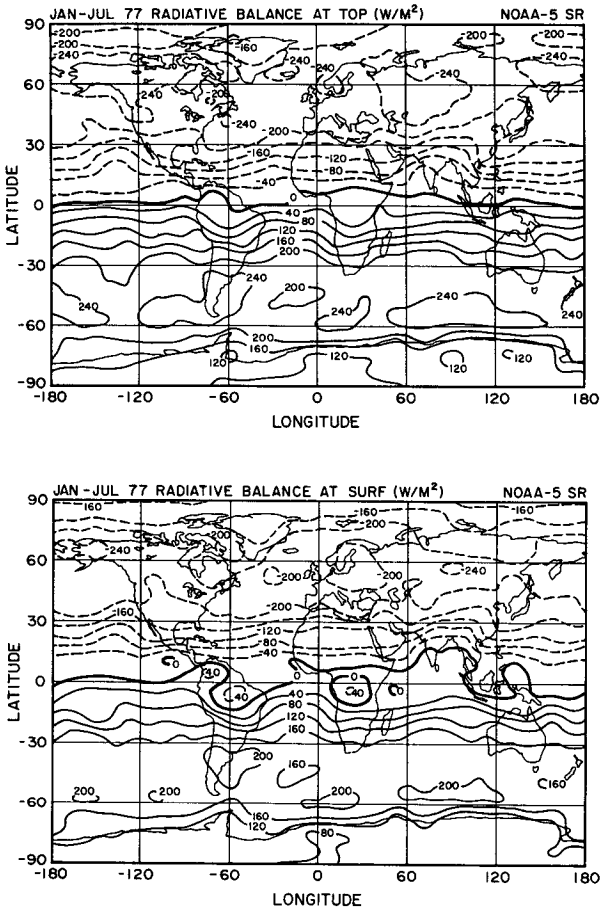

FIG. 19. Geographic distribution of differences in the January and July net radiation balances at the (a) TOA and (b) SRF.

peratures with the vertical and horizontal heat fluxes specified by current climatology).

Table 10 shows the partitioning of the net fluxes and ERB/SRB into "cloudy" and "clear" parts by showing the fraction of the global total heating/cooling provided by cloudy locations and times. The agreement of these values between the data and the GCM is quite good. The small differences between the NOAA-5 results and the GCM can be interpreted as small biases (assuming that the data are correct): 1) since the cloud cover is about the same in the data and model, the differences in surface insolation suggest that the average optical thickness of the model clouds is slightly higher than in the data, 2) that the cloudy contribution to the total reflected solar radiation is the same indicates a slightly higher surface albedo in the model as well, and 3) a lower net thermal cooling at TOA and a higher cooling at SRF suggests that the GCM clouds are slightly higher on average than in the data.

As with the radiation components themselves, the magnitude of the differences between the data and the GCM grows larger when examined at regional scale. Despite good agreement of the data and model for global mean and zonal mean cloud cover and ERB/SRB (annually averaged), Fig. 21 shows that the averaging hides larger differences (20–40 W m^{-2}) in the regional monthly mean distributions of these quantities. In Fig. 21a, the GCM has more highly cloudy regions in northern subtropics and midlatitudes than the data show but more regions with less clouds than the data in the tropics and southern subtropics. The former is caused by lower land-ocean cloud cover contrast in the model than in the data; the latter is caused by less variation of cloud cover between the ITCZ and the subtropical "clearings" over oceans in the model than in the data. Much of the dispersion in each latitude zone shown in Fig. 21a is caused by variations in the data-CC relative to a more zonally uniform model-CC.

Although both the data and model show a near-balance of ERB (Table 9), relatively more heating occurs in the subtropics in the data and less in the tropics and midlatitudes caused almost entirely by differences in cloud albedos (Fig. 21b). The stronger heating of Antarctica in the model than in the data, on the other hand, is caused by a smaller surface albedo in the model. At the surface (Fig. 21c) the data show more heating relative to the model at most latitudes generally associated with slightly higher cloud base altitudes in the model than in the data (which are determined by a fixed relation to cloud top altitudes). These differences in ERB/SRB also indicate larger variations of cloud cover and cloud optical properties in the data from region to region relative to the GCM.

TABLE 9. Annual global mean ERB, SRB, net solar heating and net thermal cooling from NOAA-5 analysis and from the GISS GCM climatology (values in parenthesis). "Cloudy" and "clear" quantities represent global values estimated by assuming completely clear or completely cloud conditions.

Quantity (w m^{-2})	Total	Cloudy	Clear	Total − clear	Cloudy − clear
ERB	12 (17)	−23 (−2)	51 (37)	−38 (−21)	−73 (−39)
SRB	128 (105)	95 (64)	163 (150)	−35 (−45)	−68 (−86)
Net Sol TOA	237 (222)	187 (166)	292 (284)	−55 (−63)	−105 (−119)
Net Sol SRF	169 (158)	113 (100)	231 (222)	−62 (−65)	−118 (−123)
Net Therm TOA	225 (205)	210 (168)	241 (247)	−16 (−42)	−31 (−79)
Net Therm SRF	41 (53)	17 (36)	67 (72)	−26 (−19)	−50 (−37)

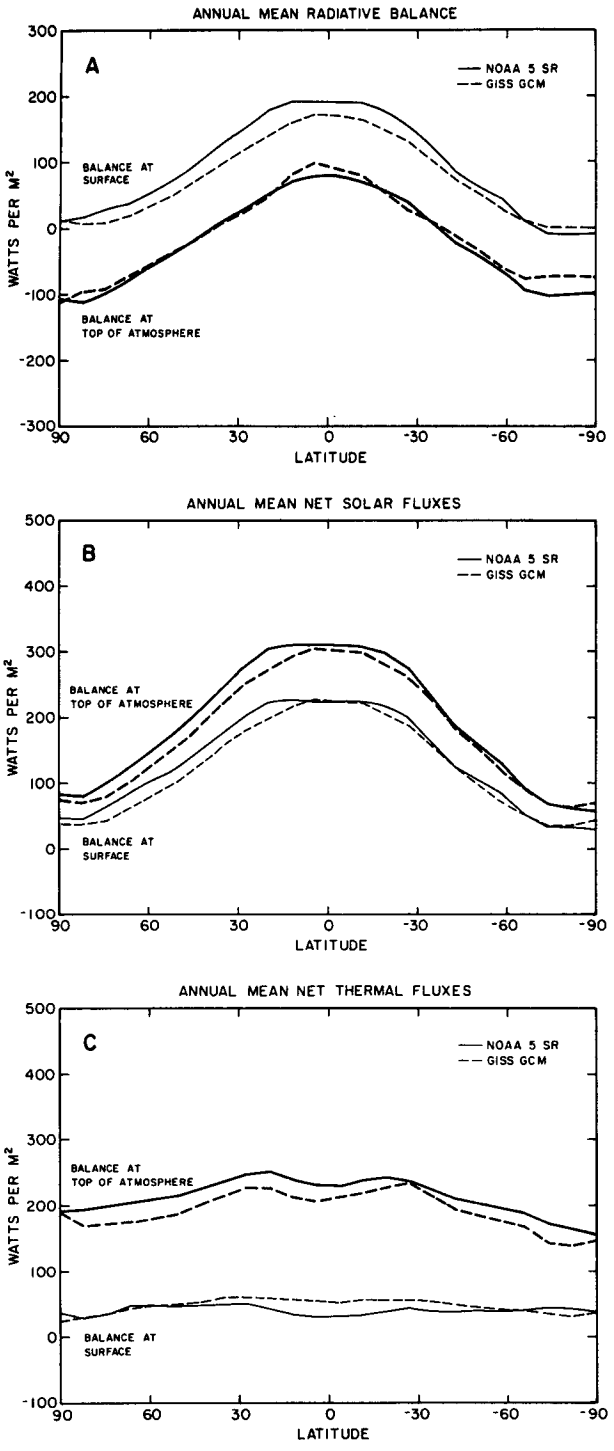

FIG. 20. Zonal annual mean (a) ERB and SRB, (b) net solar heating at TOA and SRF, and (c) net thermal cooling at TOA and SRF from NOAA-5 results (solid) and from the GISS climate GCM (dashed) (Hansen et al. 1983).

Overall, the regional differences, though explainable by differences between the model and NOAA-5 cloud and surface properties, are only slightly larger in magnitude than the differences between the NOAA-5 results and other corroborating information.

5. Summary

a. Cloud variability

1) MAGNITUDE AND COMPLEXITY OF VARIATIONS

The regional and seasonal variations of cloud optical properties (top temperatures and optical thicknesses) have been known qualitatively for some time, but never thoroughly surveyed over the globe. Most information in earlier datasets concerns cloud base heights (e.g., Warren et al. 1986, 1988) and some estimates of liquid water contents (e.g., Stephens and Webster 1981; Stephens and Platt 1987), but estimates of cloud optical thickness were limited by the availability of aircraft data and an inability to calculate the effects of the small scale variations of cloudiness. Information about cloud top temperatures is available from satellite data analyses (e.g., Minnis and Harrison 1984b; Stowe et al. 1989) but other information is restricted to simple empirical measures of cloud albedo. The kind of detailed analysis presented here seems capable of developing more useful information about optical thicknesses as well as cloud top temperatures.

Our results show that the magnitude of cloud property variations increases with decreasing scale from global and annual down to synoptic (regional $\approx$ 500–1000 km) and monthly scales. The magnitudes of seasonal variations at regional scales are generally large enough to resolve with this analysis; i.e., they are larger than the estimated analysis errors.

Cloud properties are systematically different between land and ocean: oceans have larger cloud cover with somewhat larger optical thicknesses and lower cloud top altitudes. These differences are probably biased by the limited diurnal sample of our data; however, they are also affected by the clouds that were missed, particularly low-level clouds over the ocean. Some of the largest seasonal variations of cloudiness occur in the tropics, even though the seasonal variations of the tropical surface albedo and temperature are the smallest. Cloudiness over tropical land areas undergoes larger seasonal variations than over tropical ocean areas. The largest seasonal changes of surface albedo and temperature occur at high latitudes, particularly over land, but the seasonal variations of clouds are much smaller, except near the equatorward edge of the storm track zones. The two hemispheres exhibit different styles of seasonal behavior at higher latitudes associated with their difference in land–ocean coverage. Simple linear differences between seasonal values of cloud and surface properties, as sometimes used to represent variations in climate studies, are not sufficient to describe what is actually happening even on a hemispheric or global basis (Fig. 3) since significant phase variations among different regions also occur (Fig. 8).

TABLE 10. Fractional contributions (percent) to annual global radiation from "cloudy" part from NOAA-5 analysis and from the GISS GCM (parentheses).

AREA	ERB	SRB	
52.3 (52.8)	−98 (−7)	39 (32)	
NET SOL TOA	DW SOL TOA	UP SOL TOA	
41 (39)	52.3 (52.8)	77 (77)	
NET SOL SRF	DW SOL SRF	UP SOL SRF	
35 (33)	35 (33)	36 (33)	
NET THERM TOA	NET THERM SRF	UP THERM SRF	DW THERM SURF
49 (43)	22 (36)	52 (53)	56 (56)

2) DIFFICULTY OF OBSERVATION/INTERPRETATION

Resolution of the primary scales of variation and completeness of coverage of the space/time domain appear to be crucial to obtaining accurate global and annual averages since a large cancellation of regional variations when forming space/time averaged quantities is apparent. Even though we seem to have sufficient skill to measure the larger regional variations, we do not know that the errors in "local" measurements cancel sufficiently in global/monthly averages to produce an accurate average result.

Proper detection of marginal cloud types in satellite radiance data, such as cirrus and marine stratus, depends on the threshold logic and threshold magnitudes used, which in turn depend on how accurately the clear radiances can be determined. The estimated amounts of these cloud types are probably too low in these results. The requirement for detection in both spectral bands (visible and infrared), necessitated by errors in inferring the clear radiances, is not a good idea since it causes our analysis to miss thinner cirrus that are not detected in VIS and the lower level and more broken clouds that are not detected in IR. If the accuracy of these clear radiances can be improved then more sensitive cloud detection is possible with current satellite data. Note that measurements at 0.6 μm and 11 μm are crucial since the radiance changes produced by clouds are largest at these wavelengths. An alternative is to find some nearly unique spectral signature of clouds that allows their detection in cases where the radiance differences are ambiguous (especially in the polar regions, c.f., Inoue 1987; Yamanouchi 1989); however, this approach requires new satellite instruments to obtain global, diurnal coverage. Global measurements are still made only at visible and "window" IR wavelengths (cf., Schiffer and Rossow 1983).

Available validation data are not adequate to challenge the accuracy of this type of analysis further: these results from satellite measurements already appear to have similar accuracy to other results. In effect, satellite observations of clouds may be more like a new measurement that has no independent validation but must be confirmed from "internal evidence," sensitivity studies, and subsequent "spot checks" of subsets of the observations. The ISCCP plans (WCP 1986) include all of these elements.

3) LIMITATIONS OF THESE DATA

The primary limitations of these particular results are underestimates of cirrus and marine stratus cloud amounts, lack of diurnal coverage, and coarse seasonal resolution. The limited diurnal sample probably affects the estimates of land/ocean contrasts, at least, and the coarse seasonal resolution limits the measurement of seasonal phase differences among regions and between the hemispheres.

The spatial resolution of the satellite data (25–100 km) appears sufficient to resolve the main scales of variation (cf., Sèze and Rossow 1990b); however, the effects of smaller scale cloud variations on the retrieved optical parameters are not yet understood.

b. Variations of radiation budget

1) MAGNITUDE AND COMPLEXITY OF VARIATIONS

The regional and seasonal variations of ERB/SRB have been known qualitatively for some time (e.g., Budyko 1974); only ERB is being thoroughly surveyed by satellite missions like Nimbus-6/7 (Jacobowitz et al. 1984) and ERBE (Barkstrom and Smith 1986). The kind of analysis of satellite and surface data presented here also seems capable of providing quantitatively accurate, global surveys of ERB and may be capable of doing the same for SRB but more work is necessary to confirm this. The main advantage of reconstructing ERB/SRB from atmospheric, cloud, and surface datasets, compared to their direct measurement, is that the roles of all these components of the climate

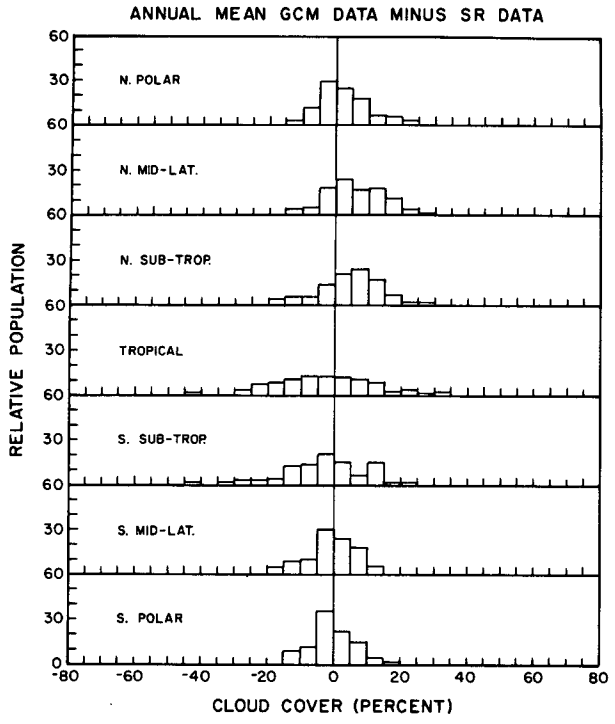

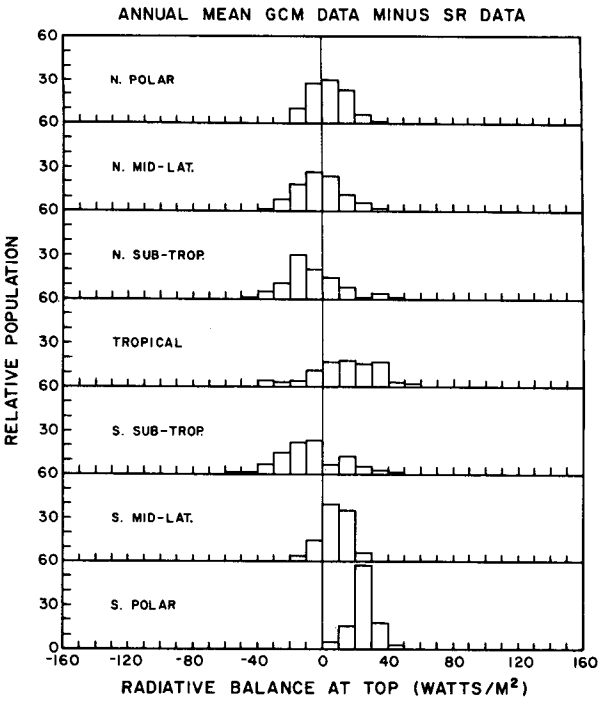

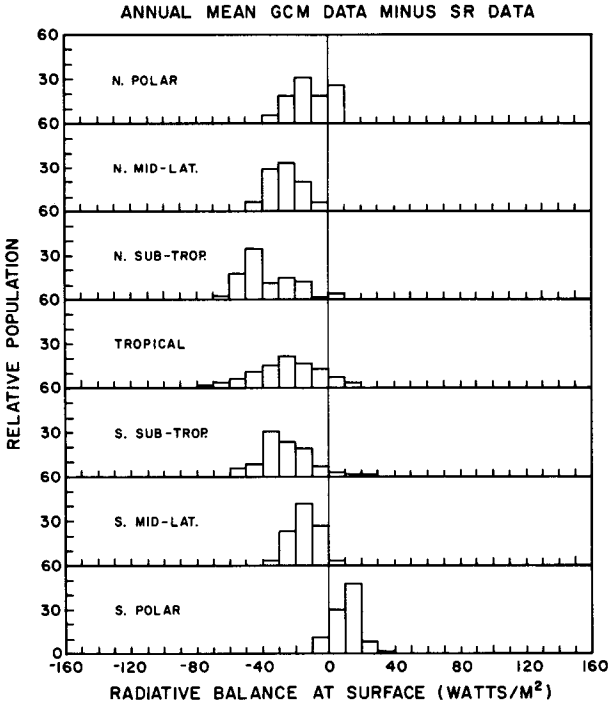

FIG. 21. Distribution of differences of annual mean (a) cloud cover, (b) ERB, and (c) SRB between the GISS climate GCM and the NOAA-5 analysis for 7.5° × 10° region in seven latitude zones: N Polar (90°N–60°N), N Midlatitude (60°N–30°N), N Subtropical (30°N–15°N), Tropical (15°N–15°S), S Subtropical (15°S–30°S), S Midlatitude (30°S–60°S) and S Polar (60°S–90°S). Positive values indicate larger values in the GCM than in NOAA-5 results.

system can then be diagnosed separately. Moreover, the effect of variations in specific cloud properties can be isolated to link them to the physical processes that form clouds.

Our results show that the magnitude of seasonal radiative flux variations increases going from global to regional scale. There is also significant cancellation among variations of the individual flux components of ERB/SRB such that changes in net fluxes and heating/cooling rates caused by cloud variations are much smaller than changes in the individual fluxes. Regional flux variations are caused by a complex interplay of changes in the atmosphere/surface and in clouds. Cloud type variations among the climate zones produce

different relations between cloud amount changes and ERB/SRB changes. Moreover, the context of such changes, determined by the atmospheric and surface properties, also changes the role of cloud variations: *even globally uniform variations of uniform clouds would not produce a globally uniform variation of the radiative fluxes.* Thus, a multivariate analysis like ours seems necessary to deduce the role of clouds in ERB/SRB.

The largest seasonal changes in net radiation occur in the 30°–60° zone in each hemisphere; the polar regions undergo a somewhat smaller seasonal change while the tropics undergo only a very small variation. The dominant reason for the seasonal variation of net radiation in the tropics is changes in the location of the convective cloud complexes; however, some changes in their properties, especially over the oceans, also contribute to the seasonal variations. The large cloud effects on individual flux components cancel almost completely when combined into the net flux. The dominant reasons for seasonal variations of net radiation at higher latitudes are changes in the solar declination and atmospheric temperature. Cloud variations serve only to modulate these basic effects somewhat and can enhance or mute the seasonal flux variations. Longitudinal changes in net radiation at higher latitudes, caused by land/ocean contrasts and the seasonal variation of land properties, are muted by the variations of cloud cover and optical properties. The net effects on latitudinal gradients of radiation are less clear. The differences in seasonal behavior between the hemispheres are associated with the difference in their land/ocean fractions.

Significant cancellation of variations of the individual flux components and the net fluxes occurs when averaging in space and time because the phases and amplitudes of their variations differ from region to region. The changing global summation of regional net radiation changes produces a "noisy" seasonal variation of the global mean values and could be one source of interannual variability. Whether this variation is just "statistical" noise, because the regional changes are nearly independent and random, or whether regional coupling (telecommunication) is strong enough that the global climate undergoes nonlinear oscillations, remains to be determined from longer-term datasets.

2) Difficulty of observation/interpretation

ERB can be constructed about as well as it can be verified with this type of comparison where we compare one particular year with another or with an average of several. Cancellation in forming average radiation quantities may mean that their use in validation studies is not definitive. Comparisons with simultaneous, collocated observations and relatively high space/time resolution are needed to further improve the validation accuracy.

The comparison of our results with other observations and with a climate GCM shows that the changes in ERB/SRB produced by clouds, that are the feedbacks on the seasonal temperature cycle, are similar in magnitude to the estimated uncertainties in both the reconstruction of ERB/SRB and their calculation by climate models. Thus, diagnosis of cloud-radiative feedbacks remains a challenging task.

Some of the key issues in the reconstruction of ERB/SRB from satellite cloud data are:

a) fidelity of the angular and spectral representation of the radiative properties of the surface and clouds in both the narrowband radiance retrieval models and the total flux models (atmospheric properties and radiative effects are probably adequately modeled),

b) completeness and accuracy of input and validating datasets, and

c) space/time sampling and averaging of input and validating datasets.

c. Cloud effects on radiation budget

Clouds cause net cooling of the current annual, global mean climate. This result has been known qualitatively for some time (e.g., Manabe and Strickler 1964).

Our results show that cloud radiative feedbacks on the seasonal temperature cycle involve complex, regionally varying relationships and cloud type dependences. The cloud properties do not all act in concert on the radiation fluxes nor do their effects vary with the same amplitudes and phases. The summation of all these regional variations produces global changes that cannot be described by simple, linear correlations. Figure 22 shows the relations of seasonal variations of the net solar and thermal fluxes at TOA with cloud cover, TAU and TC. The hemispheric mean, net solar flux increases with increasing CC, contrary to most expectations since the related variations in TAU are more important. However, the different amplitudes and phases of the hemispheric changes produce a semiannual relationship and qualitatively different effects of increasing CC and TAU in the global mean. The seasonal behavior of the hemispheric mean, net thermal fluxes is completely different between the land-dominated north and the ocean-dominated south; the global mean net thermal flux is not related to either CC or TC in a simple way.

Figure 23 shows the seasonal variations of ERB and SRB with surface temperature and cloud cover. Both hemispheres show an increase of ERB/SRB (net heating) in summer, i.e., increased TS is associated with net heating as one would expect. However, differences in seasonal amplitude and phase between the hemispheres produce the opposite relationship for global

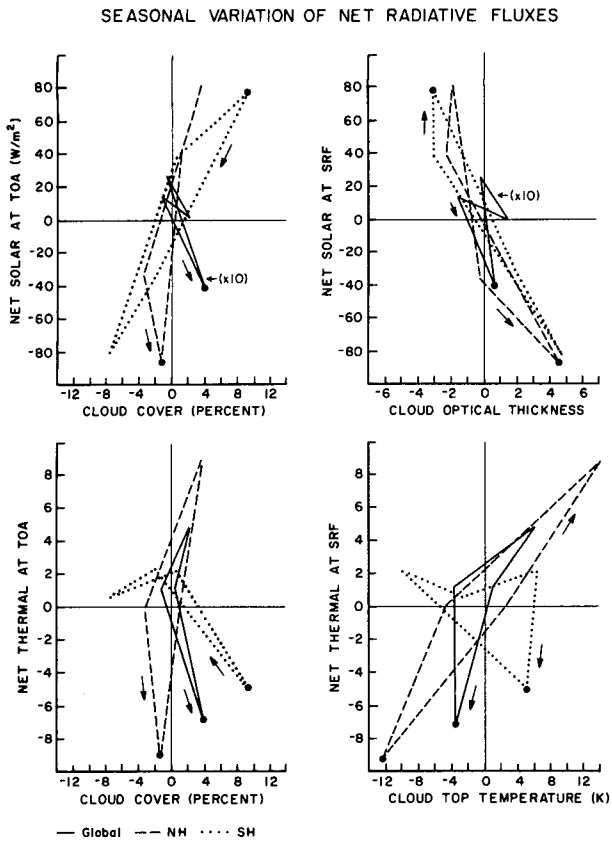

FIG. 22. Phase diagrams of the seasonal variations of net radiative fluxes at TOA for the whole globe (solid) and for the Northern/Southern Hemispheres (dashed/dotted). Deviations from global annual mean values are shown for net solar flux versus cloud cover (upper left), net solar flux versus cloud optical thickness (upper right), net thermal flux versus cloud cover (lower left) and net thermal flux versus cloud top temperature (lower right). The large dots indicate values for January and the arrows indicate the progression of time. The (×10) on the global curves refers to the vertical scale only.

ERB even though the same relation holds for SRB. The relationship of seasonal variations of ERB/SRB with those of CC approximates a linear correlation for hemispheric averages but exhibits a more complex variation for global averages.

The complex regional behavior suggests that the effect of cloud changes on seasonal temperature cycles can only be described as multiple feedbacks rather than a single "cloud feedback." There may also be no meaningful "global" cloud feedback since cloud property variations are not simple functions of global surface temperature either. Whether the fundamentally different radiative consequences of cloudiness variations at lower and higher latitudes can be attributed to a single kind of cloud response to forcing remains to be seen; however, separating the effects of clouds from those of the atmosphere and surface is absolutely essential to identification of any such general cloud behavior. This kind of diagnosis will also be necessary to determine whether the behavior of clouds, observed at short time scales (days to seasons), can be extended to climate changes.

Our preliminary evaluation of cloud effects on the radiation budget is in the form of monthly differences between radiative fluxes with and without clouds. This approach can indicate the order of magnitude of cloud effects, which shows that the magnitudes of cloud modulations of the large seasonal changes are only a little larger than the uncertainties in the analysis. Since there are significant cancellations in the global mean because of the regional phase differences, the global mean results may not be reliable. Thus, we did not pursue the determination of cloud-radiative feedbacks further.

d. Verification of GCM parameterizations of clouds and radiation

The differences between the reconstructed ERB/SRB and the climate GCM calculations are only a little

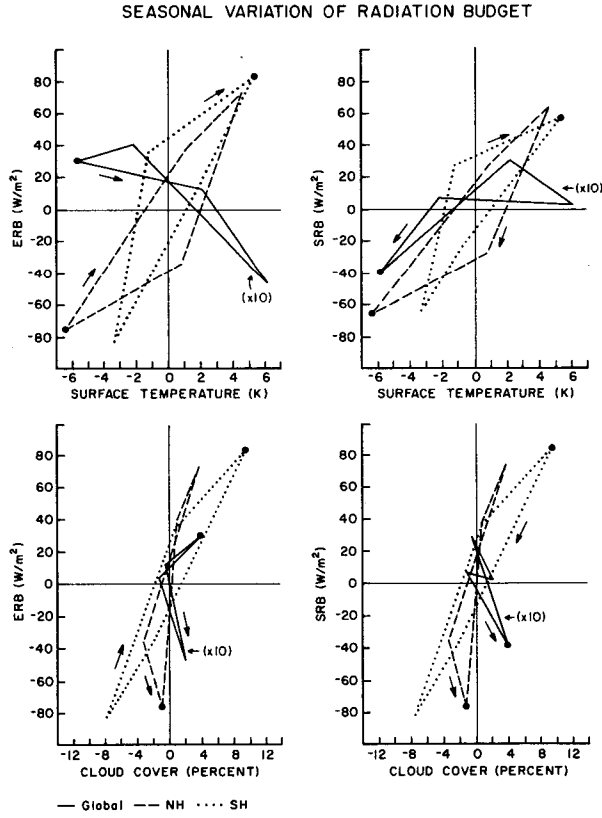

FIG. 23. Phase diagrams of the seasonal variations of ERB (left) and SRB (right) versus surface temperature (upper) and cloud cover (lower) for the whole globe (solid) and the Northern/Southern hemispheres (dashed/dotted). Changes are shown as deviations from global annual mean values. The large dots indicate values for January and the arrow indicates the progression of time. The (×10) on the global curves applies to both vertical and horizontal scales; i.e., the global variations are more than an order of magnitude smaller than the hemispheric variations.

larger in magnitude than the uncertainties in the ERB/SRB analysis and its differences with available validation. There are also a number of model/data analysis details that must be worked out to insure that the same quantities are being compared. In particular, the effective properties of the clouds and surface that can be retrieved from satellite data analyses are different from the parameters that can be retrieved from GCM diagnostics. The most notable example is the overlap assumption required to convert individual GCM layer cloud amounts and optical properties into the quantities as viewed from the satellites. Future GCM cloud diagnostics must be made consistent with quantities retrieved from satellite measurements. These include diurnal cycle statistics, frequency distributions of cloud top pressures, corresponding optical thickness distributions (weighted so as to preserve monthly cloud albedos) and cloud base pressure distributions. The latter quantity is needed for more accurate computations of SRB but is not currently available from satellite measurements. Other examples, such as the relation between the surface and cloud temperatures and their IR emissions, can usually be handled by redefining the diagnostic quantities already output by GCMs.

Some detailed differences between the GISS climate GCM and the data are, nevertheless, apparent at this stage. On average, the GCM clouds have higher mean optical thicknesses and altitudes than implied by the data, reducing net solar heating and increasing net thermal cooling (the cloud base altitude assumed in the data analysis is not necessarily more accurate than that calculated by the GCM, however). Moreover, the GCM cloudiness does not exhibit regional and seasonal contrasts that are as large as shown in the data.

Thus, to make more progress on improving our knowledge of cloud–radiation interactions and our ability to model it, we need better datasets, both for describing the attributes of the atmosphere, surface, and clouds and for validating calculations of ERB/SRB from such data. Needed improvements suggested by this study are: 1) more complete time coverage in the satellite and atmosphere/surface data (diurnal to interannual), 2) more information about clouds, especially cloud base locations and vertical structure, 3) more information about surface properties (temperature, snow and ice cover, angular and spectral dependences of optical properties) and 4) coincident, collocated observations for ERB/SRB validation data with similar space/time resolution and space/time coverage. The combination of ISCCP and ERBE data, augmented by SRB observations and improved surface/atmosphere measurements, can provide this improved dataset.

Acknowledgments. Key parts of the analysis presented here were carried out by E. Kinsella with the assistance of S. Chan (clouds) and P. J. Lu (radiation). M-S. Yao developed the first version of the software to calculate total radiation fluxes using the climate GCM radiation subroutines. Additional cloud data analyses were performed by L. C. Garder. We thank B. A. Carlson for comments on the manuscript; we also thank A. Henderson-Sellers and J. Curry for thoughtful reviews. Photographs were created using software written by J. Jonas and hardcopy was produced by P. Palmer. Graphics were drawn by L. Del Valle; word processing was done by E. Devine. Support for this research was provided by the NASA Climate Program managed by Robert Schiffer.

REFERENCES

Ardanuy, P. E., L. L. Stowe, A. Gruber, M. Weiss and C. S. Long, 1989: Longwave cloud radiative forcing as determined from Nimbus-7 observations. *J. Climate,* **2,** 766–799.

Barkstrom, B. R., and G. L. Smith, 1986: The Earth Radiation Budget Experiment: Science and implementation. *Rev. Geophys.,* **24,** 379–390.

Barton, I. J., 1983: Dual channel satellite measurements of sea surface temperature. *Quart. J. Roy. Meteor. Soc.,* **109,** 365–378.

Berlyand, T. G., and L. A. Strokina, 1980: Zonal cloud distribution on the Earth. *Meteor. Gidrol.,* **3,** 15–23.

Bess, T. D., G. L. Smith and T. P. Charlock, 1989: A ten-year monthly data set of outgoing longwave radiation from Nimbus-6 and Nimbus-7 satellites. *Bull. Amer. Meteor. Soc.,* **70,** 480–489.

Broecker, W. S., 1987: The biggest chill. *Natural History,* **96,** 74–81.

Budyko, M. I., *Climate and Life.* D. H. Miller, English Ed., Academic Press, 508 pp.

Cess, R. D., 1976: Climate change: An appraisal of atmospheric feedback mechanisms employing zonal climatology. *J. Atmos. Sci.,* **33,** 1831–1843.

——, B. P. Briegleb and M. S. Lian, 1982: Low-latitude cloudiness and climate feedback: Comparative estimates from satellite data. *J. Atmos. Sci.,* **39,** 53–59.

Desbois, M., and G. Sèze, 1984: Use of space and time sampling to produce representative satellite cloud classifications. *Ann. Geophys.,* **2**(5), 599–606.

Fortuna, J. F., and L. N. Hambrick, 1974: *The Operation of the NOAA Polar Satellite System.* NOAA Tech. Memo. NESS 60, U.S. Dept. of Commerce, Washington, DC, 127 pp.

Garand, L., 1988: Automated recognition of oceanic cloud patterns. Part I: Methodology and application to cloud climatology. *J. Climate,* **1,** 20–39.

GARP, 1975: *The Physical Basis of Climate and Climate Modeling.* GARP Publ. Ser. No. 16, 265 pp.

——, 1978: *JOC Study Conf. on Parameterization of Extended Cloudiness and Radiation for Climate Models.* Oxford, England, GARP Climate Dynamics Sub-programme, World Meteorological Organization, 37 pp.

Gates, W. L., and A. B. Nelson, 1975: A new (revised) tabulation of the Scripps topography on a 1° global grid. Part I: Terrain heights. Rep. R-1276-1-ARPA, Rand Corp., Santa Monica, 132 pp.

Gordon, A. L., 1987: Interocean exchange of thermocline water. *J. Geophys. Res.,* **91,** 5037–5046.

Hahn, C. J., S. G. Warren, J. Gordon, R. M. Chervin and R. Jenne, 1982: *Atlas of Simultaneous Occurrence of Different Cloud Types over Ocean.* NCAR Tech. Note TN-201+STR, National Center for Atmospheric Research, Boulder, 212 pp.

——, ——, ——, —— and ——, 1984: *Atlas of Simultaneous Occurrence of Different Cloud Types over Land.* NCAR Tech. Note TN-241+STR, National Center for Atmospheric Research, Boulder, 211 pp.

Hansen, J. E., and L. D. Travis, 1974: Light scattering in planetary atmospheres. *Space Sci. Rev.,* **16,** 527–610.

——, G. Russell, D. Rind, P. Stone, A. Lacis, L. Travis, S. Lebedeff and R. Ruedy, 1983: Efficient three-dimensional global models

for climate studies: Models I and II. *Mon. Wea. Rev.*, **111**, 609–662.

——, A. Lacis, D. Rind, G. Russell, P. Stone, I. Fung, R. Ruedy and J. Lerner, 1984: Climate sensitivity: Analysis of feedback mechanisms. Climate processes and climate sensitivity. *Geophys. Monogr.*, **29** (*Maurice Ewing*, 5), Amer. Geophys. Union, 130–163.

——, I. Fung, A. Lacis, D. Rind, S. Lebedeff, R. Ruedy, G. Russell and P. Stone, 1988: Global climate changes as forecast by Goddard Institute for Space Studies three-dimensional model. Climate Processes and Climate Sensitivity. *J. Geophys. Res.*, **93**, 9341–9364.

Hartmann, D. L., and D. A. Short, 1980: On the use of earth radiation budget statistics for studies of clouds and climate. *J. Atmos. Sci.*, **37**, 1233–1250.

——, V. Ramanathan, A. Berroir and G. E. Hunt, 1986: Earth radiation budget data and climate research. *Rev. Geophys.*, **24**, 439–468.

Henderson-Sellers, A., 1986: Layer cloud amounts for January and July 1979 from 3D-nephanalysis. *J. Climate Appl. Meteor.*, **25**, 118–132.

Hilsenrath, E., and B. M. Schlesinger, 1981: Total ozone seasonal and interannual variations derived from the 7 year Nimbus-4 BUV dataset. *J. Geophys. Res.*, **86**, 12 087–12 096.

——, D. F. Heath and B. M. Schlesinger, 1979: Seasonal and interannual variations in total ozone revealed by the Nimbus 4 Backscattered Ultraviolet Experiment. *J. Geophys. Res.*, **84**, 6969–6979.

Hughes, N. A., 1984: Global cloud climatologies: A historical review. *J. Climate Appl. Meteor.*, **23**, 724–751.

——, and A. Henderson-Sellers, 1985: Global 3D-nephanalysis of total cloud amount: Climatology for 1979. *J. Climate Appl. Meteor.*, **24**, 669–686.

Inoue, T., 1987: A cloud type classification with NOAA 7 split-window measurements. *J. Geophys. Res.*, **92**, 3991–4000.

Jacobowitz, H., R. J. Tighe and the NIMBUS 7 ERB Experiment Team, 1984: The earth radiation budget derived from the NIMBUS 7 ERB Experiment. *J. Geophys. Res.*, **84**, 4997–5010.

Kistler, R. E., and D. F. Parrish, 1982: Evolution of the NMC data assimilation system: September 1978–January 1982. *Mon. Wea. Rev.*, **110**, 1335–1346.

Klitch, M. A., J. F. Weaver, F. P. Kelly and T. H. Vonder Haar, 1985: Convective cloud climatologies constructed from satellite imagery. *Mon. Wea. Rev.*, **113**, 326–337.

Lacis, A. A., and J. E. Hansen, 1974: A parameterization for the absorption of solar radiation in the Earth's atmosphere. *J. Atmos. Sci.*, **31**, 118–133.

——, and V. Oinas, 1990: A description of the correlated k-distribution method for modeling non-grey gaseous absorption, thermal emission, and multiple scattering in vertically inhomogeneous atmospheres. *J. Geophys. Res.*, in press.

Lamb, H. H., 1972: *Climate: Present, Past and Future. Vol. I: Fundamentals and Climate Now.* Methuen, 613 pp.

London, J., 1957: *A Study of Atmospheric Heat Balance.* Final Report, Contract AF19(122)-165, AFCRC-TR-57-287, College of Engineering, New York University, 99 pp.

Manabe, S., and R. F. Strickler, 1964: Thermal equilibrium of the atmosphere with a convective adjustment. *J. Atmos. Sci.*, **21**, 361–385.

Masaki, G. T., 1972 (rev 1976): *The Wolf Plotting and Contouring Package.* GSFC Computer Program Lib. No. A00227, Computer Sciences Corporation, NASA Goddard Space Flight Center, 187 pp.

Matthews, E., 1983: Global vegetation and land use: New high resolution data bases for climate studies. *J. Climate Appl. Meteor.*, **22**, 474–487.

——, 1985: *Atlas of Archived Vegetation, Land-use and Seasonal Albedo Data Bases.* NASA Tech. Memo. 86199, 53 pp.

——, and W. B. Rossow, 1987: Regional and seasonal variations of surface reflectance from satellite observations at 0.6 μm. *J. Climate Appl. Meteor.*, **26**, 170–202.

McPherson, R. D., K. H. Bergman, R. E. Kistler, G. E. Rasch and D. S. Gordon, 1979: The NMC operational global data assimilation system. *Mon. Wea. Rev.*, **107**, 1445–1461.

Minnis, P., and E. F. Harrison, 1984a: Diurnal variability of regional cloud and clear sky radiative parameters derived from GOES data. Part I: Analysis method. *J. Climate Appl. Meteor.*, **23**, 993–1011.

——, and ——, 1984b: Diurnal variability of regional cloud and clear sky radiative parameters derived from GOES data. Part II: November 1978 cloud distributions. *J. Climate Appl. Meteor.*, **23**, 1012–1031.

——, and ——, 1984c: Diurnal variability of regional cloud and clear sky radiative parameters derived from GOES data. Part III: November 1978 radiative parameters. *J. Climate Appl. Meteor.*, **23**, 1032–1051.

NOAA, 1977: *Environmental Satellite Imagery.* January, April, July, October 1977. NOAA/NESS Environmental Data Service, National Oceanic and Atmospheric Administration, U.S. Department of Commerce, Washington, DC.

Ohring, G., and P. Clapp, 1980: The effect of changes in cloud amount on the net radiation at the top of the atmosphere. *J. Atmos. Sci.*, **37**, 447–454.

Oort, A. H., 1983: *Global Atmospheric Circulation Statistics, 1958–1973.* NOAA Prof. Pap. 14, NOAA Geophysical Fluid Dynamics Laboratory, U.S. Dept. of Commerce, 180 pp.

Oxford World Atlas, 1973: S. G. Cohen, Ed., Oxford University Press, 190 pp.

Parikh, J., and J. T. Ball, 1980: Analyses of cloud type and cloud amount during GATE from SMS infrared data. *Remote Sens. Environ.*, **9**, 225–245.

Platt, C. M. R., J. C. Scott and A. C. Dilley, 1987: Remote sounding of high clouds. Part III: Optical properties of midlatitude and tropical cirrus. *J. Atmos. Sci.*, **44**, 729–747.

Ramanathan, V., 1987: The role of Earth radiation budget studies in clouds and general circulation research. *J. Geophys. Res.*, **92**, 4075–4095.

——, R. D. Cess, E. F. Harrison, P. Minnis, B. R. Barkstrom, E. Ahmad and D. Hartmann, 1989: Cloud-radiative forcing and climate: Results from the Earth Radiation Budget Experiment. *Science*, **243**, 57–63.

Raschke, E., T. H. Vonder Haar, W. R. Bandeen and M. Pasternak, 1973: The annual radiation balance of the Earth-atmosphere system during 1967–70 from NIMBUS 3 measurements. *J. Atmos. Sci.*, **30**, 341–364.

Rosen, R. D., and D. A. Salstein, 1980: A comparison between circulation statistics computed from conventional data and NMC Hough analyses. *Mon. Wea. Rev.*, **108**, 1226–1247.

Rossow, W. B., (Ed), 1981: Clouds in climate: Modeling and satellite observational studies. Report of workshop held at NASA Goddard Institute for Space Studies, 29–31 Oct. '80. New York, 222 pp.

——, 1989: Measuring cloud properties from space: A review. *J. Climate*, **2**, 201–213.

——, and R. A. Schiffer, 1991: ISCCP cloud data products. *Bull. Amer. Meteor. Soc.*, in press.

——, L. C. Garder and A. A. Lacis, 1989a: Global, seasonal cloud variations from satellite radiance measurements. Part I: Sensitivity of analysis. *J. Climate*, **2**, 419–458.

——, C. L. Brest and L. C. Garder, 1989b: Global, seasonal surface variations from satellite radiance measurements. *J. Climate*, **2**, 214–247.

Saunders, R. W., 1986: An automated scheme for the removal of cloud contamination from AVHRR radiances over western Europe. *Int. J. Remote Sens.*, **7**, 867–886.

Schiffer, R. A., and W. B. Rossow, 1983: The International Satellite Cloud Climatology Project (ISCCP): The first project of the World Climate Research Program. *Bull. Amer. Meteor. Soc.*, **64**, 779–784.

——, and ——, 1985: ISCCP global radiance dataset: A new resource for climate research. *Bull. Amer. Meteor. Soc.*, **66**, 1498–1505.

Schutz, C., and W. L. Gates, 1971a: *Global Climatic Data for Surface,*

800 mb and 400 mb: January. A report prepared for Advanced Research Projects Agency, RAND, Santa Monica, R-915-ARPA, 21 pp.

——, and ——, 1971b: *Global Climatic Data for Surface, 800 mb and 400 mb: July.* A report prepared for Advanced Research Projects Agency, RAND, Santa Monica, CA, R-1029-ARPA, 22 pp.

Scorer, R., 1972: *Clouds of the World.* Lothian, 176 pp.

Sèze, G., and W. B. Rossow, 1990a: Time-cumulated visible and infrared radiance histograms used as descriptors of surface and cloud variations. *Int. J. Remote Sens.*, in press.

——, and ——, 1990b: Effects of satellite data resolution on measuring the space/time variations of surfaces and clouds. *Int. J. Remote Sens.*, in press.

Slingo, A., R. C. Wilderspin and R. N. B. Smith, 1989: Effect of improved physical parameterizations on simulations of cloudiness and the Earth's radiation budget. *J. Geophys. Res.*, **94,** 2281–2301.

Smith, F. A., and M. R. Smith, 1987: *Atlas of Earth Radiation Budget Measurements from NIMBUS 7 ERB, 1979–1983.* Florida State University, 254 pp.

Somerville, R. C. J., and L. A. Remer, 1984: Cloud optical thickness feedbacks in the CO2 climate problem. *J. Geophys. Res.*, **89,** 9668–9672.

Stephens, G. L., 1988: Radiative transfer through arbitrarily shaped optical media, II: Group theory and simple closures. *J. Atmos. Sci.*, **45,** 1837–1848.

——, and C. M. R. Platt, 1987: Aircraft observations of the radiative and microphysical properties of stratocumulus and cumulus cloud fields. *J. Climate Appl. Meteor.*, **26,** 1243–1269.

——, and P. J. Webster, 1981: Clouds and climate: Sensitivity of simple systems. *J. Atmos. Sci.*, **38,** 235–247.

Stowe, L. L., C. G. Wellemeyer, T. F. Eck, H. Y. M. Yeh and the NIMBUS-7 Cloud Data Processing Team, 1988: Nimbus-7 global cloud climatology. Part I: Algorithm and validation. *J. Climate,* **1,** 445–470.

——, H. Y. M. Yeh, T. F. Eck, C. G. Wellemeyer, H. L. Kyle and the NIMBUS-7 Cloud Data Processing Team, 1989: Nimbus-7 global cloud climatology. Part II: First year results. *J. Climate,* **2,** 671–709.

Telegadas, K., and J. London, 1954: *A Physical Model of the Northern Hemisphere Troposphere for Winter and Summer.* Sci. Rep. No. 1, AF19(122)-165, New York University, 55 pp.

Tian, L., and J. A. Curry, 1989: Cloud overlap statistics. *J. Geophys. Res.*, **94,** 9925–9935.

Van Loon, H., 1972: *Cloudiness and Precipitation in the Southern Hemisphere. Meteorology of the Southern Hemisphere.* Meteor. Monogr. No. 13, C. W. Newton, Ed., 101–104.

Wang, W-C., W. B. Rossow, M-S. Yao and M. Wolfson, 1981: Climate sensitivity of a one-dimensional radiative-convective model with cloud feedback. *J. Atmos. Sci.*, **38,** 1167–1178.

Warren, S. G., C. J. Hahn and J. London, 1985: Simultaneous occurrence of different cloud types. *J. Climate Appl. Meteor.*, **24,** 658–667.

——, ——, ——, R. M. Chervin and R. L. Jenne, 1986: *Global Distribution of Total Cloud Cover and Cloud Type Amounts Over Land.* NCAR Tech. Note NCAR/TN-273+STR (also DOE/ER/60085-H1), 29 pp., plus 200 maps.

——, ——, ——, —— and ——, 1988: *Global Distribution of Total Cloud Cover and Cloud Type Amounts Over Ocean.* NCAR Tech. Note NCAR/TN-317+STR, National Center for Atmospheric Research, 42 pp. plus 170 maps.

WCP, 1986: *International Satellite Cloud Climatology Project (ISCCP) Research Plan and Validation Strategy.* WMO/TD-No. 88, Supplement to WCP-35, World Meteorological Organization, Geneva, 18 pp.

WCRP, 1984: *Scientific Plan for the World Climate Research Programme,* WCRP Publ. Series, No. 2, WMO/TD-No. 6, World Meteorological Organization, Geneva, 95 pp.

Woodbury, G. E., and M. P. McCormick, 1986: Zonal and geographic distributions on cirrus clouds determined from SAGE data. *J. Geophys. Res.*, **91,** 2775–2785.

Wylie, D. P., and W. P. Menzel, 1989: Two years of cloud cover statistics using VAS. *J. Climate,* **2,** 280–392.

Yamanouchi, T., S. Kazuya and S. Kawaguchi, 1987: Detection of clouds in Antarctica from infrared multispectral data of AVHRR. *J. Meteorol. Soc. Jpn.*, **65,** 949–962.